CR-168297
PWA-5914-21

NASA

TURBINE BLADE AND VANE HEAT FLUX SENSOR DEVELOPMENT PHASE 1
FINAL REPORT

August, 1984

By

W. H. Atkinson
M. A. Cyr
R. R. Strange

Engineering Division
Pratt & Whitney
UNITED TECHNOLOGIES CORPORATION

Prepared For

NATIONAL AERONAUTICS AND SPACE ADMINISTRATION
Lewis Research Center
Cleveland Ohio 44135
Contract NAS3-23529

1.REPORT NO. CR-168297	2. GOVERNMENT AGENCY	3.RECIPIENT'S CATALOG NO.
4.TITLE AND SUBTITLE TURBINE BLADE AND VANE HEAT FLUX SENSOR DEVELOPMENT PHASE 1 - FINAL REPORT		5. REPORT DATE August, 1984 6. PERFORMING ORG. CODE
7.AUTHOR(S) W.H. Atkinson, M.A. Cyr, R.P. Strange		8. PERFORMING ORG. REPT. NO. PWA-5914-21
9.PERFORMING ORG. NAME AND ADDRESS UNITED TECHNOLOGIES CORPORATION Pratt & Whitney Engineering Division		10. WORK UNIT NO. 11. CONTRACT OR GRANT NO. NAS3-23529
12. SPONSORING AGENCY NAME AND ADDRESS National Aeronautics and Space Administration Lewis Research Center 21000 Brookpark Road, Cleveland, Ohio 44135		13. TYPE REPT./PERIOD COVERED FINAL REPORT 14. SPONSORING AGENCY CODE

15. SUPPLEMENTARY NOTES

16. ABSTRACT

The overall objective of this two phase program is to develop heat flux sensors suitable for installation in hot section airfoils of advanced aircraft gas turbine engines. The first phase consisted of the design, fabrication, calibration and testing of two heat flux sensor types. This will be followed by an experiment where these and other measurement techniques will be compared in an atmospheric pressure combustor rig test. This report discusses the first phase of the program. Under this phase of the program, sensors of two types, embedded thermocouple and the Gardon Gauge, were fabricated that met the geometric and fabricability requirements and could withstand the hot section environmental conditions. Calibration data indicate that these sensors yielded repeatable results and have the potential to meet the accuracy goal of measuring local heat flux to within 5%. Thermal cycle tests and thermal soak tests indicated that the sensors are capable of surviving extended periods of exposure to the environmental conditions in the turbine. Problems in calibration of the sensors caused by severe non-one-dimensional heat flow were encountered. Modifications to the calibration techniques are needed to minimize this problem and proof testing of the sensors in an engine is needed to verify the designs.

17. KEY WORDS (SUGGESTED BY AUTHOR(S))	18. DISTRIBUTION STATEMENT
Heat Flux Sensors Design Sensor Calibration Sensor Fabrication Heat Flux Sensor Testing	Unlimited

19. SECURITY CLASS THIS (REPT)	20. SECURITY CLASS THIS (PAGE)	21. NO. PGS	22. PRICE *
Unclassified	Unclassified		

* For sale by the National Technical Information Service, Springfield, VA 22161

TABLE OF CONTENTS

LIST OF ILLUSTRATIONS

LIST OF ILLUSTRATIONS (Continued)

LIST OF ILLUSTRATIONS (Continued)

LIST OF ILLUSTRATIONS (Continued)

LIST OF ILLUSTRATIONS (Continued)

1.0 SUMMARY

The overall objective of this two phase program is to develop heat flux sensors suitable for installation in hot section airfoils of advanced aircraft gas turbine engines. The first phase consisted of the design, fabrication, calibration and testing of two heat flux sensor types. This will be followed by an experiment where these and other measurement techniques will be compared in an atmospheric pressure combustor rig test. This report discusses the first phase of the program.

A literature survey and review of commercially available sensors were conducted to review the state-of-the-art of heat flux sensor technology. Conceptual designs were performed on several types of heat flux sensors for use on turbine airfoils. Preliminary analyses were then performed on these candidate designs and tests were run to determine the thermoelectric properties of various superalloys used in turbine airfoils. Based on these analyses and tests, one-dimensional embedded thermocouple sensors and Gardon gauges were identified, with concurrence of NASA, as the most promising candidates. Final designs including thermal and stress analyses were performed for these two sensor types. Sensors of both types were fabricated into turbine airfoils, calibrated, and endurance tested. The results from this phase of the program are identified below.

- Sensors of two types were fabricated that met the geometric and fabricability requirements and could withstand the hot section environmental conditions.
- Calibration data indicates that these sensors yielded repeatable results and have the potential to meet the accuracy goal of measuring local heat flux to within 5%.
- Thermal cycle tests and thermal soak tests indicated that the sensors are capable of surviving extended periods of exposure to the environmental conditions in the turbine without significant calibration change.
- Severe non-one-dimensional heat flow causes problems in calibration of the sensors. These problems are being investigated.

2.0 INTRODUCTION

Designing durable turbine airfoils which use a minimum amount of cooling air (and are, therefore, more efficient and economical) requires detailed knowledge of heat flux characteristics within the hot section of advanced aircraft gas turbine engines. Considerable development has been done on both low and high temperature heat flux sensors for such diverse purposes as basic boundary layer experiments, solar power and energy conservation investigations, research on thermal protection systems for advanced aircraft and spacecraft, and application in advanced aircraft combustors. None of those applications combines the requirement for materials compatibility, miniaturization, and survivability in a hostile environment that is necessary for a viable turbine airfoil heat flux sensor. Due to the inherent limitations of current sensors, it has been impossible to collect hard empirical data relating to the heat transfer taking place in operating turbine airfoils in aircraft gas turbine engines. As an undesirable alternative, investigators have been forced to rely on heat flux predictions derived from ad hoc analytical models. These models are themselves unverifiable due to the very lack of empirical data they seek to remedy.

From this situation, the importance of accurate and durable heat flux sensors in the development of advanced gas turbine engines becomes apparent. The development of these sensors would provide a diagnostic tool enabling the modification and verification of analytical procedures used to design improved durability and longer life turbine airfoils. These, in turn, would promote a longer component life while minimizing the amount of cooling required, thus advancing fuel efficiency and maintenance economy.

To address the requirement for heat flux sensors suitable for use on turbine airfoils, this development effort was initiated at Pratt & Whitney under the NASA Hot Section Technology (HOST) program. The objectives of this program are to first develop heat flux sensors for gas turbine engine turbine blades and vanes and then to demonstrate a variety of heat transfer measurement methods on a test piece of simple geometry in an atmospheric pressure combustor rig. This report describes the first phase of that contract, sensor development.

In the development of heat flux sensors for turbine airfoils, some unique problems must be solved. The material used must be compatible with the cast nickel and cobalt base materials and the MCrAlY coatings used in modern turbine airfoils. The sensors must survive and operate in an extremely hostile environment with regard to temperature, pressure, cycling and, in the case of turbine blades, centrifugal loading. It is necessary to design very small sensors to minimize the impact of the temperature gradient across the surface of the sensor and to obtain the spatial resolution required of the measurement. The specific goals of the contract were to develop sensors with a spatial resolution of better than 0.15 mm and an accuracy of + 5%. These sensors were to be suitable for use over heat flux levels of 0.3 to 4.5 megawatts/meters^2, at temperatures to 1250K, pressures to 40 atmospheres, Mach numbers to 1.0, and under the vibrational and centrifugal loading conditions that exist in modern gas turbine engines.

Since these heat flux sensors are being designed to measure the local heat transfer conditions that existed over hot section surfaces prior to sensor installation, the presence of the sensors must not significantly affect the local heat transfer rate. This requires that the thermal properties of the sensor must not deviate greatly from that of the host airfoil. In addition, the sensors must be designed to be installed flush with the airfoil wall to maintain aerodynamic integrity and avoid disturbing the hot side boundary layer. Finally, once the sensors have been constructed, methods must be developed to obtain accurate sensor calibrations.

3.0 SURVEY AND EVALUATION OF HEAT FLUX SENSOR CONCEPTS

A survey was conducted to identify sensor types that have the potential for meeting the requirements for the measurement of heat flux on hot section airfoils. This survey consisted of a literature search, consultation with authorities in the field of heat transfer measurement, and a review of commercially available sensors. A test program was also initiated to evaluate the suitability of advance airfoil superalloys for use as thermoelectric materials.

3.1 LITERATURE SURVEY

A computer assisted literature survey was performed to identify the state-of-the-art in heat flux sensor development. This survey was conducted through the United Technologies Research Center library using interlibrary loans on requested materials. Also reviewed were materials gathered in a literature survey for a previous contract, (Reference 1). The new search included heat flux work on blades and vanes. A complete listing of the literature reviewed is contained in Appendix A.

In most of the literature, heat transfer coefficients were calculated from measurements of gas and metal temperatures rather than being directly measured. Both transient and steady state sensors have been used (Ref. 2). Where direct measurements have been made most of these direct measurements of heat fluxes reported were conducted with thin film transducers at low temperatures. One direct measurement at high temperature, Dunn and Hause (Ref. 12), measured heat flux using a thin film heat flux gauge constructed of platinum painted on a Pyrex insulating substrate with a magnesium fluoride vapor deposited coating as a protection against abrasion. The sensor, classified as a transient sensor, was then attached to turbine components using epoxy and used at high temperatures. Other transient sensors include calorimeters, thin foil heat flux sensors and one-dimensional transient heat flux sensors. One of the disadvantages of these sensors is that they require a step change in net heat flux to the sensor to yield data. Under steady state conditions, or under transients that are slow compared to sensor response time, these sensors yield no data.

Steady state sensors are sensors whose operation are based on heat conduction through a thermal barrier. One-dimensional steady state sensors determine heat flux by measuring the temperature differential across a material of known thermal conductivity. These sensors, which the literature search indicated were the most feasible for the turbine airfoil application, include the Gardon gauge sensors, one-dimensional steady-state laminated sensors and the thin foil sensors. The thin foil sensors are, however, only applicable to low temperature use and are therefore not of interest for this program. The steady state heat flux sensors for use at high temperature conditions, discussed by Atkinson and Strange (Ref. 1), are the most likely candidates for turbine blade and vane installations.

During the literature survey, discussions were held with a wide range of authorities in the field of heat flux measurement. These included experts within educational institutions, industry, and the government. While these experts were in agreement with the desirability of steady state heat flux sensors for use on hot section airfoils, none were aware of the existence of such a high temperature, high pressure sensor.

3.2 SURVEY OF COMMERCIALLY AVAILABLE HEAT FLUX SENSORS

In parallel with the literature survey, a survey was conducted of the commercially available heat flux sensors to determine if any of these sensors would be suitable for adaption to the turbine blade and vane application. A wide range of transient and steady state sensors are available. Thin nonperturbing sensors were identified that are being used for relatively low temperature boundary layer experiments. There also are high temperature sensors available for energy conversion studies and investigation in high temperature furnaces. No commercially available sensors were, however, identified that had all the characteristics of high temperature capability, extreme ruggedness, nonperturbing qualities, and small size demanded by the turbine blade and vane application.

3.3 THERMOELECTRIC TESTS ON SUPERALLOYS

Several of the proposed sensor designs used airfoil materials as a portion of the thermoelectric circuit. A series of thermoelectric tests was, therefore, run on various turbine blade and vane materials to determine the suitability of these materials as thermocouple elements to be used in the fabrication of heat flux sensors. The tests were run by taking samples with large length to diameter ratios and installing a Chromel/Alumel thermocouple at each end. One end of the sample was heated while the other was held at ambient temperature. Figure 3.3-1 shows a schematic of that test procedure. The two end temperatures plus the differential output between the Alumel wires were recorded during test. The output from the two Alumel wires was representative of the output of the sample material versus Alumel referred to the ambient temperature. This value was then corrected to a 273°F reference temperature.

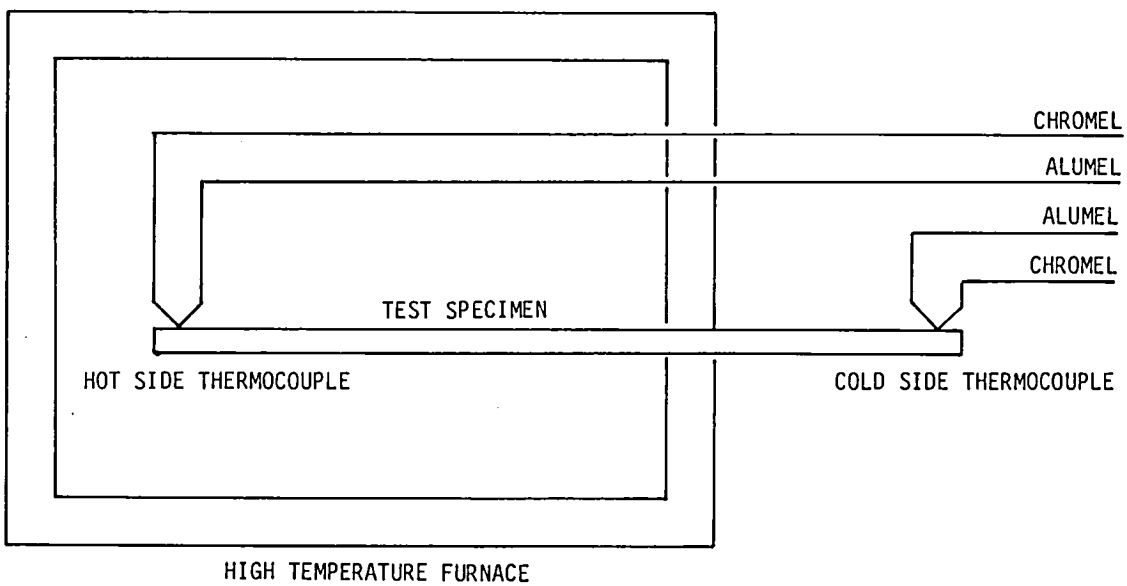

Figure 3.3-1 Thermoelectric Test Schematic

The materials tested are listed in Table 3.3-I. All of the nickel base blade alloys and cobalt base vane alloys tested exhibited stability with time and temperature to 1250K, and produced millivolt outputs versus Alumel that make them acceptable as thermocouple elements.

Curves showing the thermoelectric characteristics of the various hot section alloys are included in Appendix C. For ease of comparison with data in the literature, the output of the alloys is presented versus platinum. The output versus platinum was calculated from the test data and the Alumel versus platinum thermoelectric reference tables.

A discussion of the stability, magnitude, and uncertainty of the thermoelectric properties of hot-section materials appears in reference 50.

TABLE 3.3-I

HOT SECTION MATERIALS FOR WHICH THERMOELECTRIC DATA WAS OBTAINED

Nickel Base Materials		Cobalt Base Materials	
Alloy 454	(PWA 1480)	Mar-M-509	(PWA 647)
B-1900	(PWA 663)	WI-52	(PWA 653)
B-1900 + Hf	(PWA 1455)		
Hastelloy-X	(PWA 1038)		
Inconel 792	(PWA 1456)		
Inconel 713C	(PWA 655)		
Mar-M-247	(PWA 1447)		
Mar-M-200 + Hf	(PWA 1422)		

4.0 HEAT FLUX SENSOR DESIGN

Following the evaluation of the various sensor types, two types of steady state heat flux sensors were chosen by NASA to be designed for use in turbine blades and vanes. These were embedded thermocouple sensors and Gardon Gauge sensors.

4.1 MECHANICAL DESIGN

The embedded thermocouple sensors require installation of lead wires in both the hot and cold side of the airfoil wall. In order to maximize thermocouple wire size to increase durability while keeping the required slots small, these sensors were designed with three single conductor swaged wires. Figure 4.1-1 illustrates the design for the embedded thermocouple sensors. In this design, both an Alumel and Chromel wire are embedded in the cold side of the blade or vane and an Alumel wire is embedded on the hot side. The sensor output is obtained as a differential signal from the Alumel wires. The Chromel/Alumel thermocouple yields a reference temperature.

The Gardon Gauge sensors require installation of lead wires on only the cold side of the airfoil. In order to minimize machining, these sensors were designed with a single sheathed three conductor cable. Figure 4.1-2 shows schematic for the Gardon Gauge sensors. For this design, two Alumel wires and one Chromel wire are installed in a single sheath that was embedded in the cold side surface. This unique three conductor cable was produced to our specifications by Idaho Labs[1]. A cavity is electro-machined into the airfoil. One Alumel lead is attached to the bottom center of the cavity; the other Alumel lead and the Chromel lead are attached to the wall of the cavity near the bottom. Sensor output is obtained from the two Alumel wires, while a reference temperature is obtained from the Chromel and Alumel wires attached to the wall. The cavity made for the Gardon Gauge is filled with a ceramic cement which provides aerodynamic integrity on the cold side as well as support and oxidation protection for the fine thermocouple wires.

4.2 THERMAL AND STRESS ANALYSIS

Thermal analyses were performed on both the Gardon Gauge and embedded thermocouple sensors using the Pratt & Whitney Thermal Calculation (TCAL) program. This program performs three-dimensional finite difference heat transfer analyses. The program allows material properties (thermal conductivity and specific heat) to vary with temperature and allows both transient and steady state analyses to be performed. A comparison with the more complex STAN5 boundary layer program under a previous NASA contract (Ref. 1) showed that TCAL was an accurate cost effective tool for sensor screening.

[1] Idaho Laboratories Corporation
2101 Hemmert Avenue
Idaho Falls, ID 83401

This program was used to analytically investigate variations in the dimensions and geometry of the instrumentation in order to optimize the sensor designs. For purposes of this analysis, both steady-state and transient conditions were imposed. The hot and cold side boundary conditions were chosen to give representative heat fluxes and airfoil temperatures.

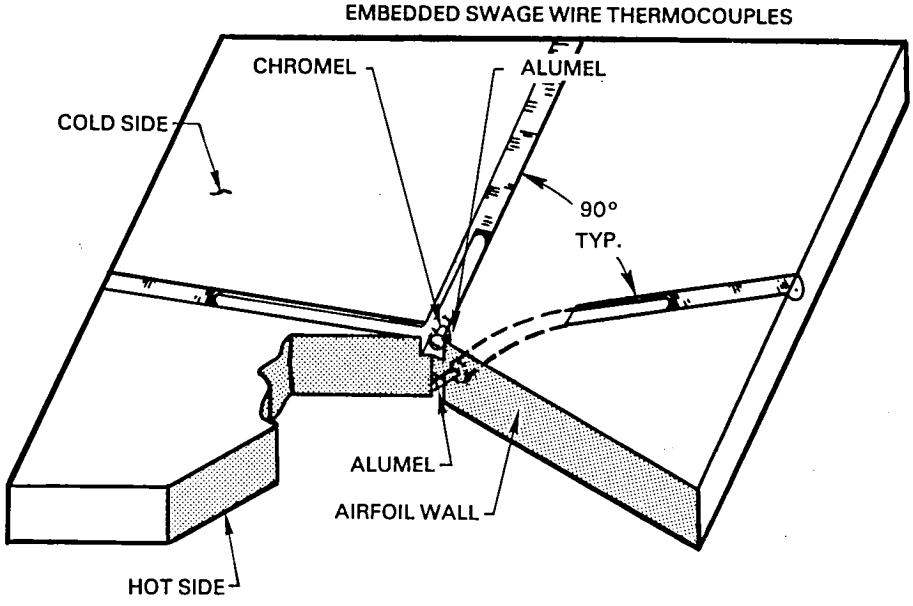

ELECTRICAL SCHEMATIC EMBEDDED THERMOCOUPLE SENSOR

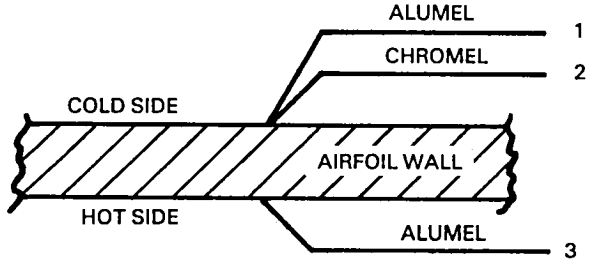

1-3 = SENSOR OUTPUT

1-2 = REFERENCE TEMPERATURE

Figure 4.1-1 Schematic of the Embedded Thermocouple Heat Flux Sensor

GARDON GAUGE

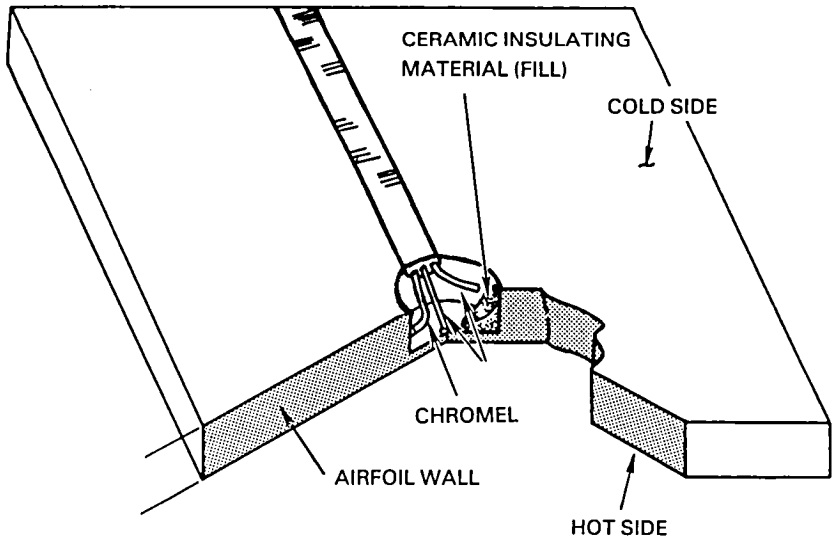

ELECTRICAL SCHEMATIC GARDON GAUGE SENSOR

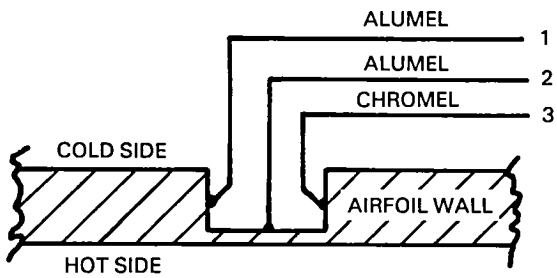

1-2 = SENSOR OUTPUT

1-3 = REFERENCE TEMPERATURE

Figure 4.1-2 Schematic of the Gardon Gauge Heat Flux Sensor

4.2.1 Steady-state Heat Transfer Analysis

The two steady-state cases analyzed were a high heat flux case and a low heat flux case. For the high heat flux case, boundary conditions were chosen to give a heat flux into the unperturbed surface of $\approx 5.0 \times 10^6$ W/m^2 and an average airfoil temperature of $\approx$ 1255K. The conditions chosen were:

Hot Side	h	= 7.3 kW/m^{2}K
	t_{gas}	= 2030K
Cold Side	h	= 12.5 kW/m^{2}K
	t_{gas}	= 755K

For the low heat flux case, boundary conditions were chosen to give a heat flux into the unperturbed surface of $\approx 6.3 \times 10^5$ W/m^2 and an airfoil temperature of $\approx$ 1115K. The conditions chosen were:

Hot Side	h	= 1.9 kW/m^{2}K
	t_{gas}	= 2030K
Cold Side	h	= 2.7 kW/m^{2}K
	t_{gas}	= 865K

The material properties used throughout these analyses are tabulated in Appendix B.

A steady state analysis was conducted for the embedded thermocouple sensor installed into a MAR-M-509 airfoil to simulate a turbine vane installation. The airfoil thickness used was 1.14 mm, which is a typical value for airfoil walls. The grooves were modeled as 0.25 mm squares with 0.25 mm swaged thermocouple wires installed in the grooves. At the lower heat flux, the thermal perturbation was less than 1K in the area of the thermocouple junction while at the higher heat flux a 4K perturbation was calculated. Figures 4.2-1 and 4.2-2 show the thermal profiles across the sensor predicted for the two cases. Sensor output for the lower heat flux was calculated to be 0.366 millivolts and the sensitivity was 0.532 μV/kW/m^2. For the higher heat flux case the output and sensitivity was calculated to be 2.528 millivolts and 0.516 μV/kW/m^2, respectively. The heat flux into the airfoil with the sensor installed was compared with the heat flux into the airfoil prior to sensor installation. The difference in both cases was negligible ($< 0.3\%$) and produced negligible errors in the heat flux measurement.

The embedded thermocouple configuration will remain the same for all heat flux ranges. The Gardon Gauge sensor, however, must be optimized for each heat flux condition. The Gardon Gauge configuration chosen for this analysis included a 0.038 mm thick foil on the hot side in an MAR-M-509 airfoil with a total wall thickness of 1.14 mm. This was done in order to obtain a useful output from the sensor at low heat fluxes. The design for a high heat flux condition would use a thicker foil. The trade-off between thermal perturbations and sensor output are determined by changing the foil dimensions. The sensor output may be increased by increasing the diameter or depth of the Gardon Gauge cavity. This ability to increase sensor output can be important especially for rotating components where the signal from the heat flux sensor must be transmitted through a slip ring or a telemetry package. The increase in sensor output is, however, accompanied by an increase in thermal perturbation and the accompanying sensor error. This tradeoff should be carefully considered for each sensor installation. The configuration chosen was optimized for fluxes on the order of 3×10^5 W/m^2. This is representative of the levels anticipated in the cylinder in crossflow experiment required under the contract as well as the low heat flux section of some hot section airfoils.

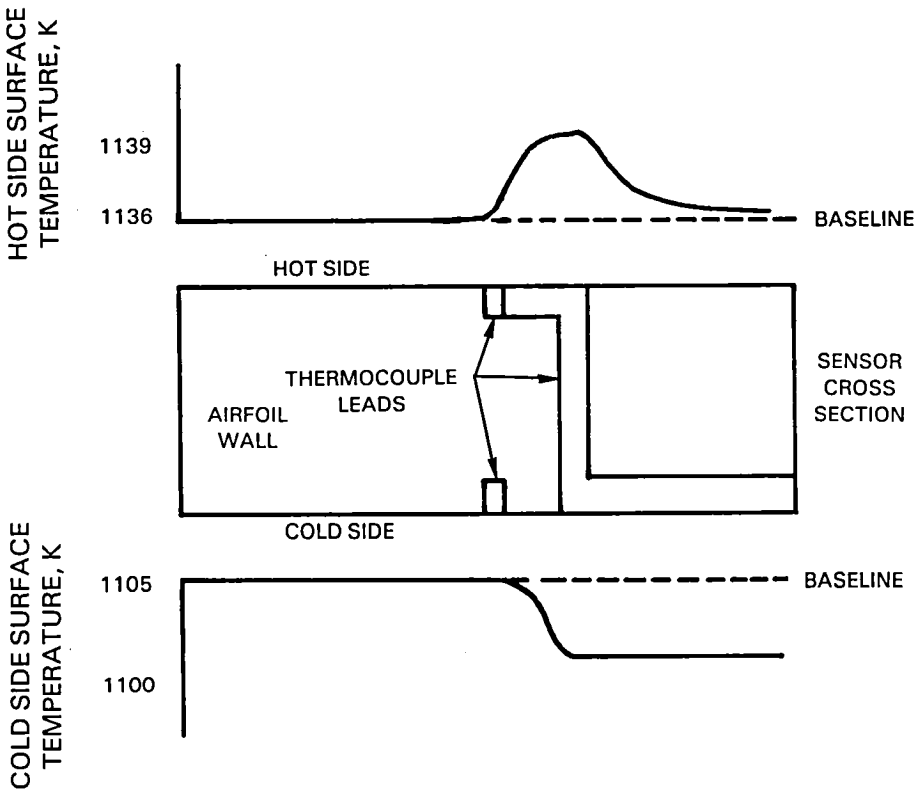

Figure 4.2-1 Embedded Thermocouple Perturbations at Low Heat Flux

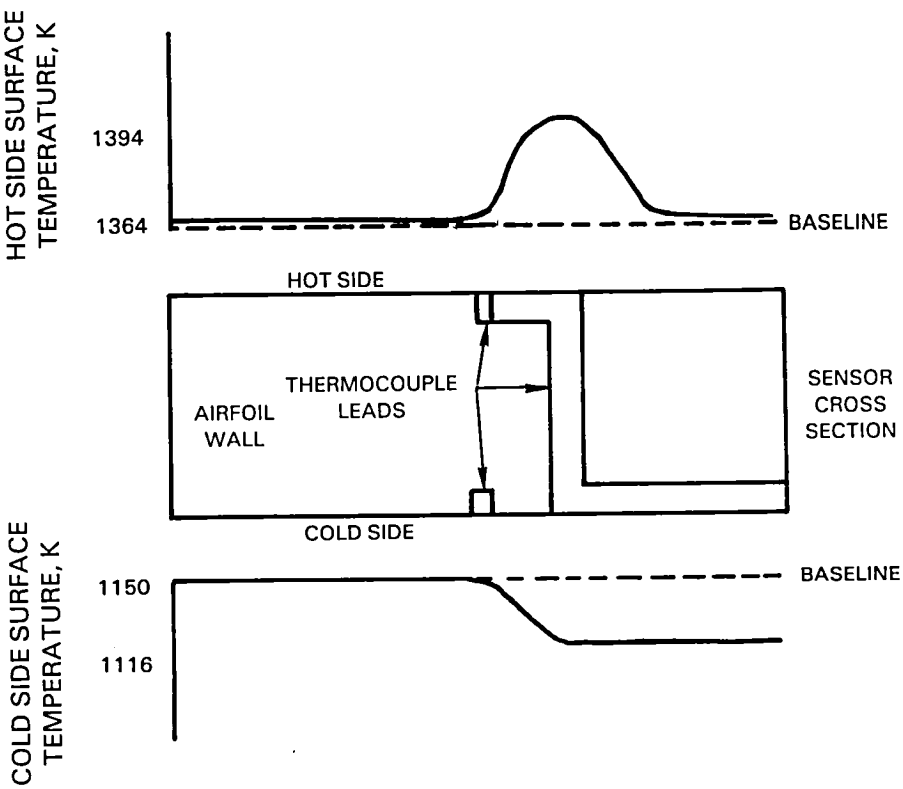

Figure 4.2-2 Embedded Thermocouple Perturbations at High Heat Flux

The maximum hot side thermal perturbation introduced by the Gardon Gauge for the low heat flux case was 17K. Figure 4.2-3 shows the thermal profile across the sensor. The sensor output was calculated to be 0.573 millivolts and the sensitivity was 0.899 $\mu V/KW/M^2$. The heat flux into the airfoil with the sensor installed was compared with the heat flux into the airfoil prior to sensor installation. The maximum difference was 5.1% at the center of the Gardon Gauge foil. This results in a sensor error of -3.5% for these test conditions.

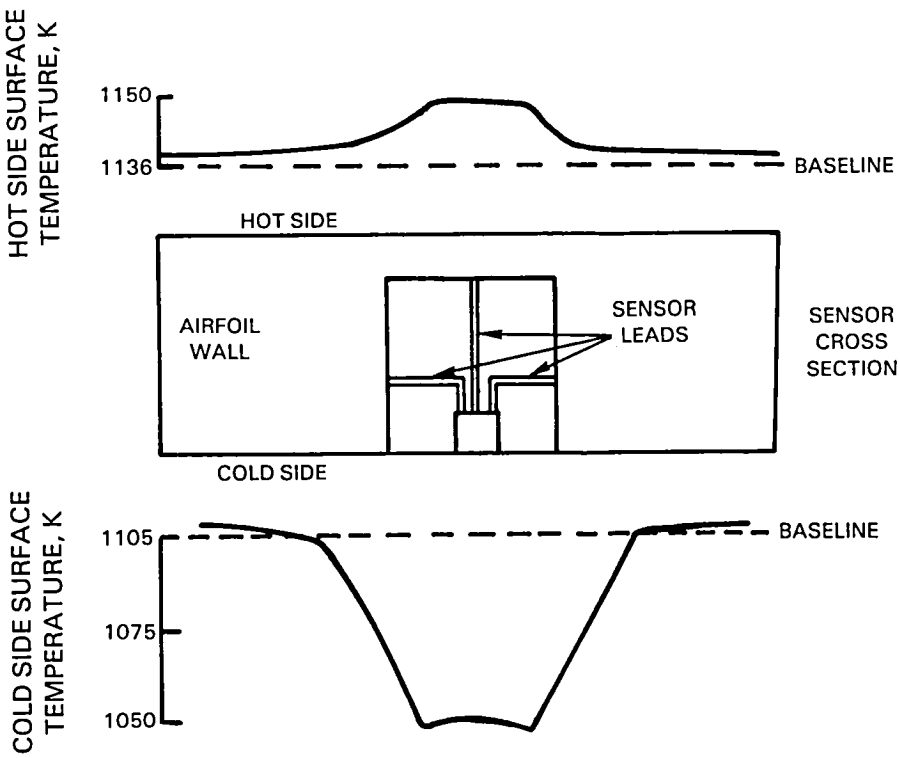

Figure 4.2-3 Gardon Gauge Perturbations at Low Heat Flux

The above analyses were repeated for both the embedded thermocouple and Gardon Gauge sensor mounted in a blade of Alloy 454 (PWA-1480). The geometry was kept identical to the cases discussed above; only the airfoil material was changed. The results were very similar to those for the vane alloy. The baseline temperatures changed slightly due to the slightly lower thermal conductivity of Alloy 454 versus MAR-M-509 but the magnitude of the perturbation resulting from the heat flux sensor installation showed no significant change.

A steady-state analysis was performed to determine the validity of the assumption that the blade could be modeled as a flat plate internally. A comparison was made between the thermal and heat flux profiles for a flat plate and a plate with turbulators. Two comparisons were conducted. The first used a constant heat transfer coefficient on the cold side and the second used an imposed heat transfer coefficient gradient between turbulators. This gradient was from available P&W test data. Both cases indicated that the internal blade or vane profile could be modeled as a flat plate for the sensor area with negligible error.

4.2.2 Transient Heat Transfer Analysis

Transient cases were run through the TCAL program to determine the feasibility of using transient slug calorimeters as an alternative sensor type. The airfoil chosen for analysis was a MAR-M-509 vane with a wall thickness of 1.14 mm. A section of the airfoil wall was used for the slug calorimeter. The airfoil was initially overcooled, and the transient was created by modeling an abrupt cut off of the coolant air. The conditions used for the analysis are given in Table 4.2-I, and the resulting thermal transient is shown in Figure 4.2-4. At an airfoil temperature of $\approx$ 1150K the rate of change of airfoil temperature would be approximately 37 K/sec. While this is a rapid change, this sort of transient is within the measuring capabilities of modern data systems. The results indicate that transient sensors might be a possible alternative. The transient sensors would probably only be used in vanes which are nonrotating. The cooling to the vanes can be varied relatively easily whereas the cooling could not easily be changed to the rotating blades.

TABLE 4.2-I

BOUNDARY CONDITIONS FOR TRANSIENT HEAT FLUX ANALYSES

Initial condition

h	hot side	7.0 kW/m^2K
T	hot side gas	1477 K
h	cold side	5.3 kW/m^2K
T	cold side gas	866 K

At time t = 0.9 sec, the cold side heat transfer coefficient was changed to 0 kW/m^2K.

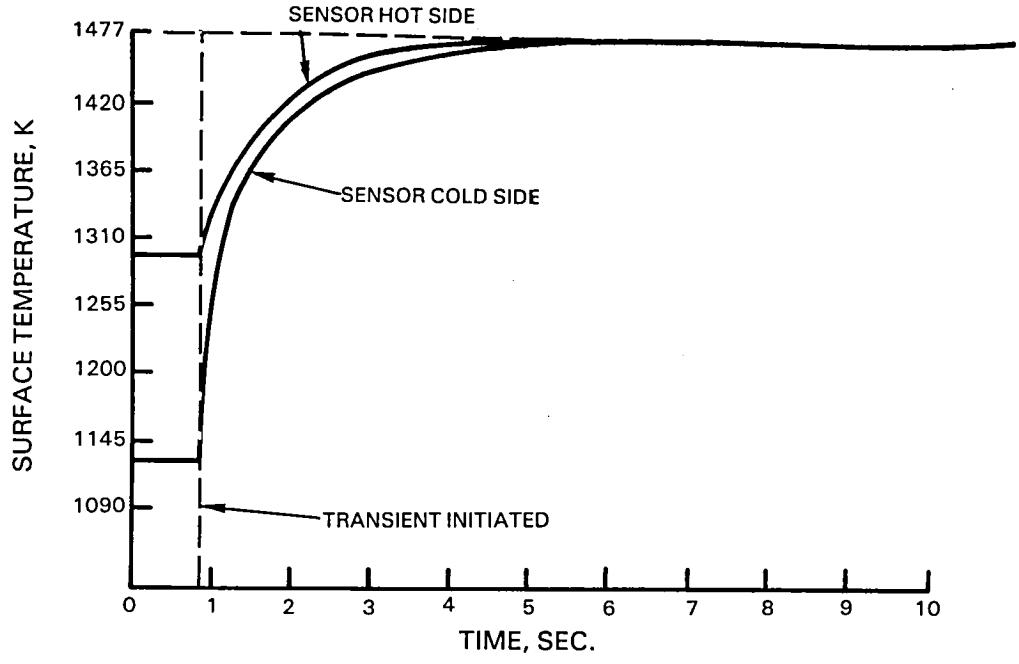

Figure 4.2-4 Results of Transient Heat Flux Sensor Analysis

4.2.3 Stress Analysis

When a heat flux sensor is installed in a blade or vane, thermal perturbations are introduced. The resulting thermal expansions will result in thermally induced airfoil stresses and ultimately thermally induced airfoil strain. These considerations are especially important for turbine blades which are already highly loaded due to centrifugal effects.

A worst case condition would exist if there was a sharp thermal gradient at the edge of the sensor area. In that case the maximum shear stress at the edge of sensor is given by:

$$\tau = 1/2\,\Delta T\,\alpha E$$

Where

τ = Shear Stress
ΔT = Temperature Drop Across the Sensor
α = Modulus of Elongation
E = Young's Modulus

The worst case thermal perturbations will take place if a Gardon Gauge designed for a relatively low heat flux were run in a high heat flux condition. Such a case was used for the stress analysis.

Calculations for blade and vane materials yielded thermal stresses of 23.2 MPa and 41.8 MPa, respectively. These stresses yielded an increase in strain of 0.03%. This represents a ten percent increase in the airfoil design strain of 0.3%. Such an increase would cause a slight decrease in airfoil life but is not a concern for parts that will be run only in experimental engines.

5.0 FABRICATION OF HEAT FLUX SENSORS

The same general procedure would be used for the fabrication of heat flux sensors into any airfoil. This general procedure will be described followed by a description of the sensors fabricated into test pieces for this contract.

5.1 GENERAL FABRICATION PROCEDURE

Both the embedded thermocouple sensor and the Gardon Gauge sensor selected for development are fabricated into the airfoil wall. The embedded thermocouple sensor is formed by machining a groove into the hot side wall and two grooves into the cold side wall to accept the thermocouple wires. The grooves are cut by electrical discharge machining and are 0.3 mm wide and 0.3 mm deep. At the thermocouple junction end of the groove, the depth is reduced to 0.13 mm to keep the thermocouple junction as close to the surface as possible. The thermocouple junctions are directly opposite each other on the airfoil wall and the grooves are approximately 90 degrees apart to reduce the structural impact. In the case of the rotating blades, the leadwires are routed in a serpentine pattern to accommodate the centrifugal loading on the wires. The thermocouple wire used is 0.25 mm diameter single conductor swaged Chromel and Alumel wire. The swaged thermocouple wires are installed in the grooves and held in place by fillet wires of Chromel P which are resistance welded in place. After the thermoelectric junctions are made by resistance welding, the area around the thermocouple junction is filled with powdered MgO insulation material to protect the thermoelectric junctions. A Hastelloy-X cap is then welded over the sensing area, and the entire groove is filled with Chromel P fillet wire. After the wires are installed, the area is smoothed by hand to restore the aerodynamic integrity.

The Gardon Gauge sensor is fabricated by machining a cavity 1.5 mm in diameter into the cold side surface to a depth that leaves a sensor foil of the desired thickness at the the bottom of the cavity. A groove is machined into the cold side wall for the leadwire that is 0.55 mm wide and 0.55 mm deep. In the case of rotating blades, the leadwire routing is in a serpentine pattern to accommodate the centrifugal loading on the wires. The wire used to fabricate these sensors is a three conductor swaged wire 0.5 mm in diameter with two Alumel and one Chromel conductor. The thermocouple wire is installed in the channel utilizing the technique discussed above using Chromel P as a fillet wire. One Alumel wire is attached by resistance welding in the center at the bottom of the cavity. The other Alumel wire is attached to the sidewall of the cavity at the bottom and is oriented in the direction where the minimum temperature gradient is anticipated. The Chromel wire is attached to the sidewall of the cavity directly opposite the Alumel wire and is also located near the bottom of the cavity. After the thermocouple junctions are made, the cavity is filled with M-Bond GA100 ceramic cement. This cement provides both structural protection and oxidation resistance for the small wires. After the ceramic is given an oven cure, the surface is smoothed by hand to restore the aerodynamic integrity.

In the generation of the designs for the heat flux sensors, consideration was given to maintaining the structural and aerodynamic integrity of the airfoils. These same considerations were applied to the installation of the sensors into the airfoils. The sensor designs chosen for this work dictate that we must have access to the inside wall of the airfoil to install the heat flux sensors.

For vanes, it was considered feasible to remove a section of the vane wall opposite the proposed sensor location. This provides a window through which the sensor can be installed. If the window is removed using electrical discharge machining, the width of the cut can be held to 0.13 mm. After the instrumentation is installed, the window can be reinstalled in the vane by Heliarc welding. The weld junction is then smoothed by hand to restore the aerodynamic integrity of the vane surface.

For rotating blades, the concept of using a large window in the surface represents a compromise of the structural integrity of the blade. Access through the wall can be obtained while maintaining structural integrity by a series of holes no larger than 2.5 mm in diameter along the path of the leadwire. However, the machining cannot be accomplished through these holes and the ability to install instrumentation is severely limited. For these reasons two piece bonded blades were chosen for test pieces.

5.2 FABRICATION OF TEST HARDWARE

These two piece blades were engine airfoil manufactured from Mar-M-200+Hf (PWA 1422). Two sensors were installed in the suction side of each test blade, one in a forward cavity where the blade wall thickness was $\approx$1.07 mm and one in a rear cavity where the blade thickness was $\approx$1.37 mm. The 1.5 mm diameter Gardon Gauge foil thickness chosen for these sensors was 0.38 mm. The relatively thin foil was chosen to give reasonable output at relatively low heat flux levels. The use of two piece blades allowed installation of the instrumentation on the blade half prior to assembling the blade. The normal method of joining the blade halves is to use transient liquid phase (TLP) bonding. A previous study conducted by P&W indicated that thermocouple installations would not survive the TLP bond cycle of 20 hrs at 1475 K. The TLP bond is required for service hardware to produce a long low cycle fatigue life. It was decided that the instrumented blade would not require a long low cycle fatigue life in an experimental installation, and alternative methods of joining the blade halves, such as a lower temperature braze material or Heliarc welding, could be considered. The strength of the bond is not critical and bond failure would not result in loss of structural integrity of the blade. In a separate experiment, instrumented blade halves were joined with a 1200K braze and demonstrated that this method is feasible for joining experimental instrumented blades.

For test purposes under this contract, the blade halves were joined together by tack welding small metal strips around the periphery of the blade. This method of joining the blade halves permitted the blades to be disassembled for inspection or repair of the heat flux sensors. Installation of heat flux sensor in a blade to be run in an engine would require that the lead wires be embedded from the sensor location to the root of the blade in order to protect the leads from centrifugal loading and the hot side gas stream. The leads for these test blades were only embedded for a distance of 1 to 2 cm from the sensor. This minimized machining and assembly cost and increased the repairability of the test sensors.

Figures 5.2-1 through 5.2-5 show a sequence of photographs taken during installation of embedded thermocouple sensor. A similar sequence for the Gardon Gauge sensor is shown in Figure 5.2-6 through 5.2-9.

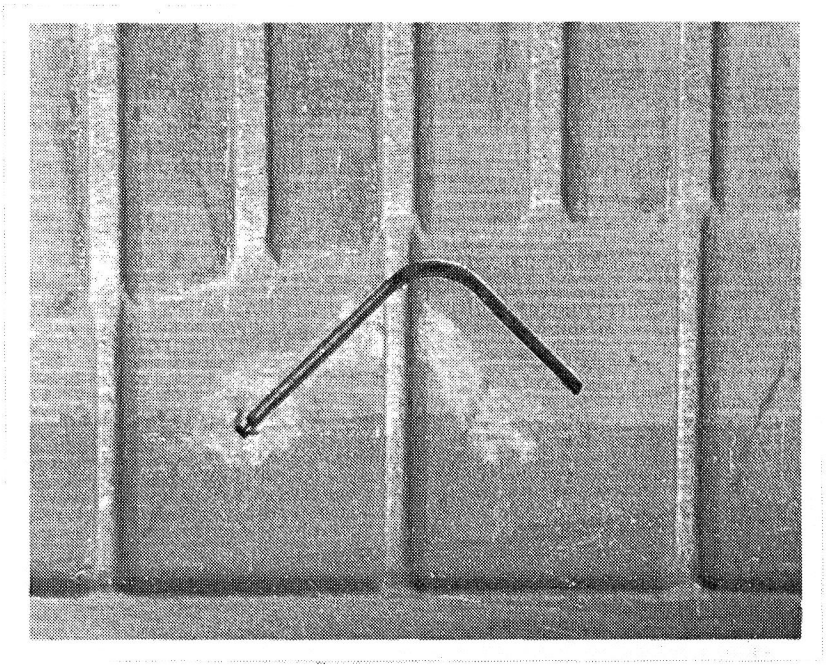

Figure 5.2-1 Embedded Thermocouple Sensor - First of Two Grooves Eloxed Into Internal Blade Wall for Heat Flux Sensor Wire Installation

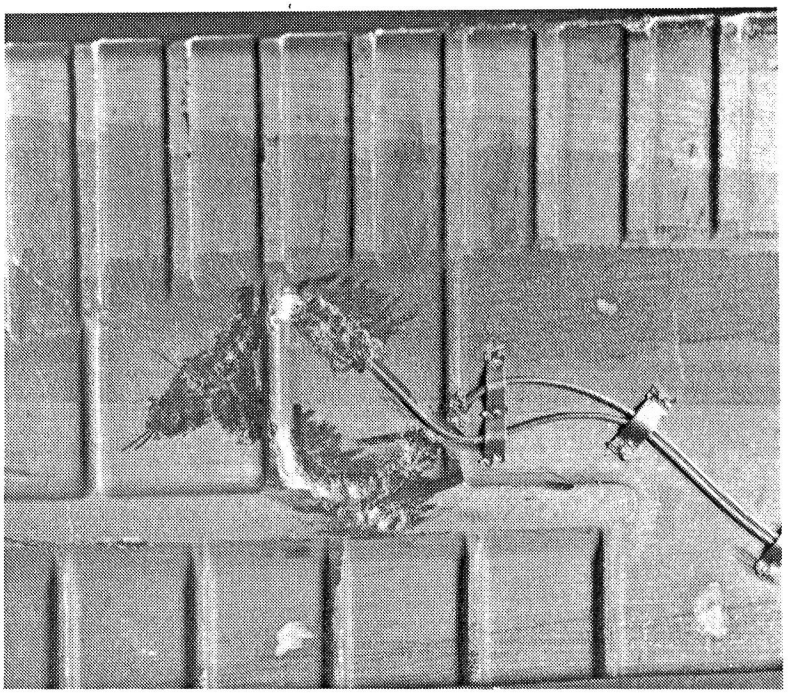

Figure 5.2-2 Embedded Thermocouple Sensor - Chromel and Alumel Leads Installed in Blade Inside Surface Rear Cavity

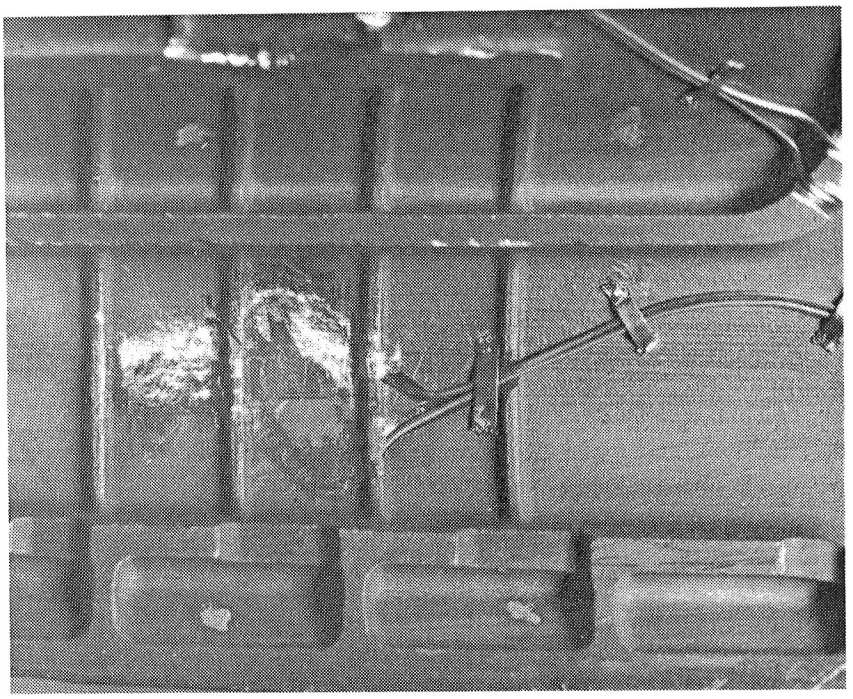

Figure 5.2-3 Embedded Thermocouple Sensor - Chromel and Alumel Leads Installation in Blade Inside Surface Forward Cavity

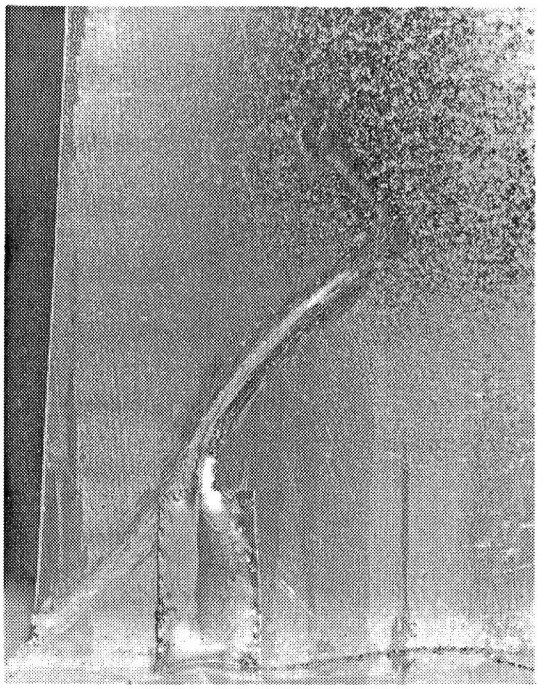

Figure 5.2-4 Embedded Thermocouple Sensor - Alumel Wire Installed in Blade Hot Side Surface. (The wire is covered by a thin foil after emerging from surface for protection during calibration.)

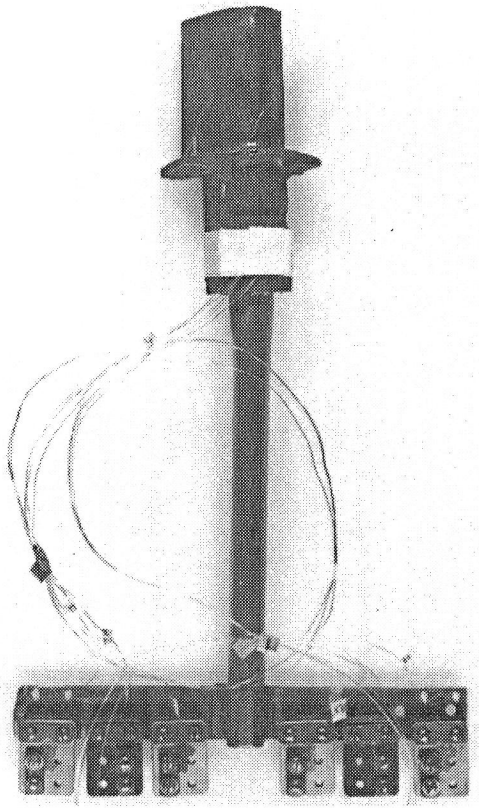

Figure 5.2-5 Assembled Blade with Two Embedded Thermocouple Sensors Installed

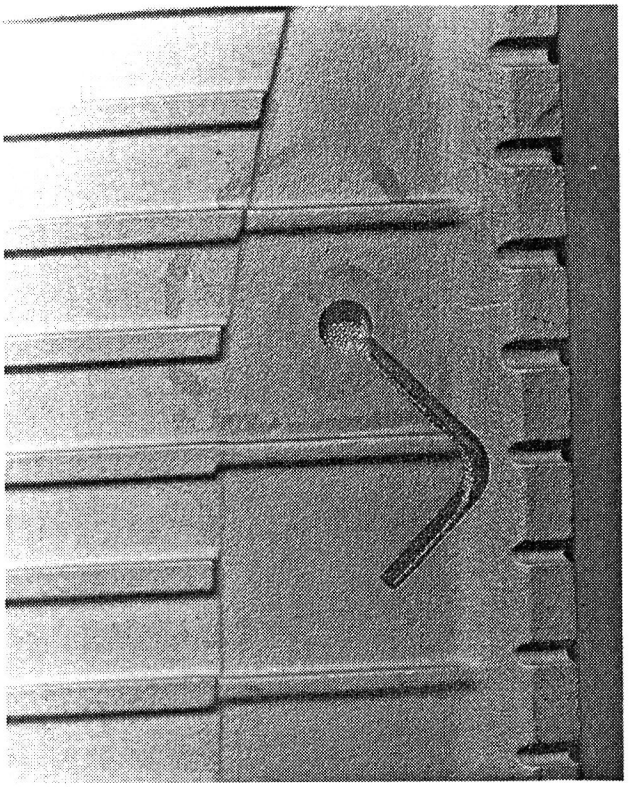

Figure 5.2-6 Gardon Gauge Sensor - Cavity and Groove Eloxed into Internal Blade Wall for Heat Flux Sensor

Figure 5.2-7 Gardon Gauge Sensor - Three Conductor Wire Installed

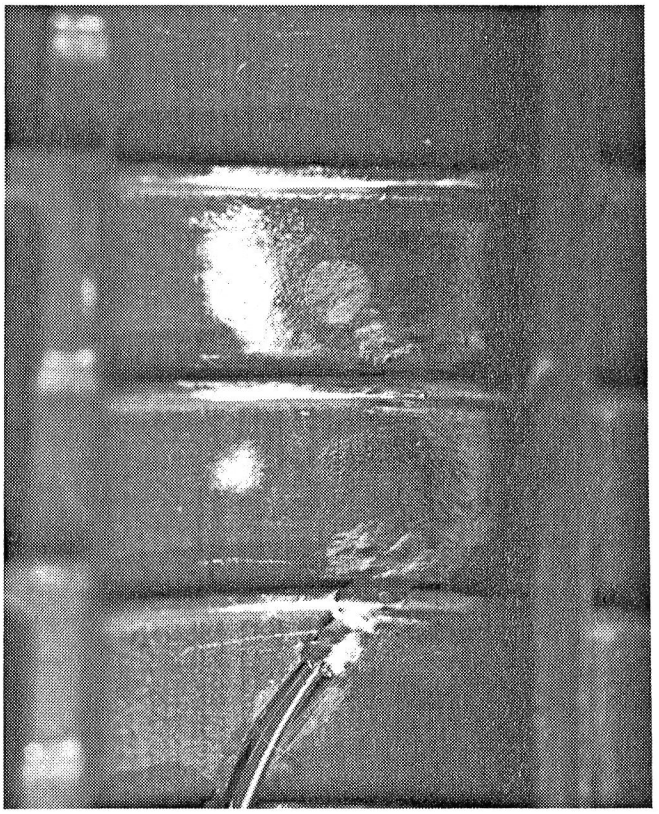

Figure 5.2-8 Gardon Gauge Sensor - Ceramic Cement in Place

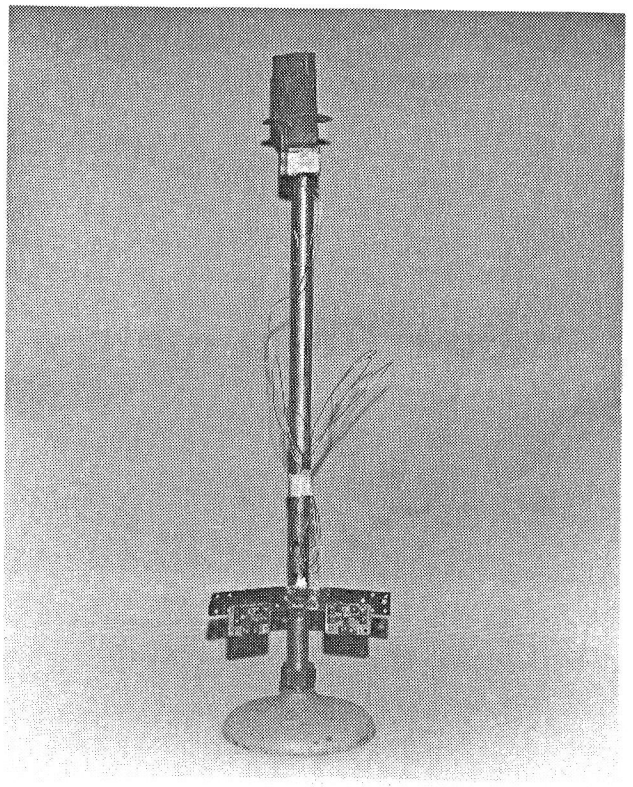

Figure 5.2-9 Assembled Blade with Two Gardon Gauge Sensors Installed

6.0 CALIBRATION AND LABORATORY TESTING

After fabrication, a program was undertaken to provide calibrations of the heat flux sensors to determine the output versus transmitted heat flux relationship and to provide durability testing of the sensors when subjected to thermal cycle and thermal soak conditions. A quartz lamp bank test facility was used for all testing and the airfoils were cooled with internal cooling air. The heat source was a quartz lamp bank with six parallel quartz halogen bulbs each rated at 6 kW. The bulbs are 25.4 cm long and the width of the lamp assembly is 7.6 cm. This lamp assembly is capable of producing a maximum heat flux incident on the sensors of 1.7 MW/m^2. During routine operation, the lamp is operated to approximately 1.0 MW/m^2 to maximize lamp life.

A photograph of the lamp face is shown in Figure 6.0-1. The reflector on the lamp is water cooled and the bulbs are air cooled to permit continuous operation. The airfoil under test is positioned below the lamp and is surrounded with polished water-cooled shields to concentrate the energy onto the airfoil. This shielding arrangement is shown in Figures 6.0-2 through 6.0-4. The airfoil is positioned so that the surface of the sensor area is parallel to the plane of the lamps and as close to the lamps as possible. The polished shields are adjustable to accommodate the various airfoil orientations. The heat flux output of the lamp is monitored by a reference heat flux sensor mounted in the shield. After the shields are positioned for a particular airfoil orientation, the airfoil is removed from the lamp assembly and a second reference sensor is mounted in the same location as the airfoil sensor. A calibration of the assembly is then performed to determine the relationship between the heat flux incident at the blade location to that at the reference sensor location. This relationship is used to correct the data measured by the reference sensor during the blade calibration. The position of the two reference sensors is exchanged and the calibration is repeated to eliminate any bias on the reference sensor calibrations. An overall view of the rig is shown in Figure 6.0-5. A probe was also fabricated to measure the convective heat transfer coefficient at the surface of the airfoil. The probe consists of an I^2R heater assembly with a thin foil heat flux sensor laminated on the surface. This probe was used to measure the heat transfer coefficient resulting from both free air convection and lamp coolant air leakage on the airfoil surface, and the measured value was used in the calculation of the heat losses from the sensor surface.

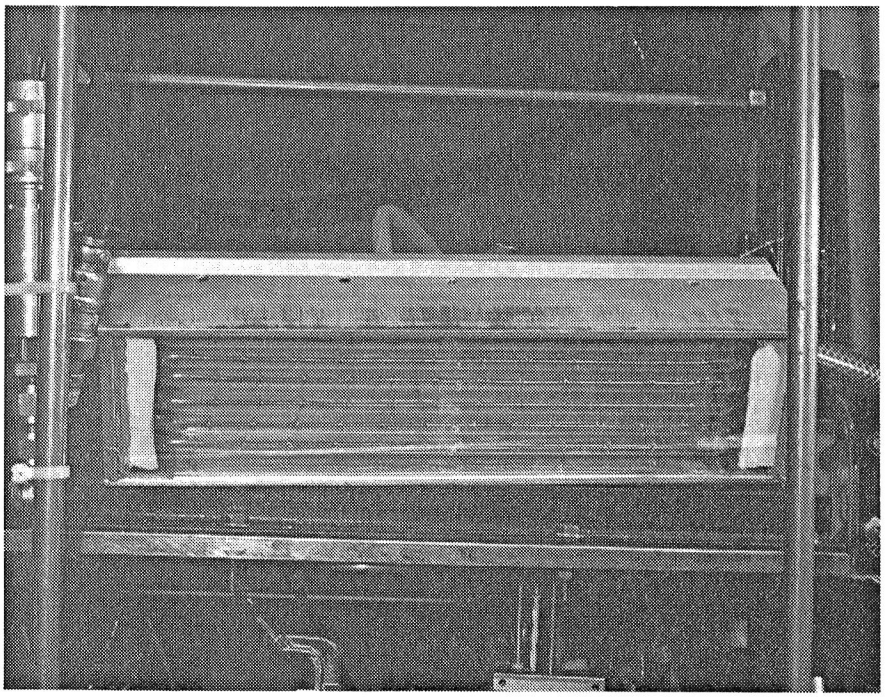

Figure 6.0-1 Lamp Face of the Quartz Lamp

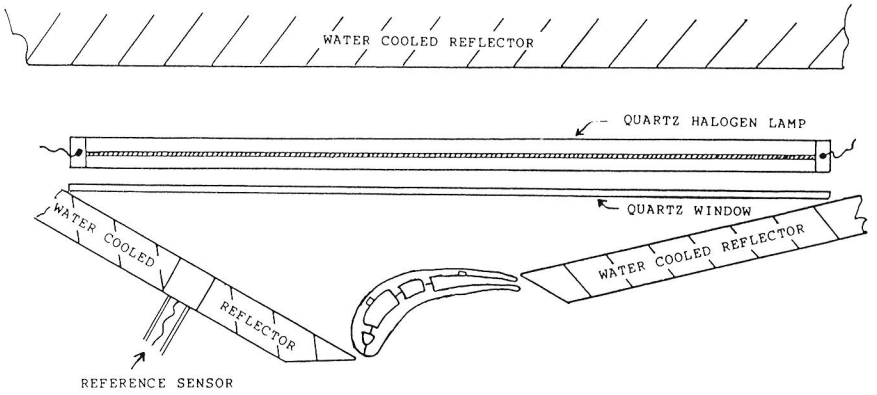

Figure 6.0-2 Calibration Setup Showing Assembled Blade in the Quartz Lamp Facility and Arrangement of the Reflectors

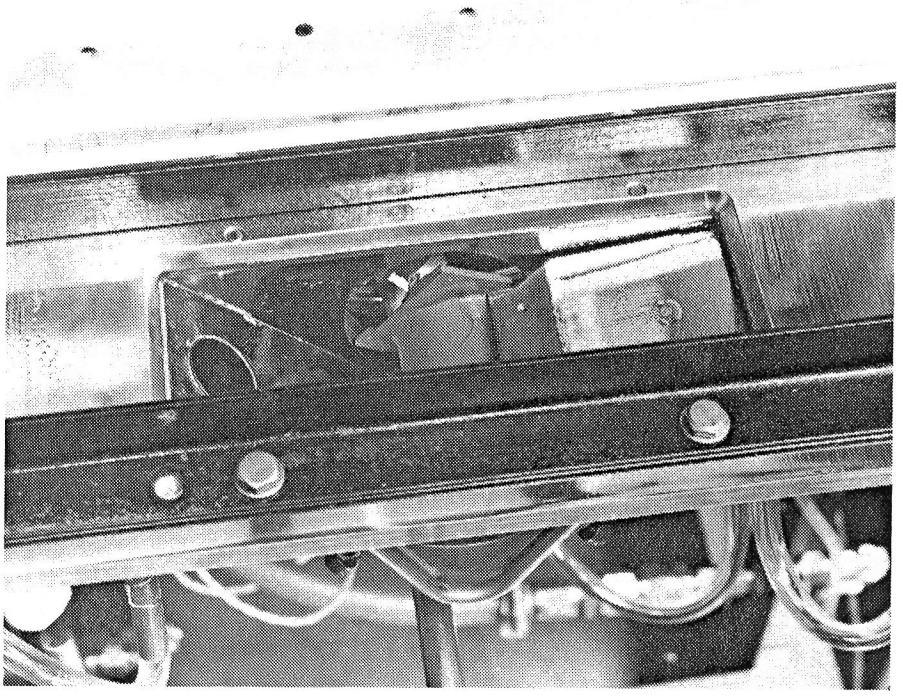

Figure 6.0-3 Quartz Lamp Facility Shielding Arrangement

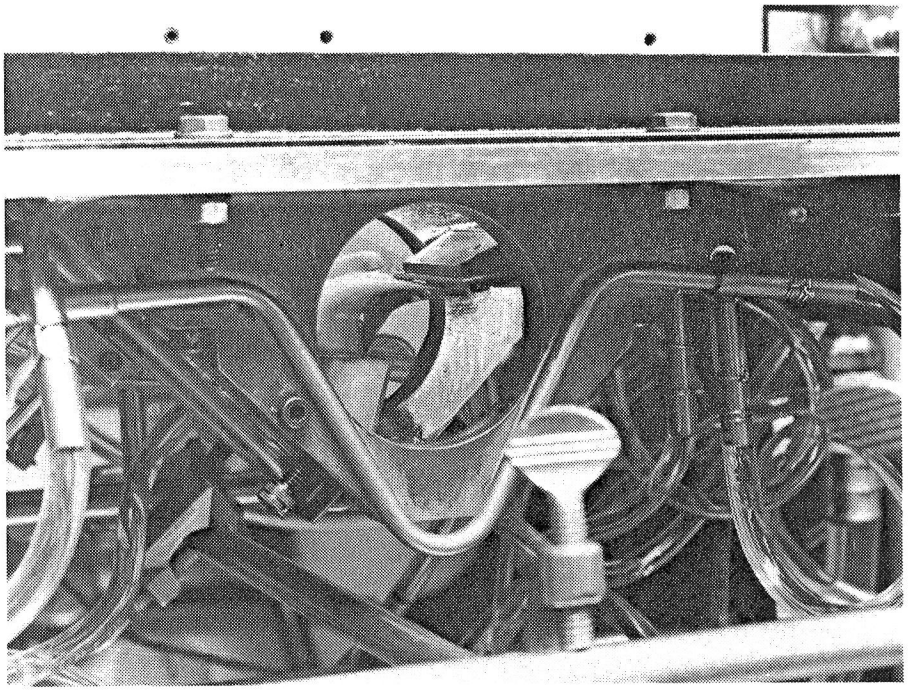

Figure 6.0-4 Quartz Lamp Facility Shielding Arrangement

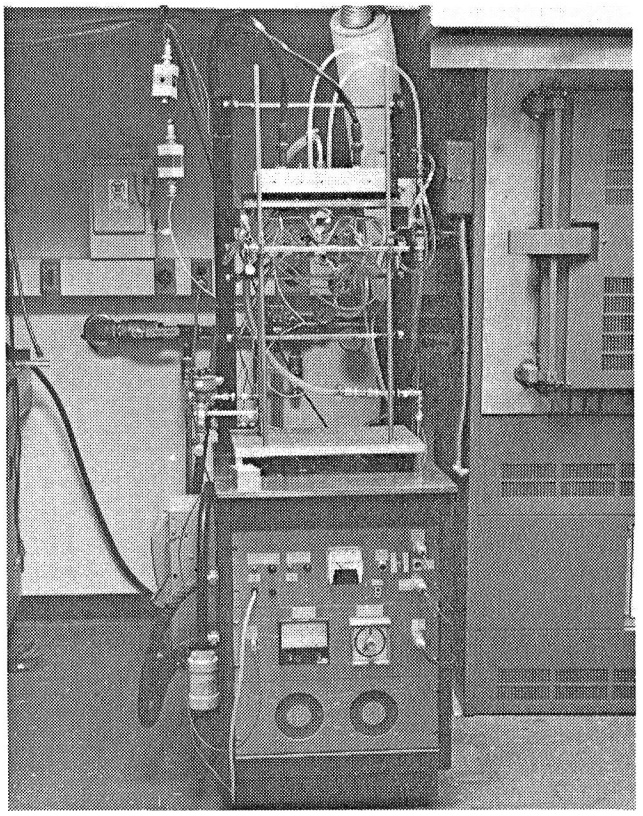

Figure 6.0-5 Overall View of Quartz Lamp Rig

The data from the calibrations is acquired with a microcomputer based data acquisition system. The system, shown in Figure 6.0-6, consists of a computer, scanner, voltmeter, disk storage and a printer. The computer controls the lamp assembly and cooling air and automatically acquires the data in a prescribed sequence. The data at each calibration point is output to the printer and is also stored on the disk for later data analysis and plotting.

Figure 6.0-6 Data Acquisition System for the Quartz Lamp Facility

6.1 SENSOR CALIBRATIONS

In our initial attempts to calibrate the heat flux sensors fabricated into blade halves, we tried to calibrate the blade half with impingement cooling on the back of the sensor. It was found that the calibration data obtained with impingement cooling was not repeatable between calibration runs. Subsequent investigation revealed that the sensor output was extremely dependent on the relative positioning of the blade half and the cooling nozzle. This dependency is believed to be due to both the curvature of the blade wall and the internal structure of the blade protruding off the rear face. Slight changes in the angle of incidence of the cooling air produced large changes in the thermal profile of the airfoil wall. As a result of this testing, it was determined that valid calibration data could be obtained only by assembly of the blades and cooling the airfoil by passing air through the internal coolant passages.

For calibration purposes, the blade halves were joined together by tack welding thin metal straps at numerous locations. This method of attachment makes it possible to easily separate the blade halves to inspect or repair the sensors. The cooling air is fed to the blades through the root section, passes through the internal passages of the blade and is exhausted through the trailing edge slot. The blade was coated with "Zynolyte 1000F Hi-Temp"[2] black paint to provide a constant known emittance of 0.89 for calibration.

The calibrations were conducted under two sets of conditions; varying incident heat load at a constant sensor temperature and varying incident heat load at constant blade coolant flow. The heat flux transmitted through the airfoil wall was calculated by determining the heat absorbed and subtracting the heat losses from the front face by convection and reradiation. The absorbed heat flux is equal to the incident heat flux as measured by the reference sensor, corrected to the test sensor location, times the emittance of the airfoil surface. The convective loss is equal to the convection heat transfer coefficient as measured with the convective probe times the temperature differential between the sensor surface and the ambient air temperature. The reradiation loss is the emittance times the difference in the fourth powers of the sensor surface temperature and the sink temperature. The sink temperature was experimentally determined as 394K for this calculation. The calibration data was then normalized to a constant sensor temperature of 1150K. This normalization analytically accounts for the changes in thermal conductivity with temperature and the changes in thermoelectric output with temperature. A detailed error analysis of this calibration procedure was presented in Reference 1 and will not be reported here.

Four blades were fabricated with two heat flux sensors in each blade. Two blades were instrumented with embedded thermocouples and two blades were instrumented with Gardon gauge sensors. The calibration results on these sensors are presented in Figures 6.1-1 to 6.1-8.

---

[2]Zynolite Products Company
15700 South Avalon
Compton, CA 90224

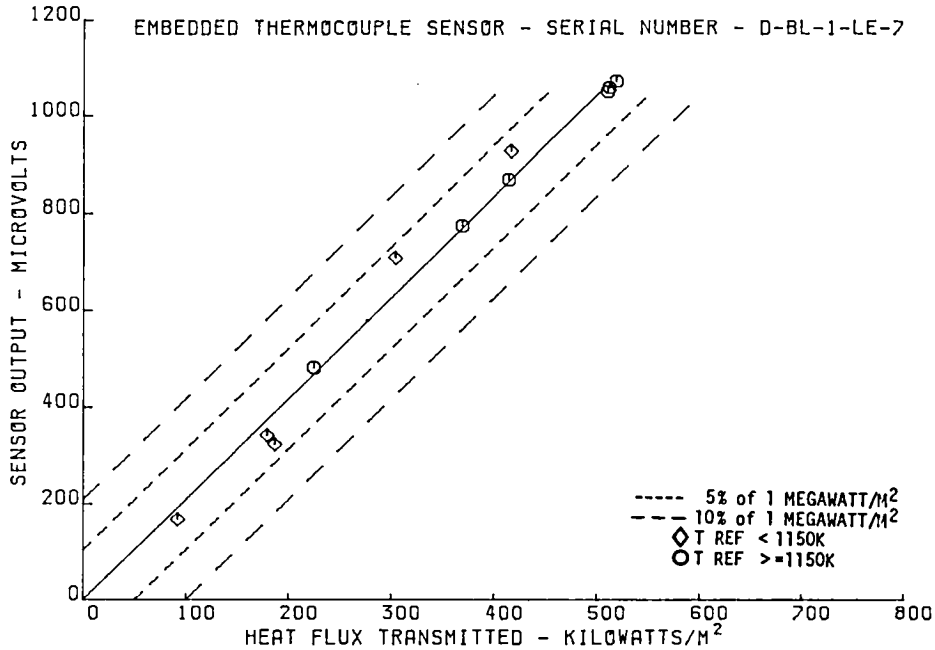

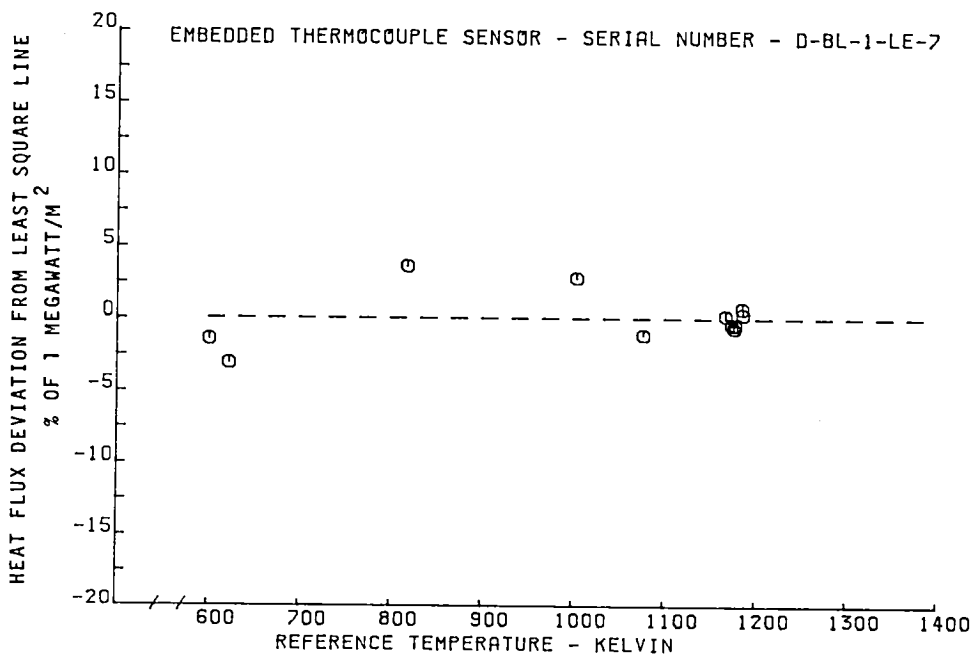

Figure 6.1-1 Calibration Data for Embedded Thermocouple Sensor

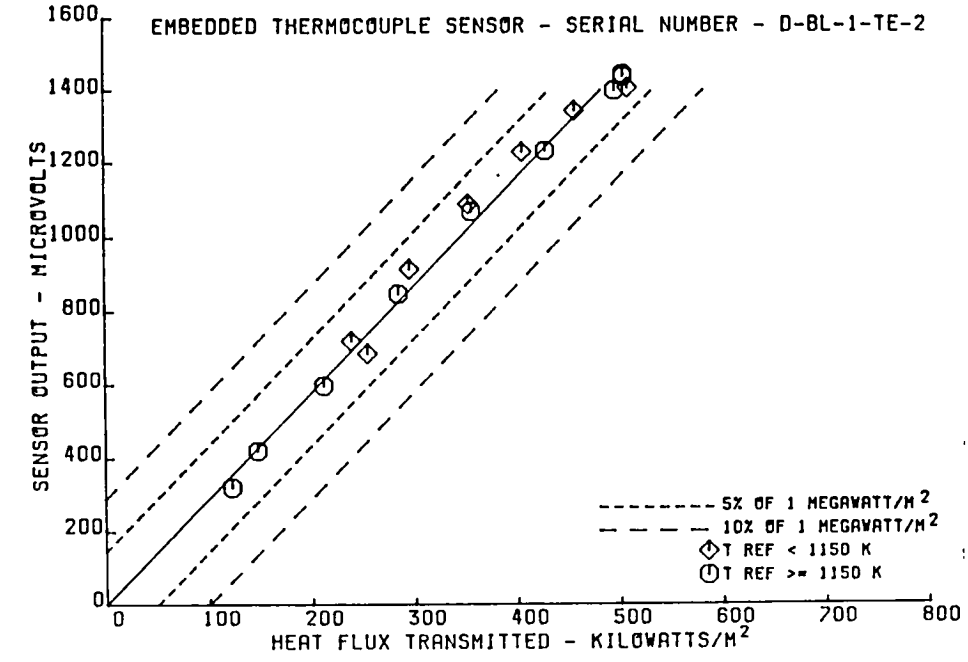

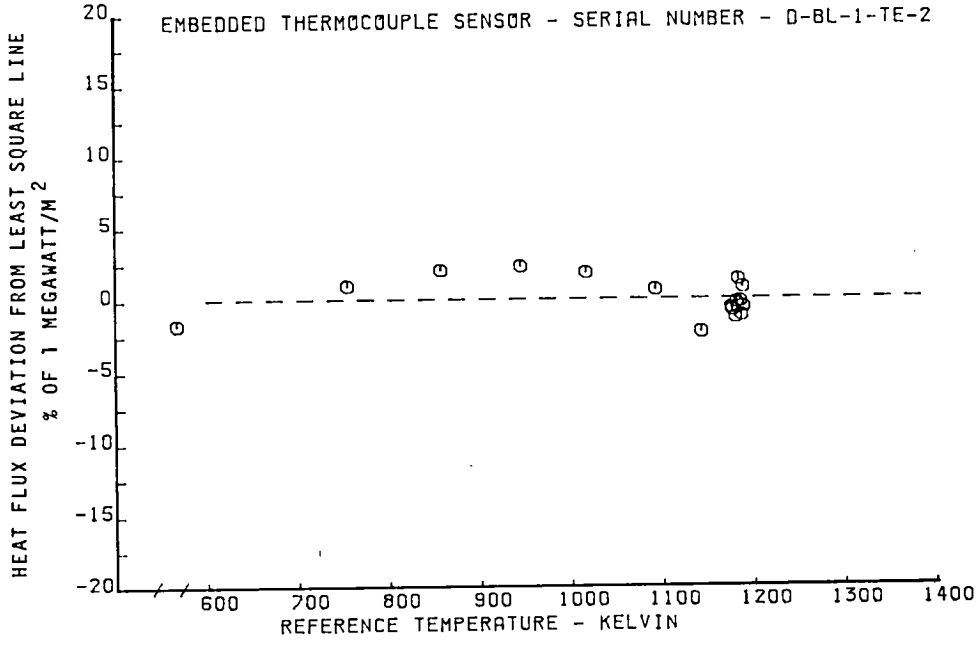

Figure 6.1-2 Calibration Data for Embedded Thermocouple Sensor

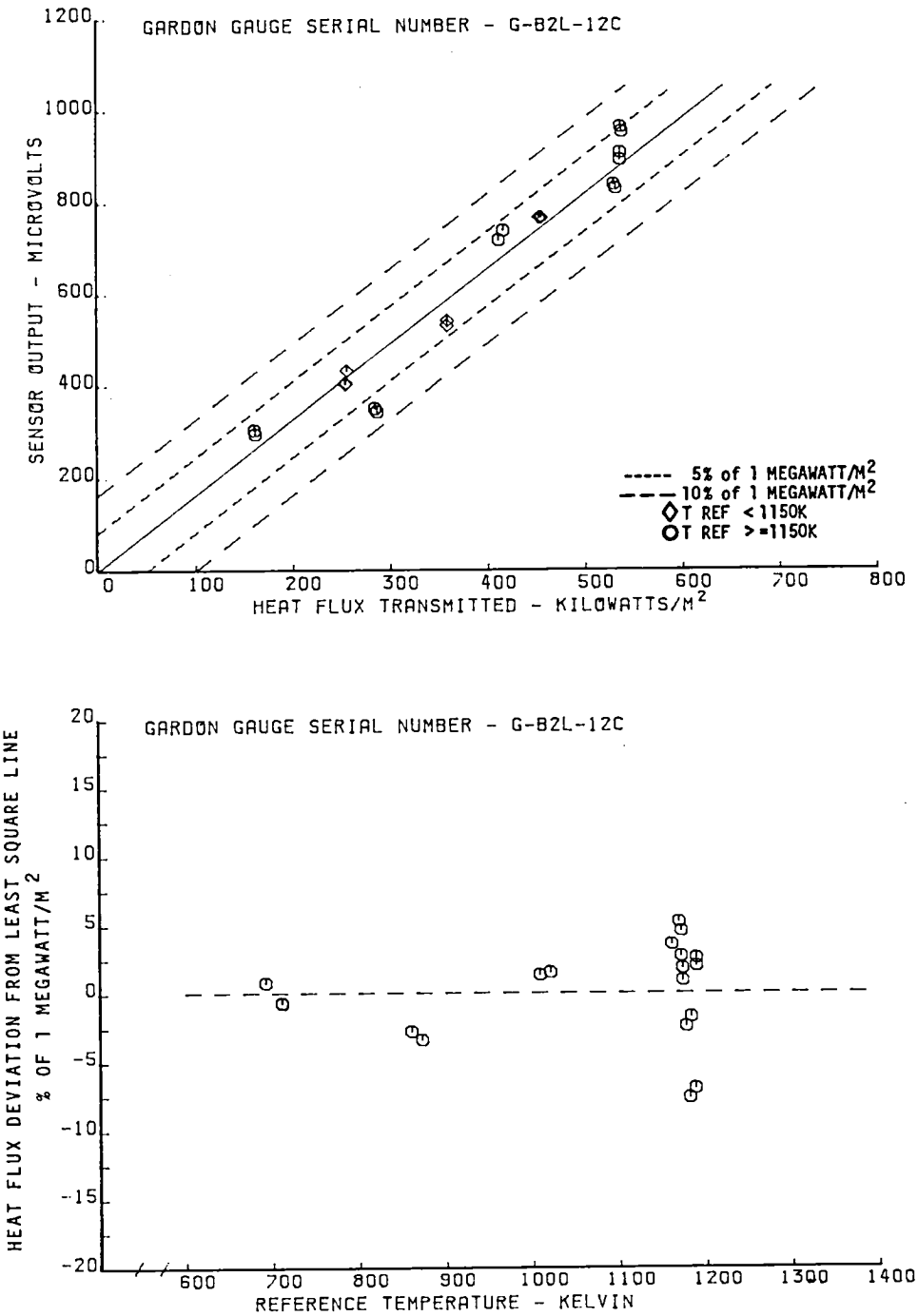

Figure 6.1-3 Calibration Data for Gardon Gauge Sensor

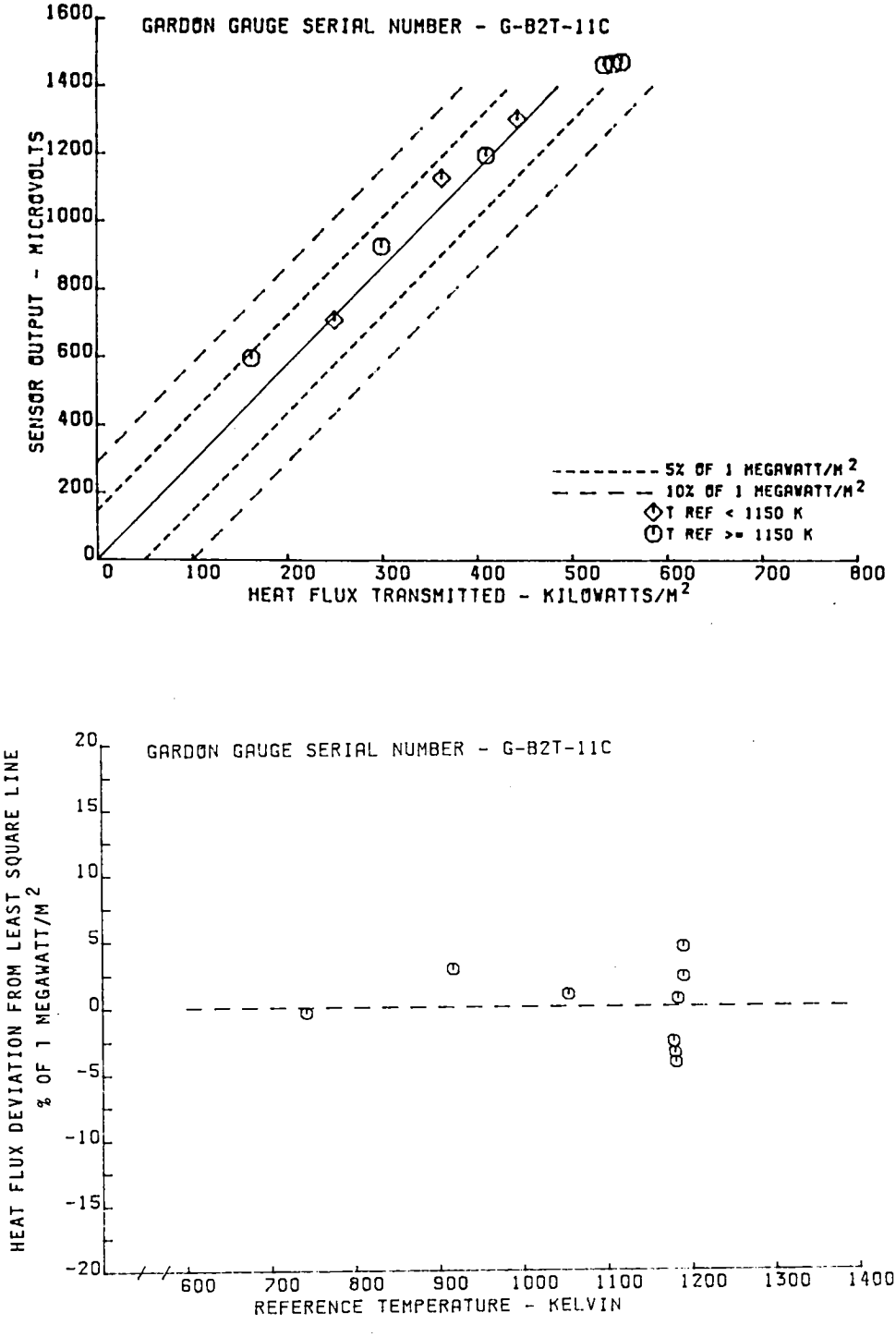

Figure 6.1-4 Calibration Data for Gardon Gauge Sensor

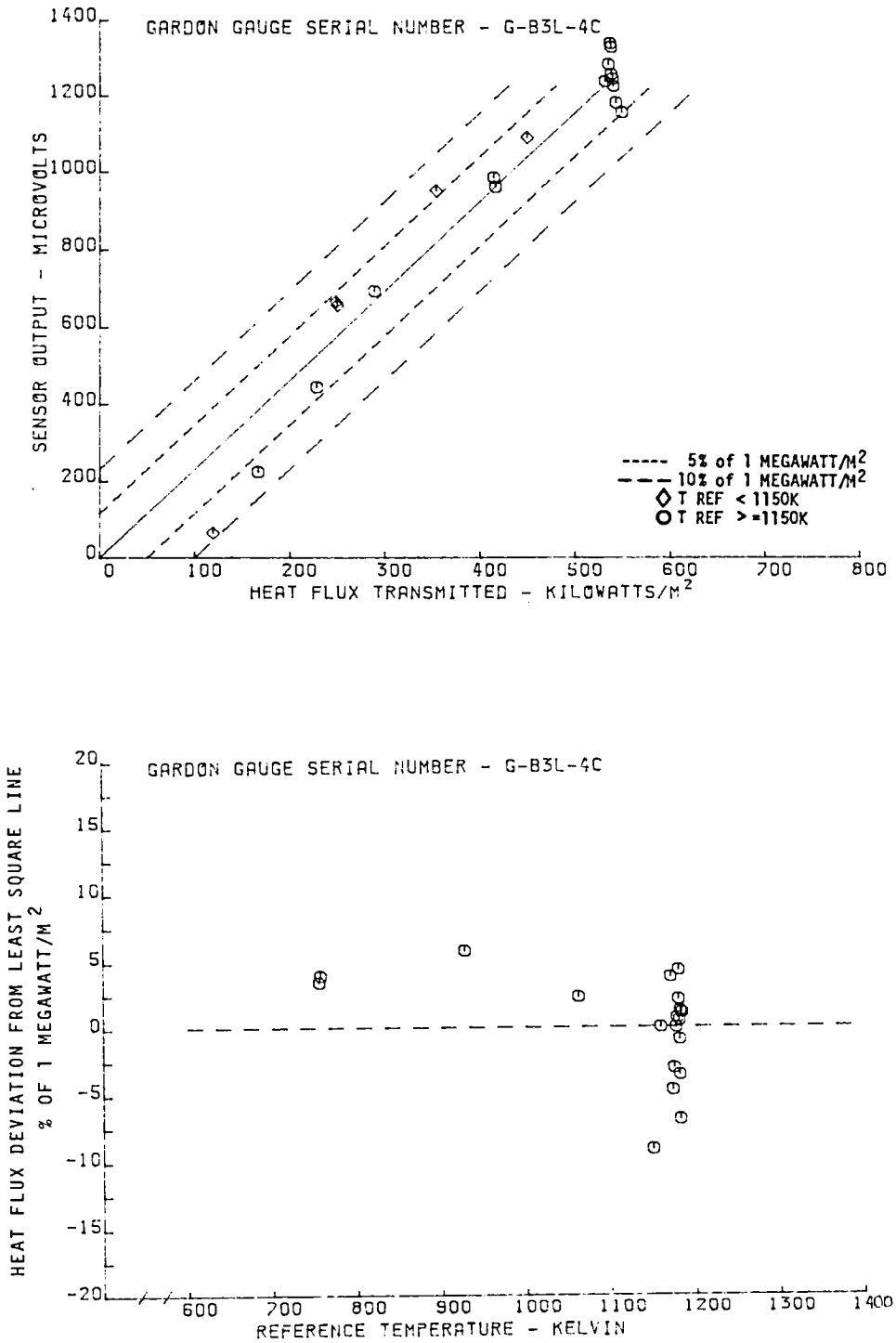

Figure 6.1-5 Calibration Data for Gardon Gauge Sensor

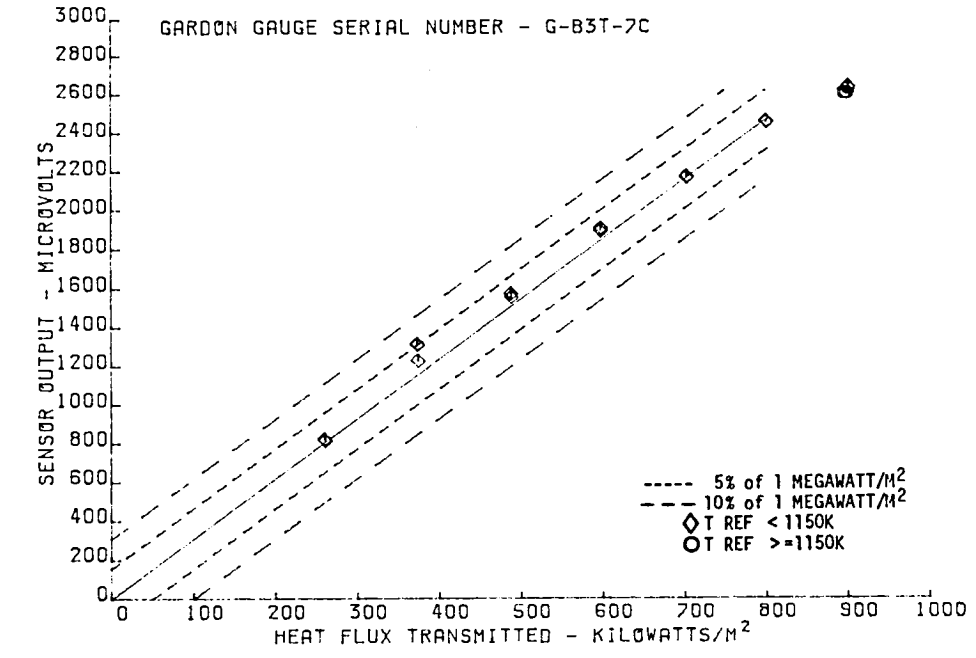

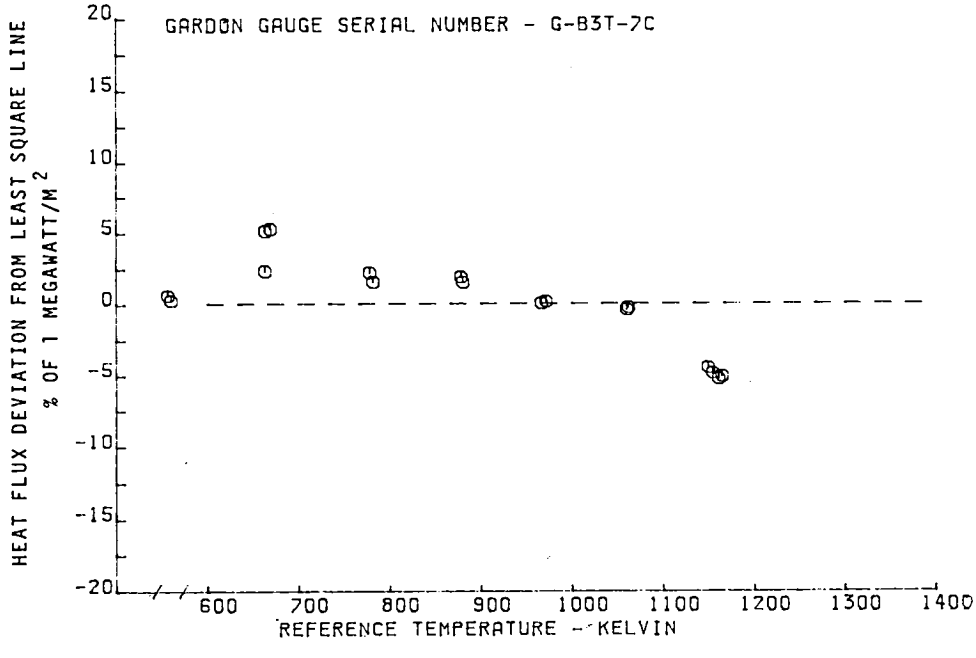

Figure 6.1-6 Calibration Data for Gardon Gauge Sensor

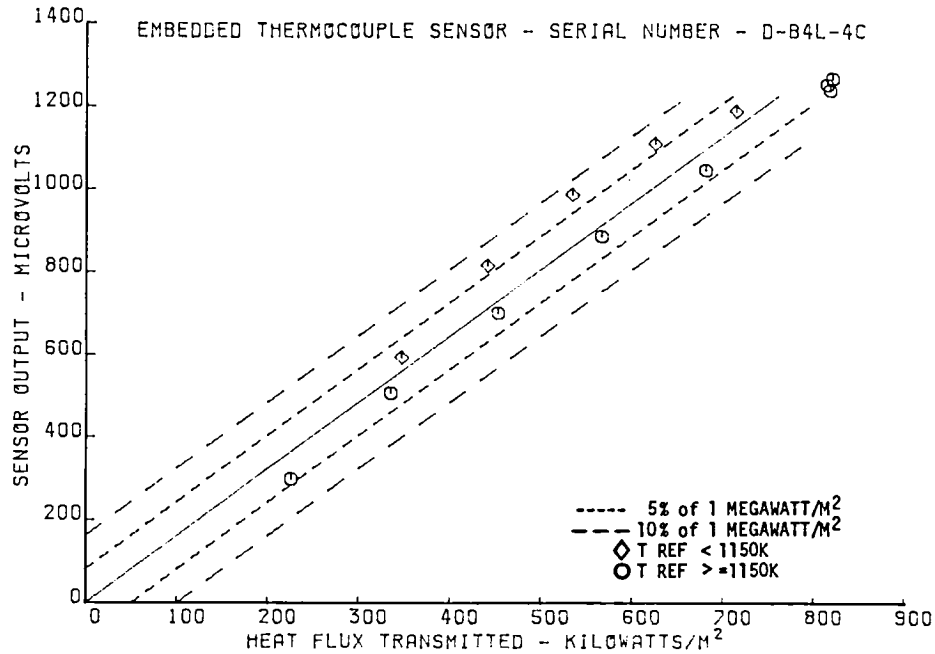

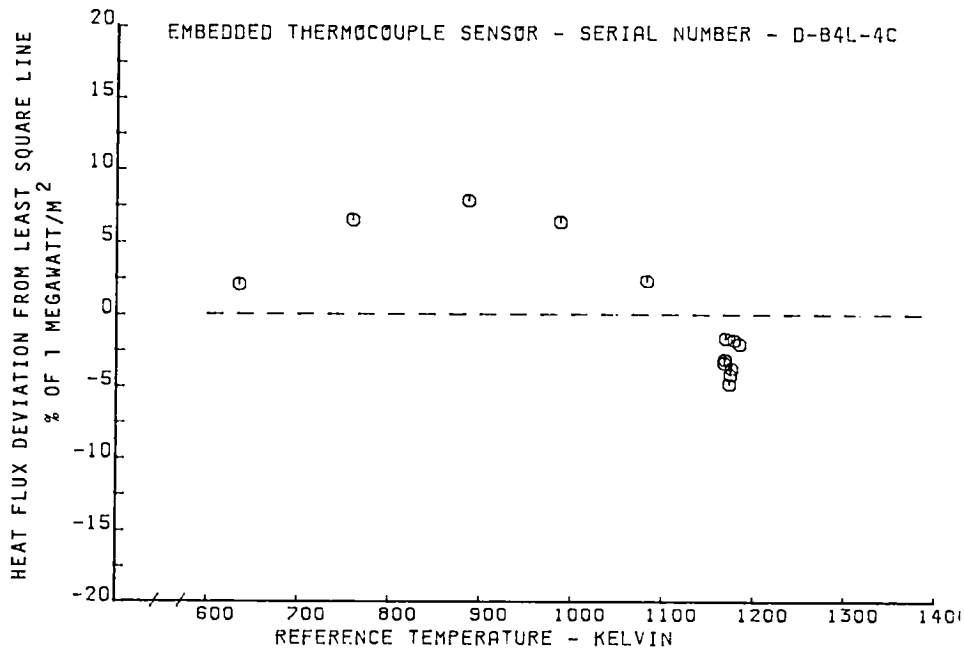

Figure 6.1-7 Calibration Data for Embedded Thermocouple Sensor

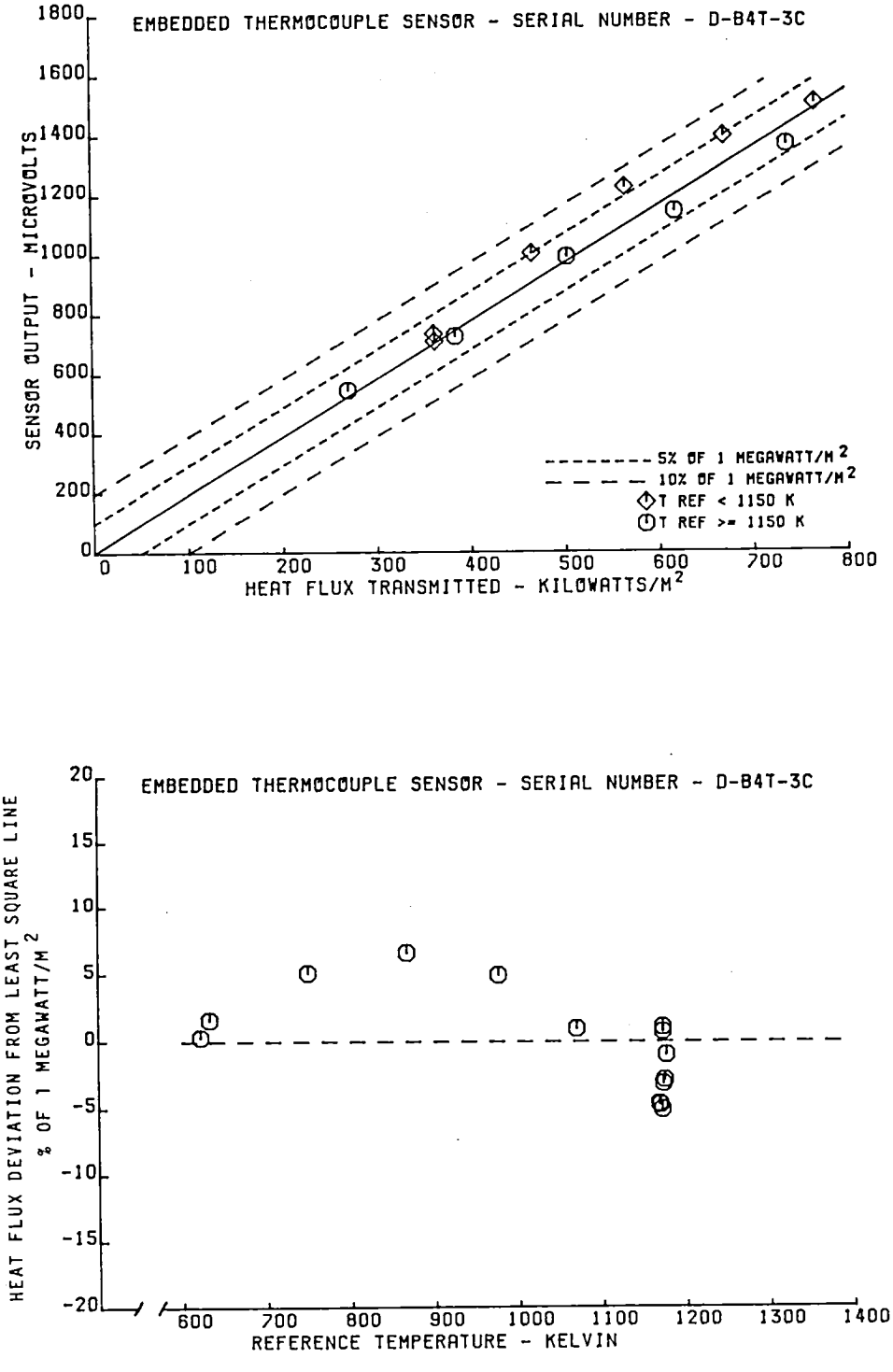

Figure 6.1-8 Calibration Data for Embedded Thermocouple Sensor

When the data was normalized it was found that the calibration data from varying temperatures does not always collapse perfectly onto the data from constant temperature. This is an indication that there is non-one-directional flow through the sensors as a result of temperature gradients across the sensor area. These gradients arise from the non-uniform cooling created by the cooling passages internal to the blades. During the calibration testing, it was also noted that at certain coolant flows the output of the sensor changed dramatically with small changes in coolant flow. This effect was traced to a separation of the blade halves by internal pressurization. The halves were not rigidly attached together and tended to open when sufficient internal pressure was achieved. When the blades opened, cooling air spilled over the internal ribs between cooling passages. This in turn caused a change in the cooling pattern and in the thermal profile on the blade surface. The change in temperature profile resulted in a change in the amount of non-one-directional flow and affected sensor output. This effect is most apparent in the sensors located in the center cooling cavity and as expected had very little effect on the sensors mounted in the trailing edge cavity.

To confirm this effect, a series of thermographic tests were run in front of the quartz lamp bank on a pair of blades, one firmly brazed together, and the other held together with tack welded strips. The results of those tests are shown in Figure 6.1-9. The lamp was set at a constant output, and data was taken at three flow levels for each blade. The coolant flow for the brazed blade passed through the interval coolant passages and exited through the blade trailing edge. The resistance welded blade had the same flow passages but allowed leakage of some coolant air through the blade tip and leading edge. This resulted in a difference in thermal pattern between the two blades. The tack welded blade ran cooler at the leading edge due to leakage of cooling air through that area. The trailing edge of the tack welded blade ran hotter since less coolant air passed through that area due to the leakage from the leading edge and tip. Data could not be taken under actual calibration conditions due to lack of optical access to the rig. The data above, however, clearly shows that calibration techniques for heat flux sensors in airfoils must consider the effect of non-one-dimensional heat flow if optimum accuracy is to be obtained.

6.2 THERMAL CYCLING TESTS

The heat flux sensors used on turbine airfoils may be exposed to several thermal cycles. These cycles may result either from repeated start and shutdown cycles or as the result of engine or rig power lever movements. Tests were, therefore, conducted to evaluate the affect of thermal cycling on the survivability of the heat flux sensors. These tests were conducted in the same quartz lamp test facility used for sensor calibration. A thermal cycle consisted of turning on the quartz lamp bank and rapidly heating the sensor to ~1200K with a transmitted heat flux of ~570 kW/m^2. This condition was held for 2 minutes. The heat source was then shut down and the sensor was rapidly cooled to near room temperature for 4 minutes. This process was repeated for a total of 50 cycles. Data were automatically acquired twice during each cycle, once 1.8 minutes after the quartz lamp bank was turned on, and again 3.5 minutes after it was turned off.

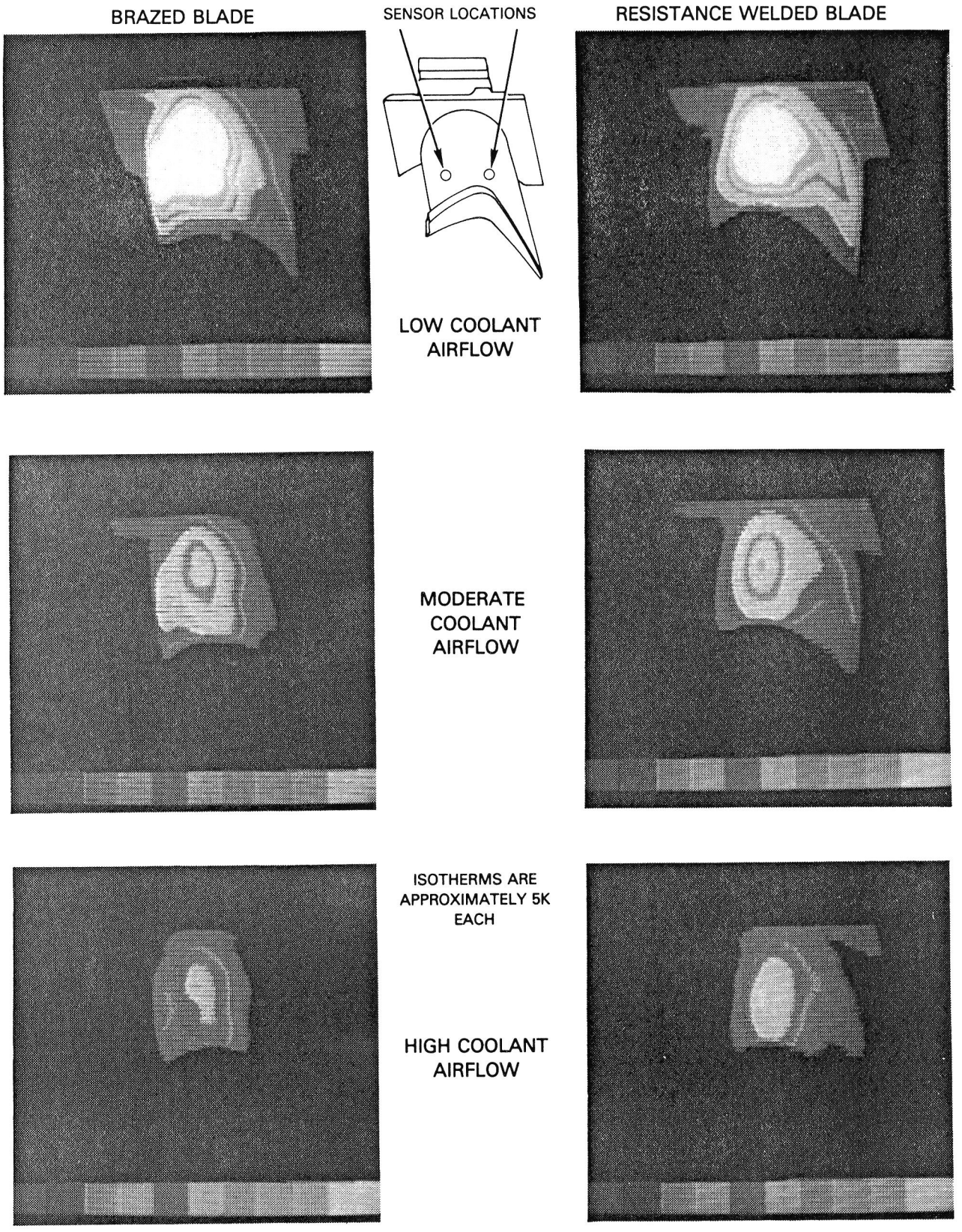

Figure 6.1-9 Thermographic Test Results for Turbine Blades

One sensor of each type was subjected to the thermal cycle tests, the leading edge embedded thermocouple sensor on blade one, and the trailing edge Gardon Gauge sensor on blade two. Both sensors survived through the full fifty cycles of the tests. Figure 6.2-1 shows a comparison of the pre-test and post-test calibration results for the embedded thermocouple sensor. Figure 6.2-2 shows the sensor sensitivity (output per unit heat flux transmitted) as a function of cycle number. This same information is shown for the Gardon Gauge sensor in Figures 6.2-3 and 6.2-4. It can be seen that while there is some cycle to cycle variability, both sensors show good agreement between the pre-test and post-test calibrations. This data combined with a visual inspection indicates that the thermal cycling produces no serious degradation of either the embedded thermocouple or Gardon Gauge sensors.

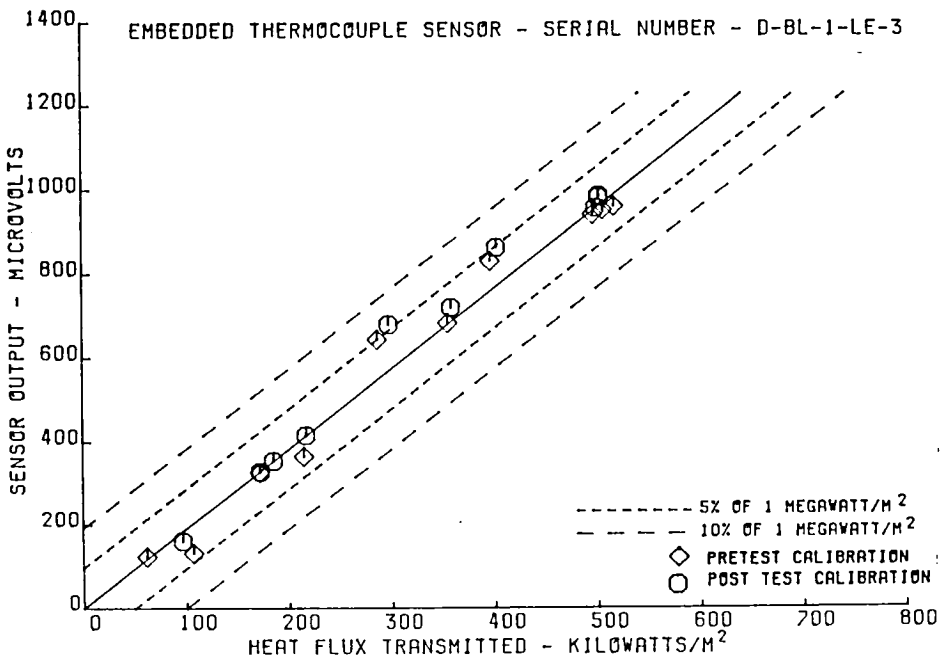

Figure 6.2-1 Pre- and Post-Thermal Cycle Test Calibration Data for the Embedded Thermocouple Sensor

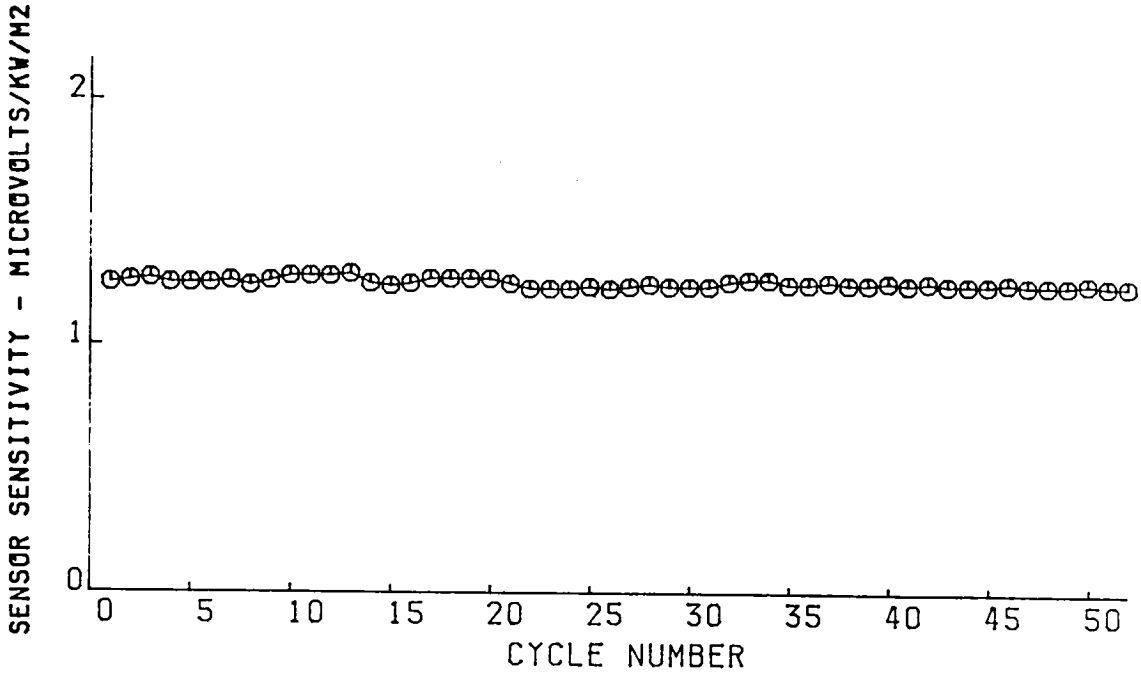

Figure 6.2-2 Sensitivity (output per unit heat flux transmitted) for the Embedded Thermocouple Sensor

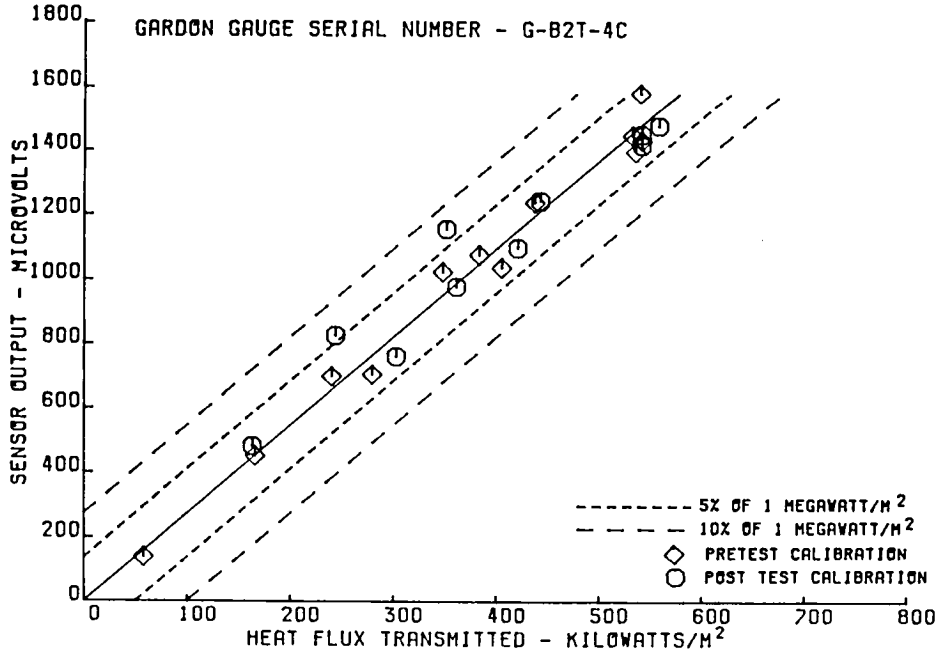

Figure 6.2-3 Pre- and Post-Thermal Cycle Test Calibration Data for the Gardon Gauge Sensor

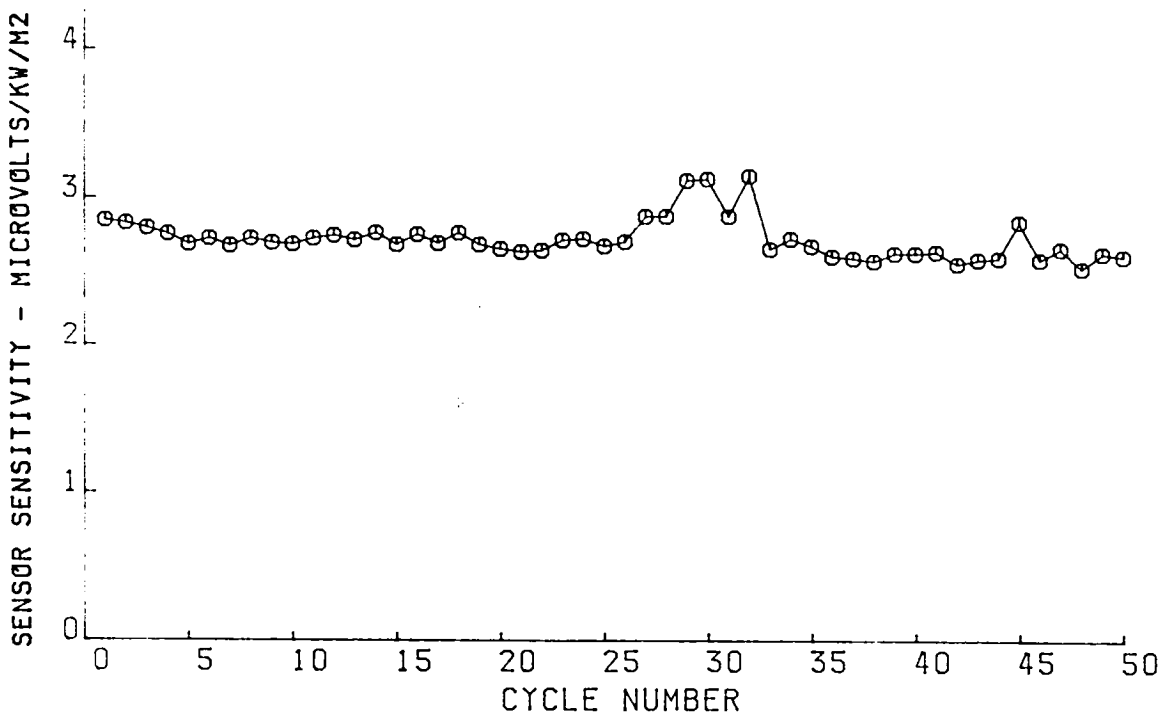

Figure 6.2-4 Sensitivity (output per unit heat flux transmitted) for the Gardon Gauge Sensor

6.3 THERMAL SOAK TESTS

In addition to thermal cycling, sensors suitable for use on hot section airfoils must be capable of surviving for extended periods of time at elevated temperatures. Tests were conducted to evaluate the affect of high temperature thermal aging on the survivability and durability of the sensors. These tests were conducted in the quartz lamp test facility. After the turbine blade sensor was installed in the test facility, the quartz lamp was turned on and the sensor ramped to a temperature of ~1200K with a transmitted heat flux of ~570 kW/m^2. The sensor was maintained under these conditions for a period of 10 hours with the data being automatically acquired every 1/4 hour. At the end of the 10 hour test, the sensor was rapidly cooled to room temperature.

One sensor of each type was subjected to the thermal soak test program. These were the same two sensors that had previously survived the thermal cycle testing. Both sensors survived the full ten hour test. Figure 6.3-1 shows a comparison of the pre-test and post-test calibration results for the embedded thermocouple sensor and Figure 6.3-2 shows the sensor sensitivity as a function of time throughout the aging test. This same information is shown for the Gardon Gauge sensor in Figures 6.3-3 and 6.3-4. It can be seen that while there is some scatter in the data, both sensors show good agreement between the pre-test and post-test calibration as well as good stability throughout the test. This data combined with a post-test visual inspection indicates that the thermal aging produced no serious degradation of either the embedded thermocouple or Gardon Gauge sensor.

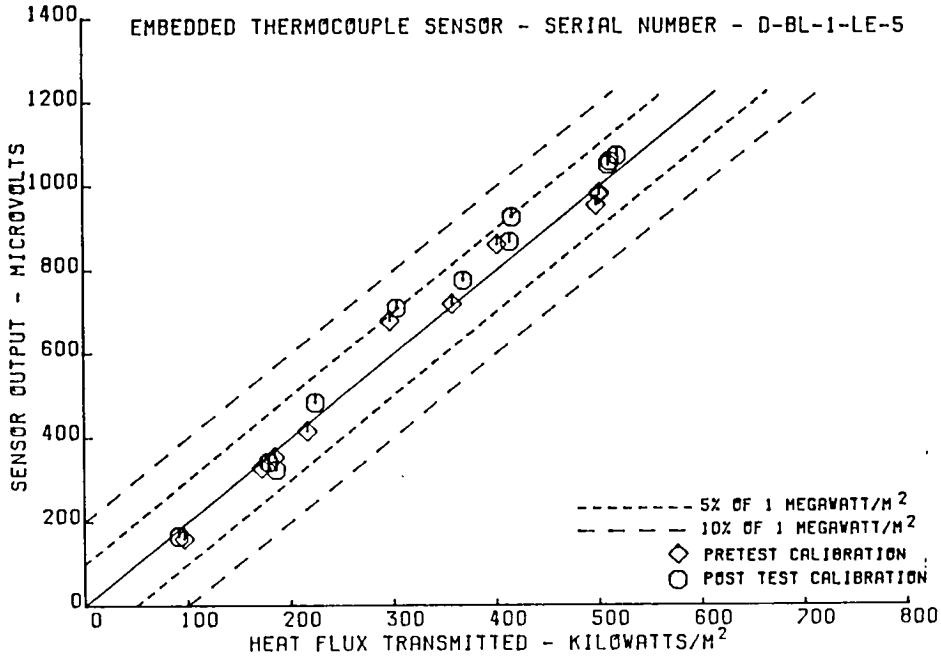

Figure 6.3-1 Pre- and Post-Thermal Soak Test Calibration Data for the Embedded Thermocouple Sensor

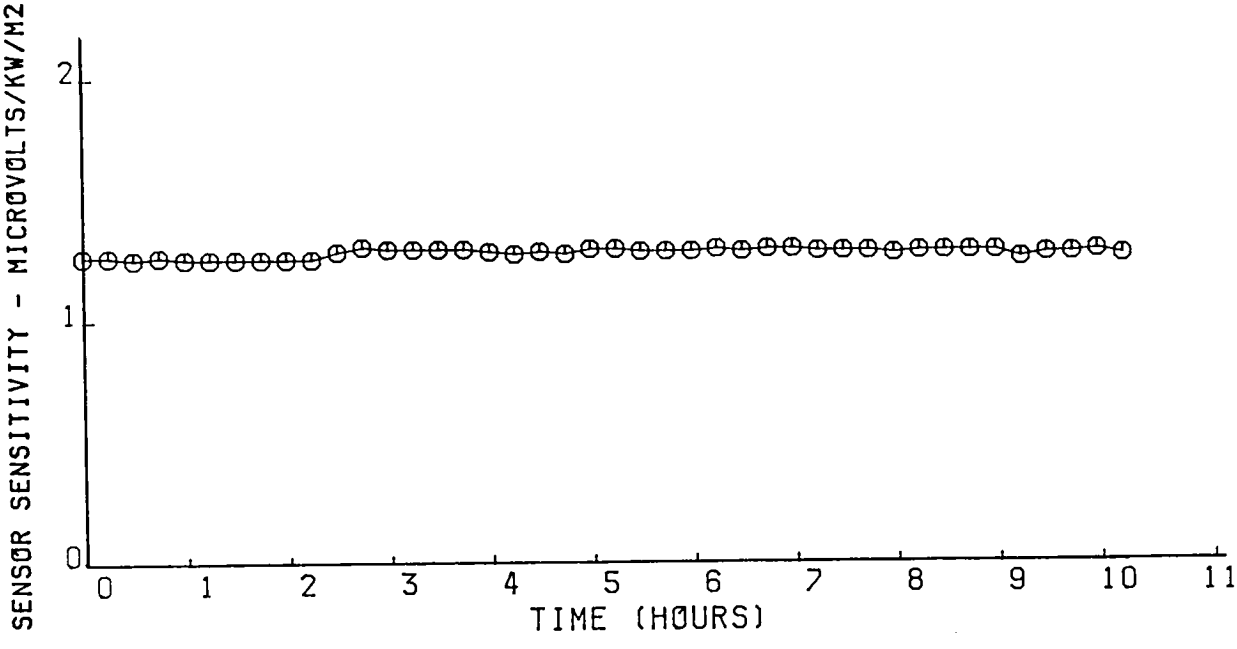

Figure 6.3-2 Sensitivity (output per unit heat flux transmitted) for the Embedded Thermocouple Sensor

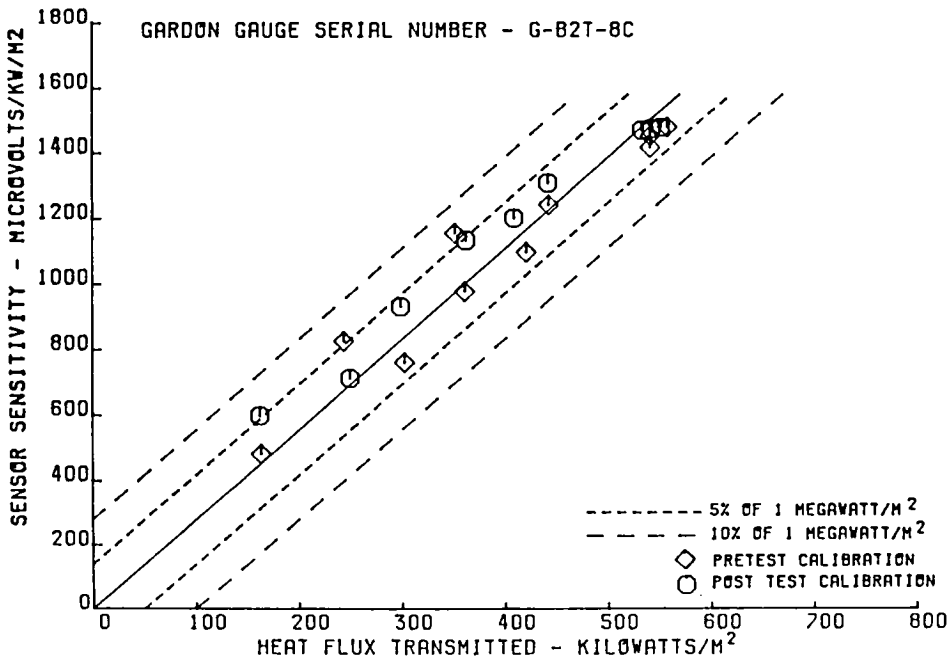

Figure 6.3-3 Pre- and Post-Thermal Soak Test Calibration Data for the Gardon Gauge Sensor

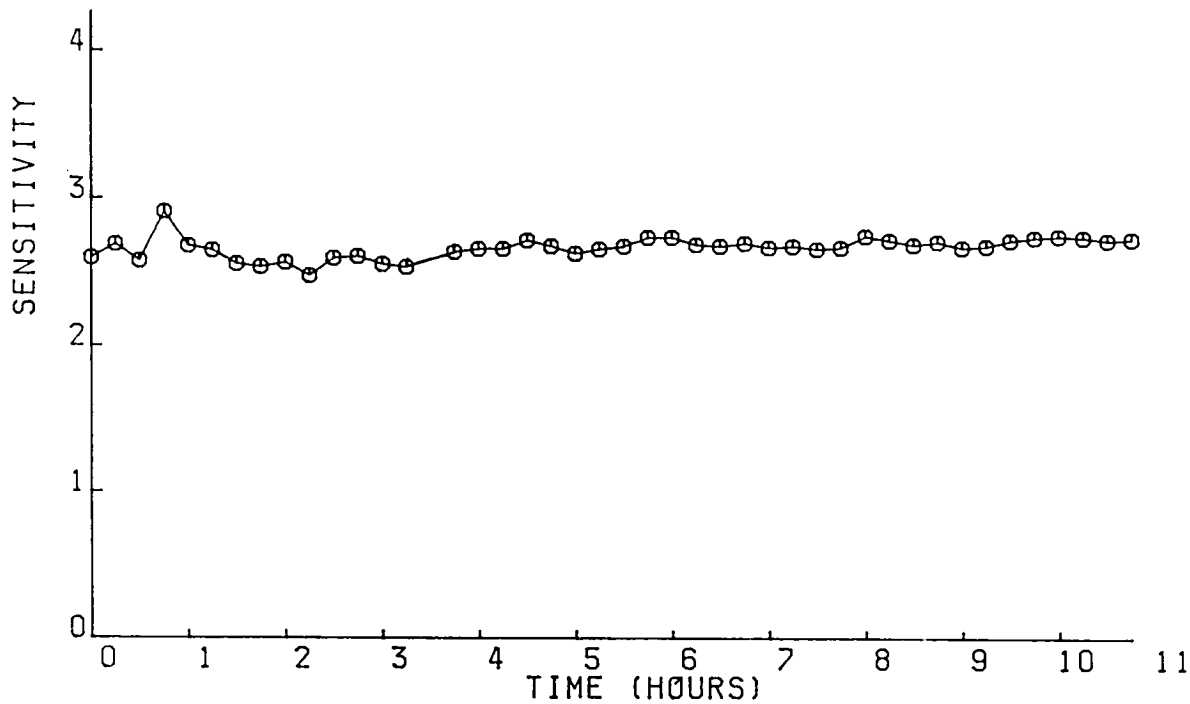

Figure 6.3-4 Sensitivity (output per unit heat flux transmitted) for the Gardon Gauge Sensor

6.4 SENSOR LEADWIRE FAULTS

During the course of the test program, leadwire problems were encountered with three sensors, all Gardon gauge sensors fabricated with three conductor swaged wire. The problem in each of the three sensors was an open leadwire. The first occurred prior to the initial calibration and was traced to an open in the Chromel leadwire internal to the blade but not in the sensor. This sensor was repaired by replacing the leadwire. The second sensor, also in a blade, had undergone numerous calibrations and had been subjected to 50 thermal cycles and a 10 hour thermal soak. The sensor was recalibrated after the tests and was operational and stable. The sensor then failed when undergoing further calibrations. The failure was traced to a break in the Alumel leadwire, at the sensor, where the wire exited the sheath. The situation was corrected by replacing the leadwire and rebuilding the sensor. The third sensor was one that had been installed in a vane for the High Pressure Facility. The Chromel lead to the sensor was found to be open before the initial calibration. The sensor was still operational although no reference temperature could be measured. The location of the open was not determined since to determine if the break was in the leadwire external or internal to the vane, the lead would have had to be cut, rendering the sensor totally useless. The retention of an operational sensor was considered to be more important than determining the exact location of the open. Repair of this sensor was impractical since the window used to install the instrumentation had been welded back in place. The number of open leadwires encountered is not considered to be excessive and represents a quality control problem with the leadwire rather than a flaw in the basic sensor design.

7.0 FABRICATION OF HARDWARE FOR DELIVERY

Four MAR-M-509 vanes from the NASA High Pressure Facility were instrumented with heat flux sensors as deliverable items. Two of the vanes have two Gardon Gauge sensors on the pressure side and two have two embedded thermocouple sensors on the pressure side. The vanes were fabricated and instrumented according to the techniques reported in Section 5.0 of this report. Figures 7.0-1 through 7.0-5 show a sequence of photographs tracing the installation of instrumentation for a vane with two embedded thermocouple sensors. A similar sequence for a vane with two Gardon Gauge sensor is shown in Figures 7.0-6 to 7.0-8. Figures 7.0-9 through 7.0-11 shows the closure of the instrumentation window. The heat flux sensors were then calibrated with the Quartz Lamp Calibration Facility described in Section 6.0 of this report. The vanes were calibrated at two coolant gas flow conditions: at 124.1 kPa inlet pressure with a flow of 103 kilograms per hour and at 48.3 kPa inlet pressure with a flow of 55 kilograms per hour. The data from these calibrations indicated that there were still difficulties with non-one-directional flow problems. It was also noted that the trailing edge section of the vane was running hotter than the rest of the vane surface. A ceramic shield was fabricated to slip over the trailing edge to keep from overtemperaturing this area. The installation of this shield altered the calibration values by a small amount by reducing the amount of non-one-directional flow. All reported calibrations were run with the trailing edge shield in place. The calibration data for these sensors are presented in Figures 7.0-12 through 7.0-19.

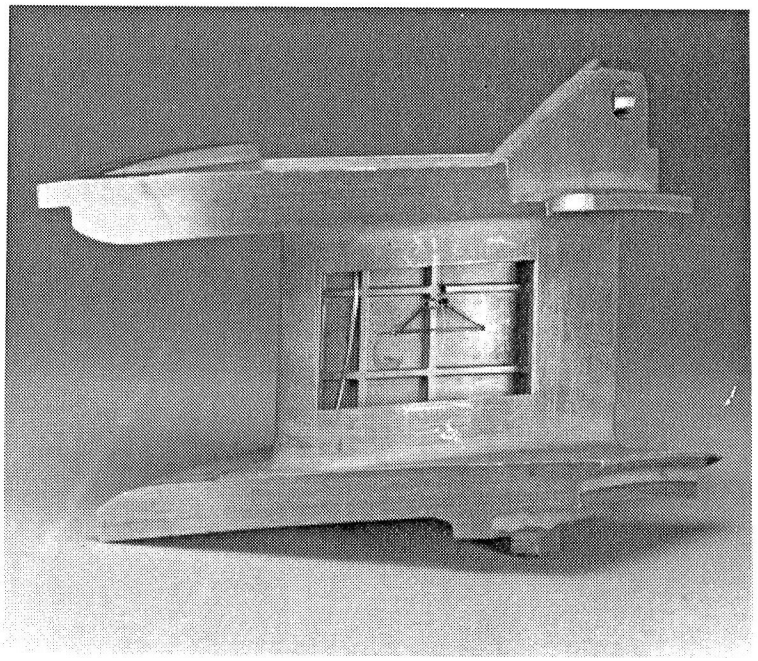

Figure 7.0-1 Vane with Instrumentation Window Removed and Slots Eloxed on Pressure Surface Inside Wall for Construction of Embedded Thermocouple Sensors

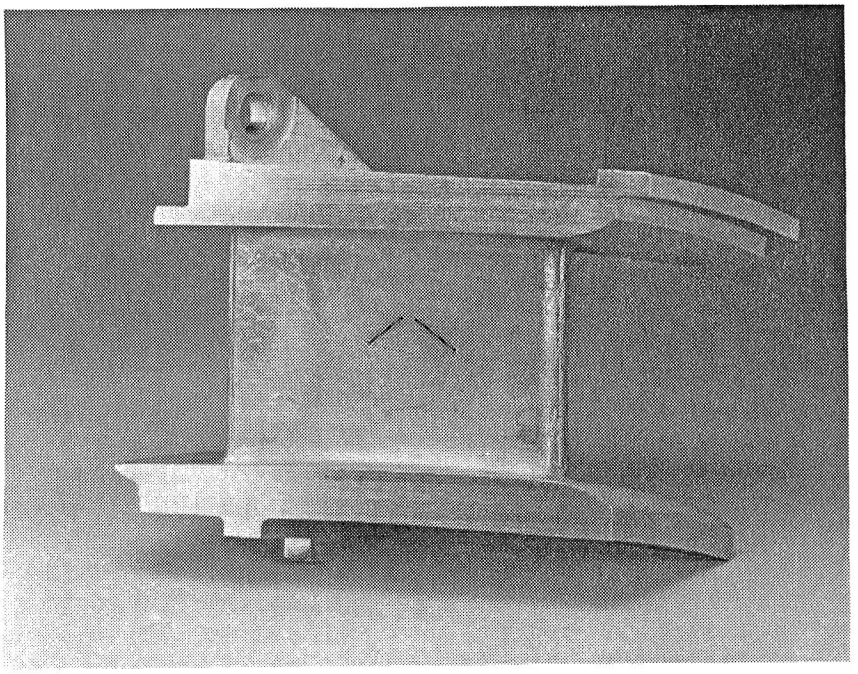

Figure 7.0-2 Vane with Slots Eloxed on Pressure Surface Hot Side Wall for Construction of Embedded Thermocouple Sensors

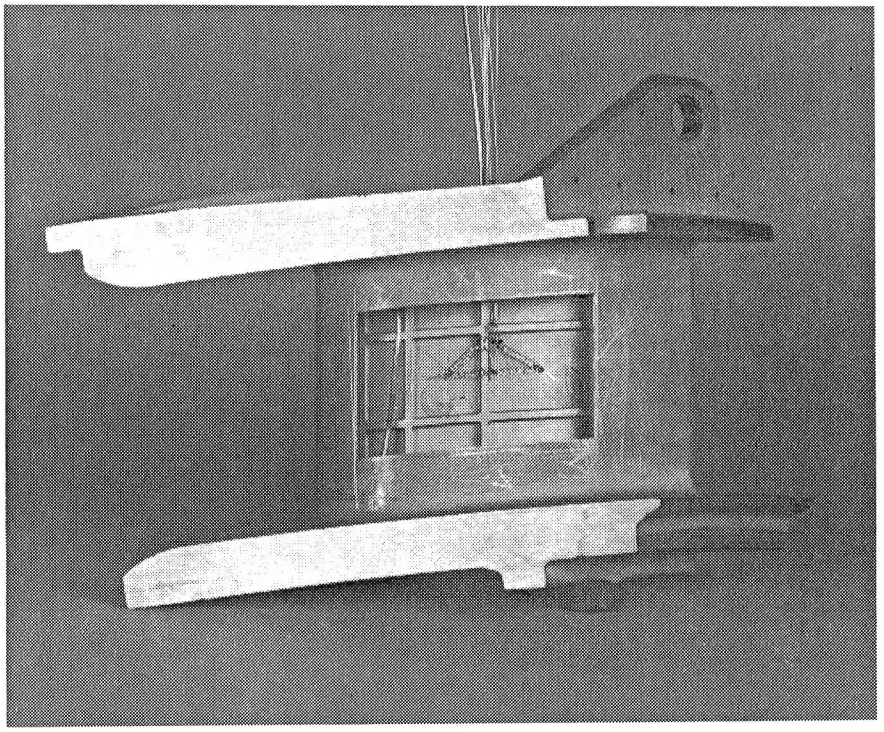

Figure 7.0-3 Vane with Internal Leads Installed for Embedded Thermocouple Sensors (surface not yet smoothed)

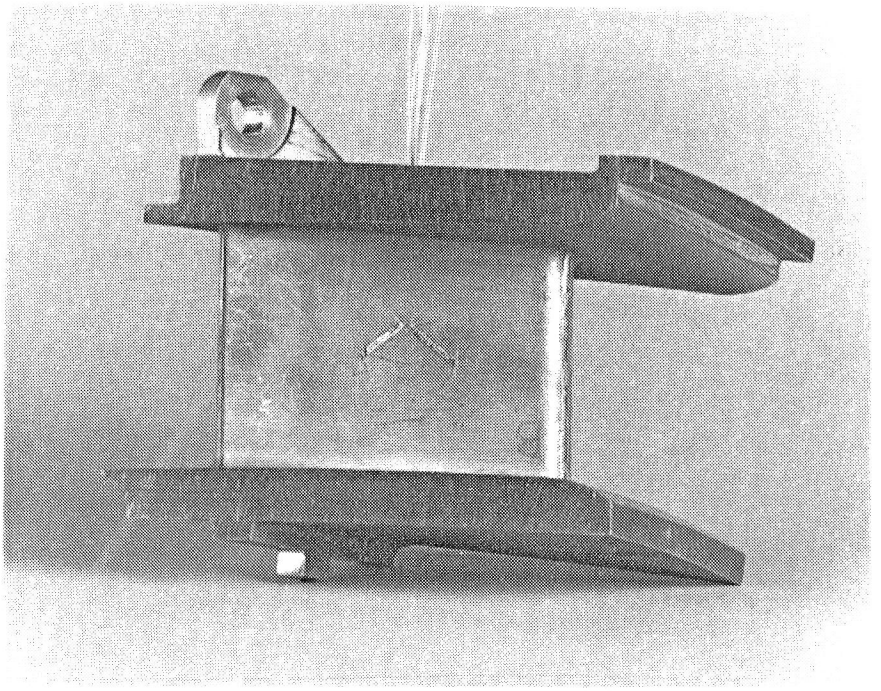

Figure 7.0-4 Vane with External Leads Installed on Pressure Surface Hot Side Wall for Embedded Thermocouple Sensors (surface not yet smoothed)

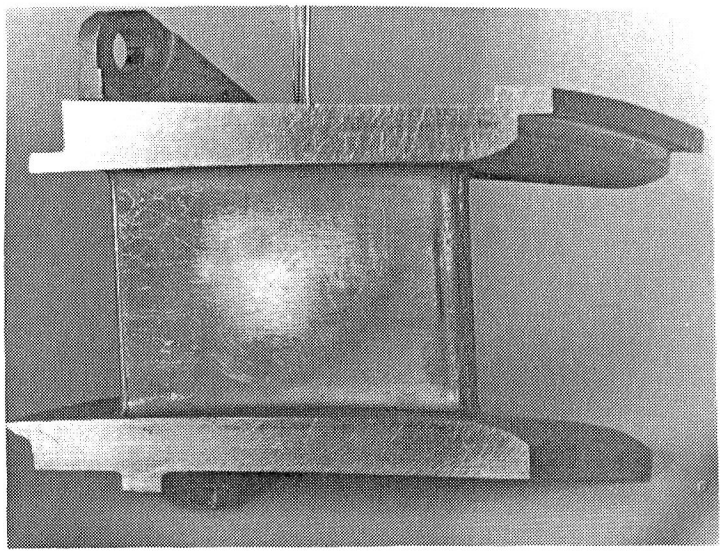

Figure 7.0-5 Vane with External Leads Installed on Pressure Surface Hot Wall for Embedded Thermocouple Sensor (after smoothing)

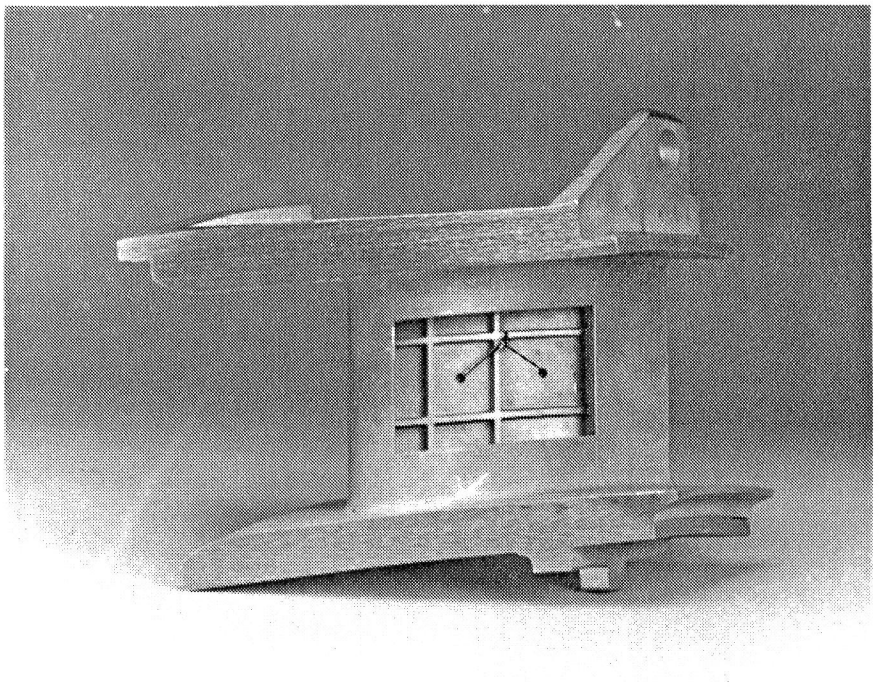

Figure 7.0-6 Vane with Instrumentation Window Removed and Eloxing Complete for Construction of Gardon Gauge Sensors

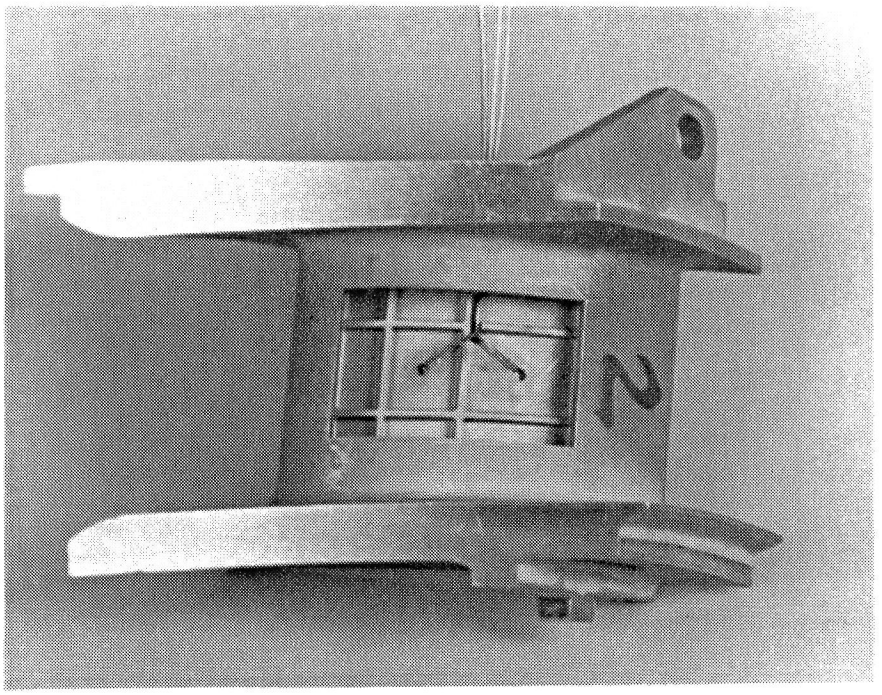

Figure 7.0-7 Vane with Leads Installed for Gardon Gauge Sensors (ceramic not yet installed and surface not yet smoothed)

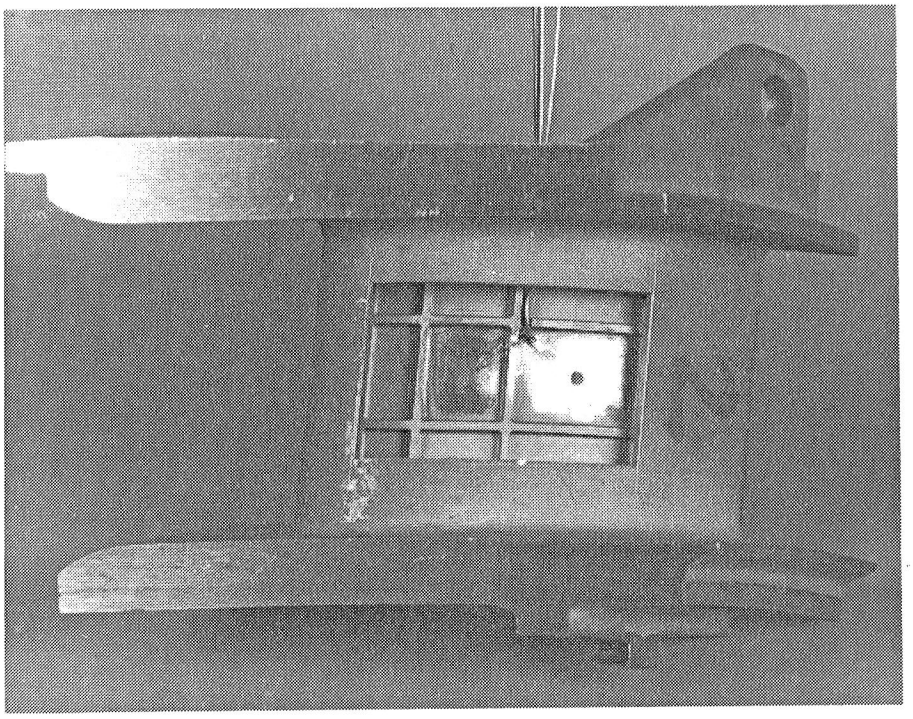

Figure 7.0-8 Vane with Completed Gardon Gauge Sensors

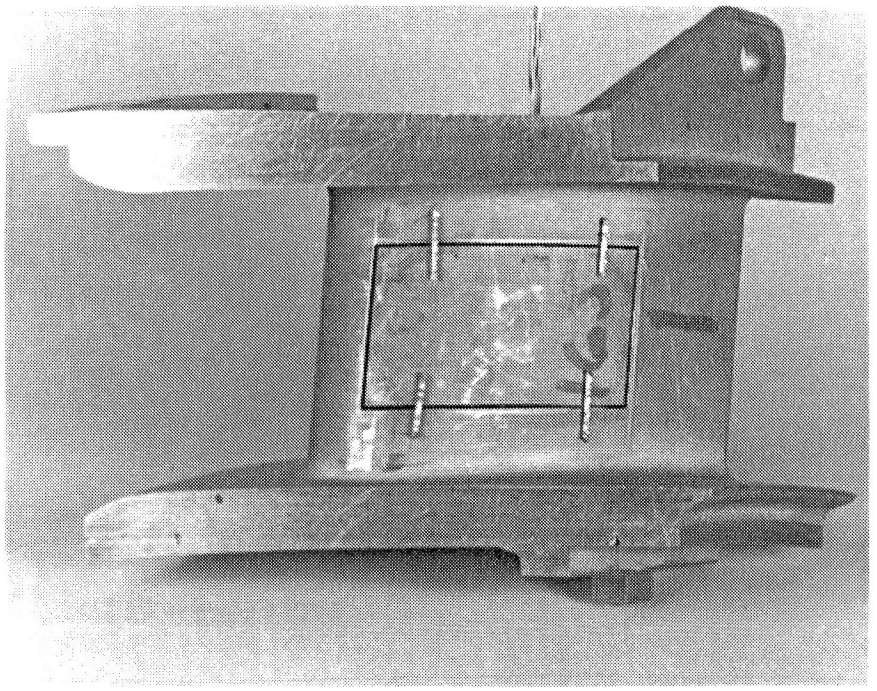

Figure 7.0-9 Vane with Window that was Removed for Instrumentation Held in Place by Tackwelded Strip for Rewelding into Vane

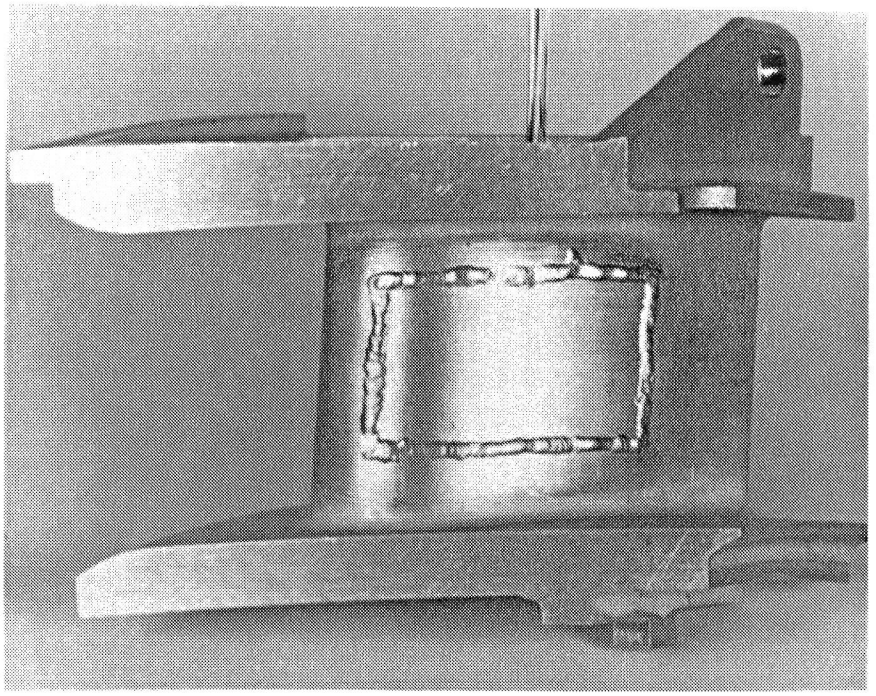

Figure 7.0-10 Vane with Instrumentation Window Rewelded into Place

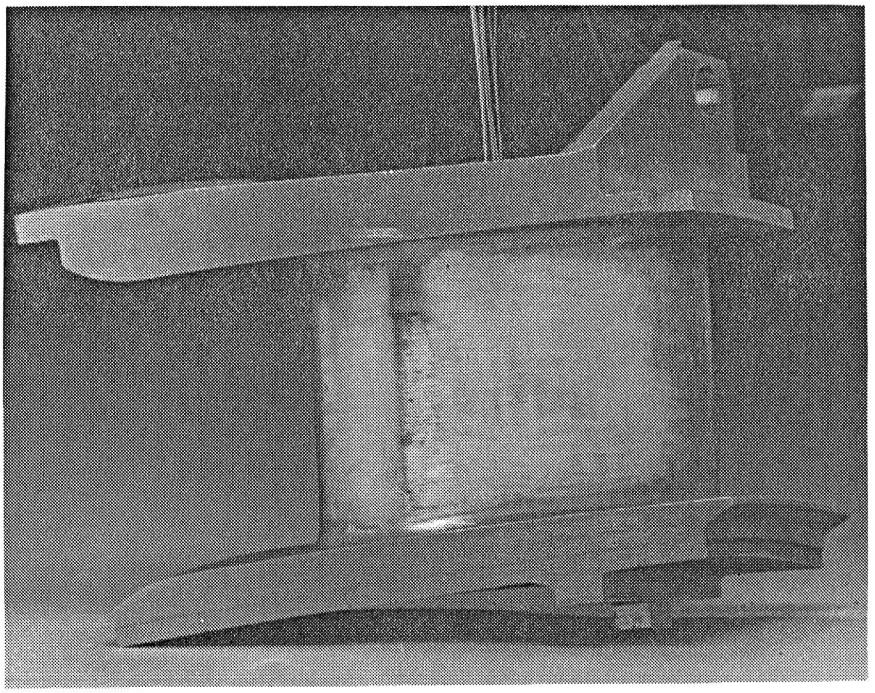

Figures 7.0-11 Completed Vane with Rewelded Instrumentation Window Smoothed

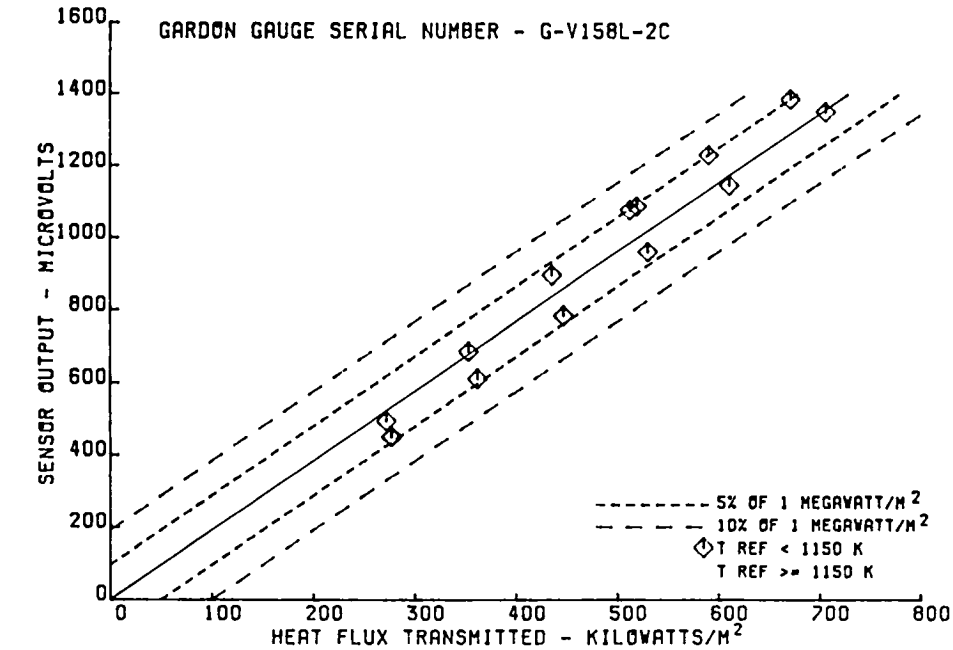

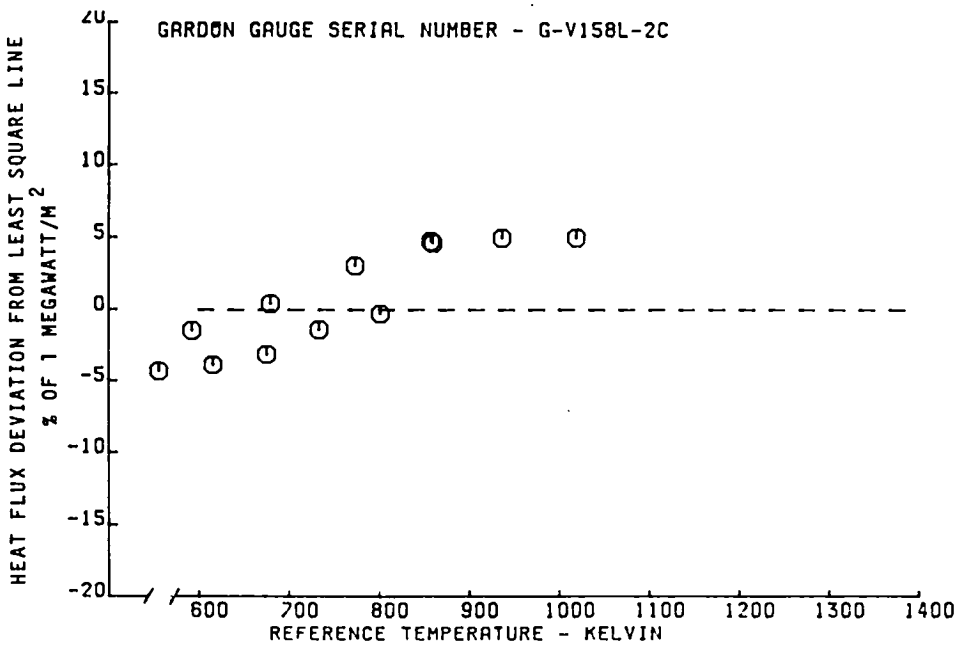

Figure 7.0-12 Calibration Data for Gardon Gauge Sensors Installed in Vanes for the High Pressure Facility

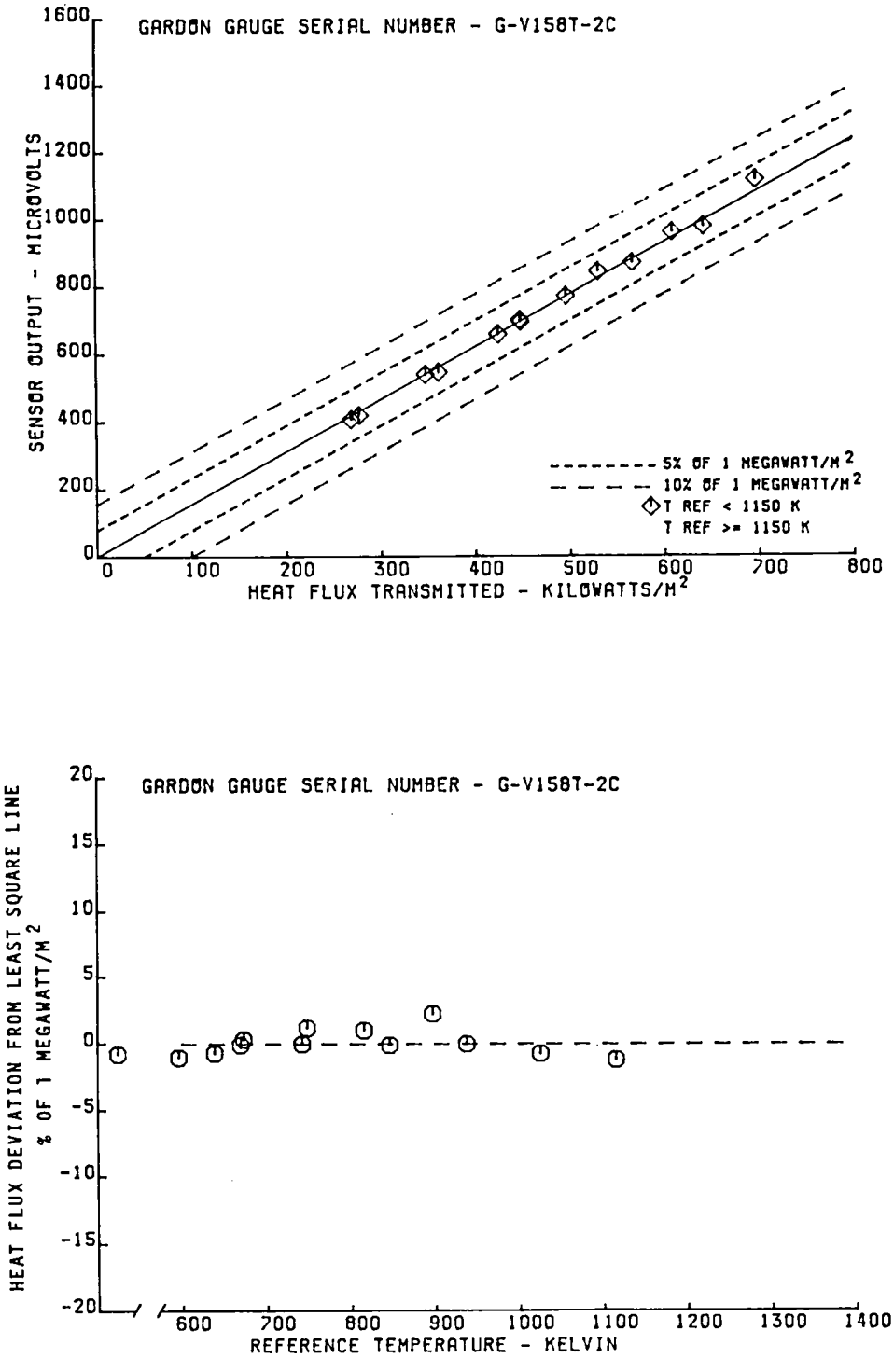

Figure 7.0-13 Calibration Data for Gardon Gauge Sensors Installed in Vanes for the High Pressure Facility

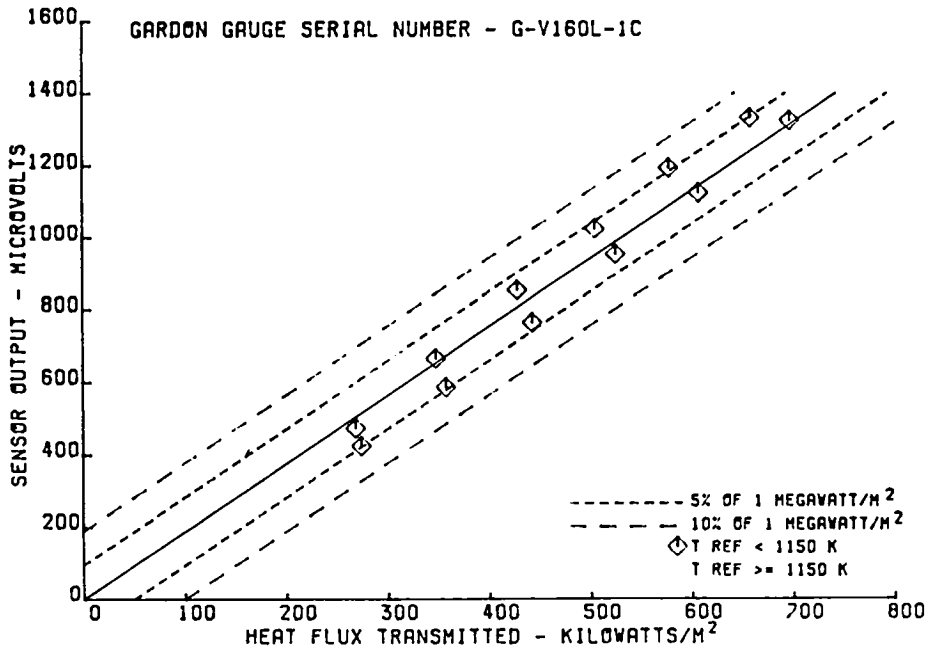

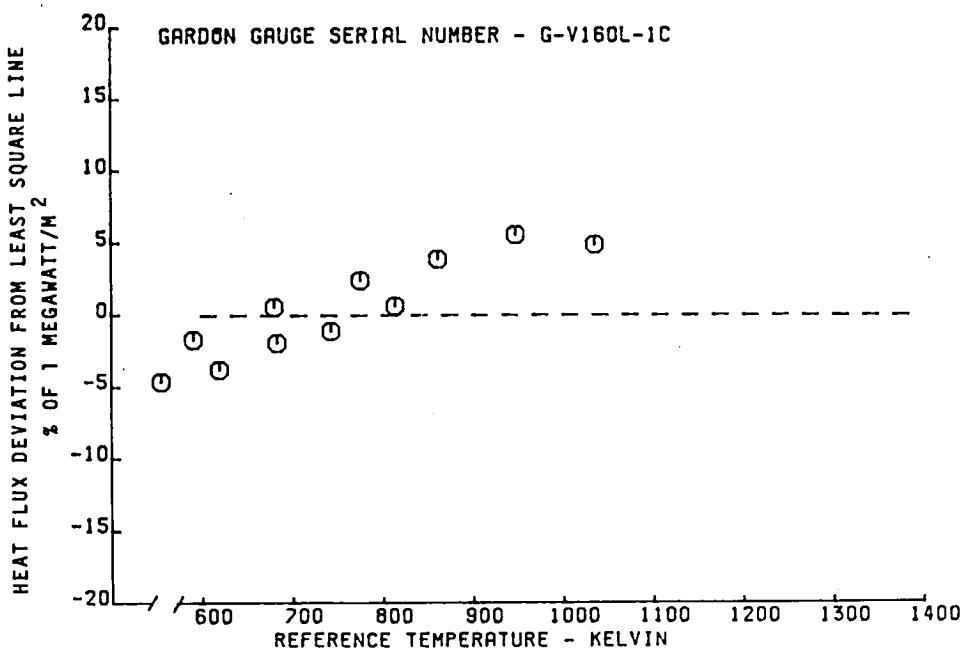

Figure 7.0-14 Calibration Data for Gardon Gauge Sensors Installed in Vanes for the High Pressure Facility

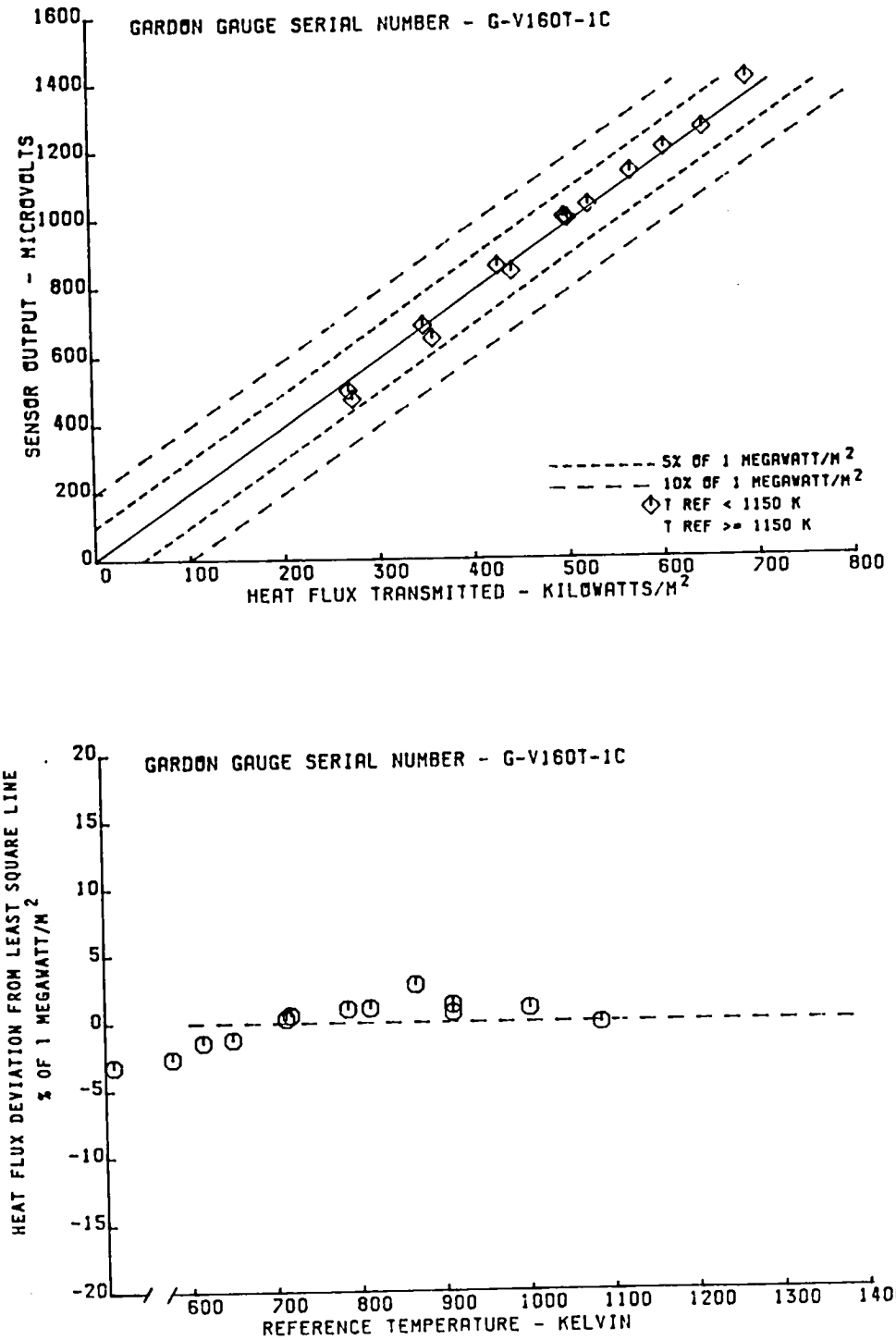

Figure 7.0-15 Calibration Data for Gardon Gauge Sensors Installed in Vanes for the High Pressure Facility

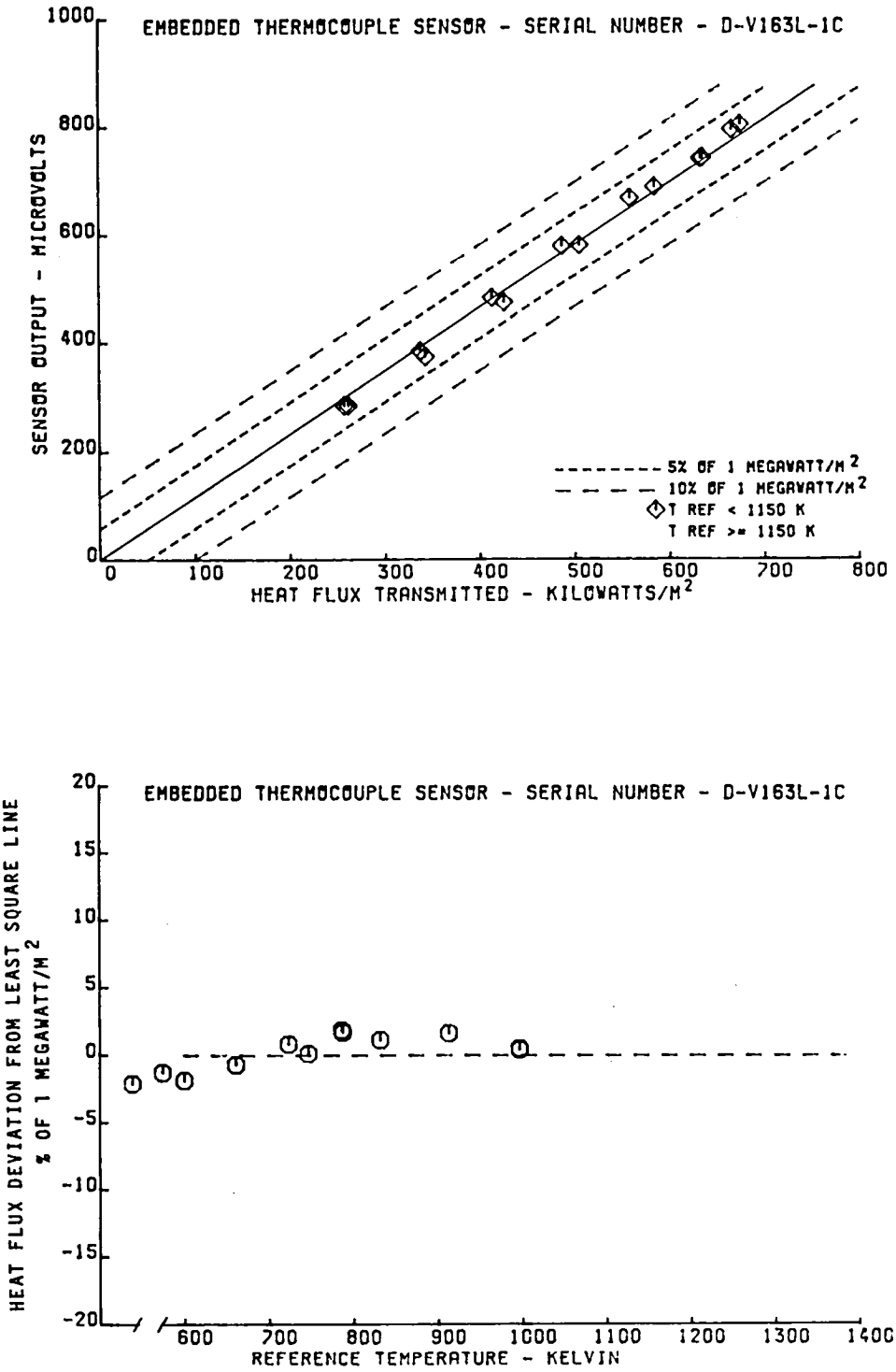

Figure 7.0-16 Calibration Data for Embedded Thermocouple Sensors Installed in Vanes for the High Pressure Facility

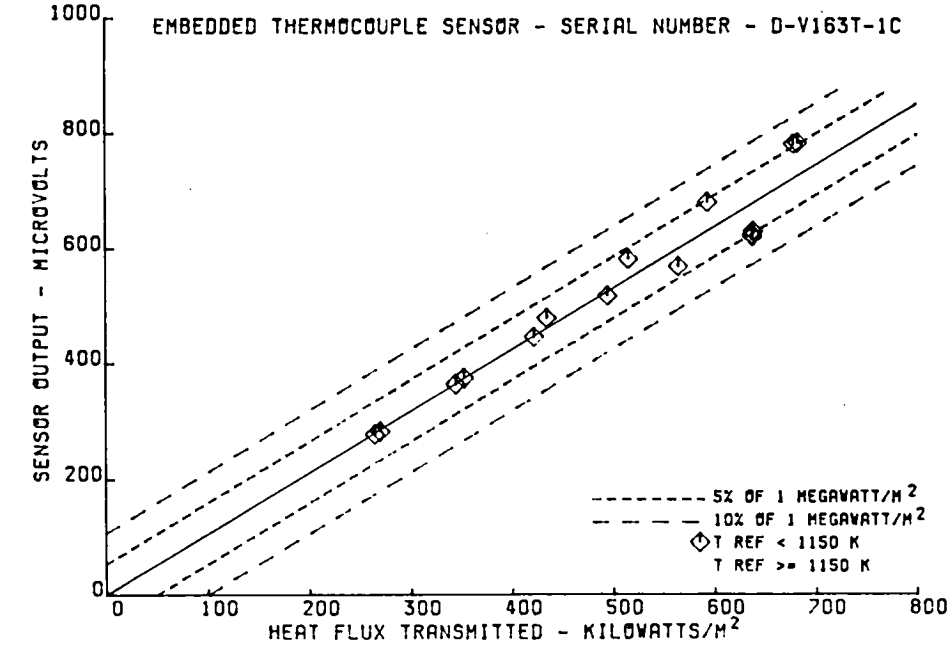

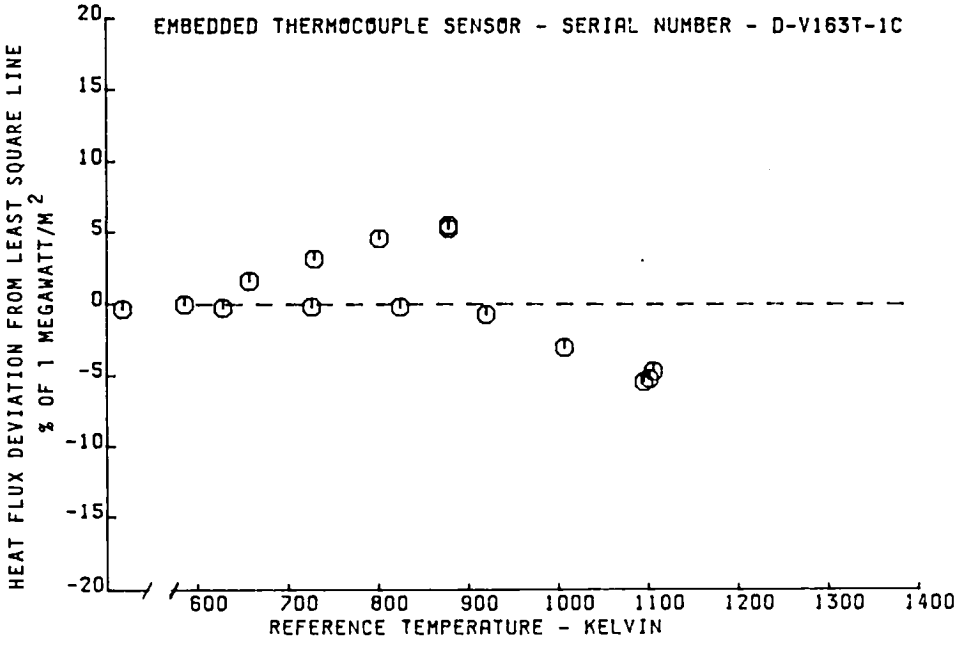

Figure 7.0-17 Calibration Data for Embedded Thermocouple Sensors Installed in Vanes for the High Pressure Facility

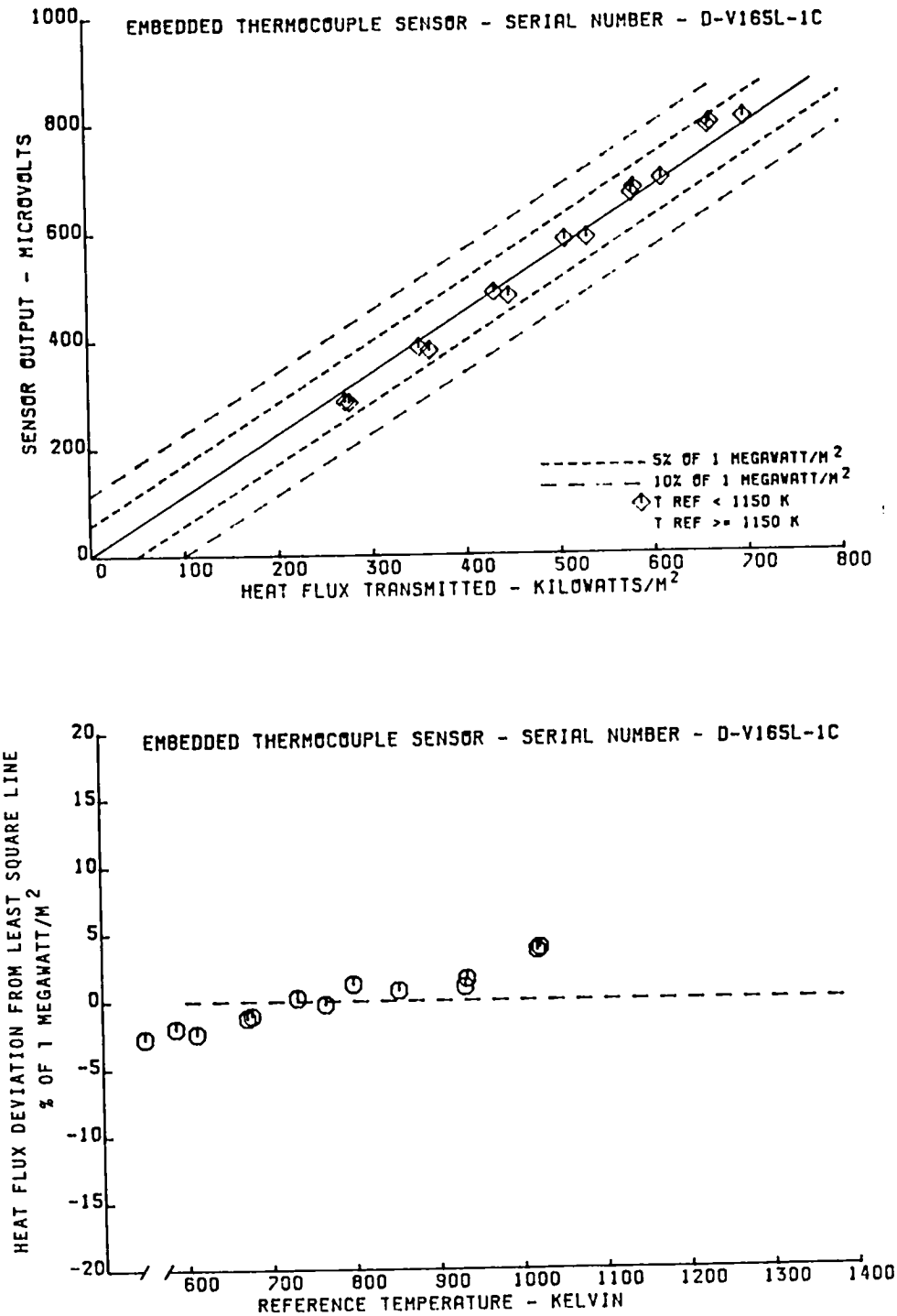

Figure 7.0-18 Calibration Data for Embedded Thermocouple Sensors Installed in Vanes for the High Pressure Facility

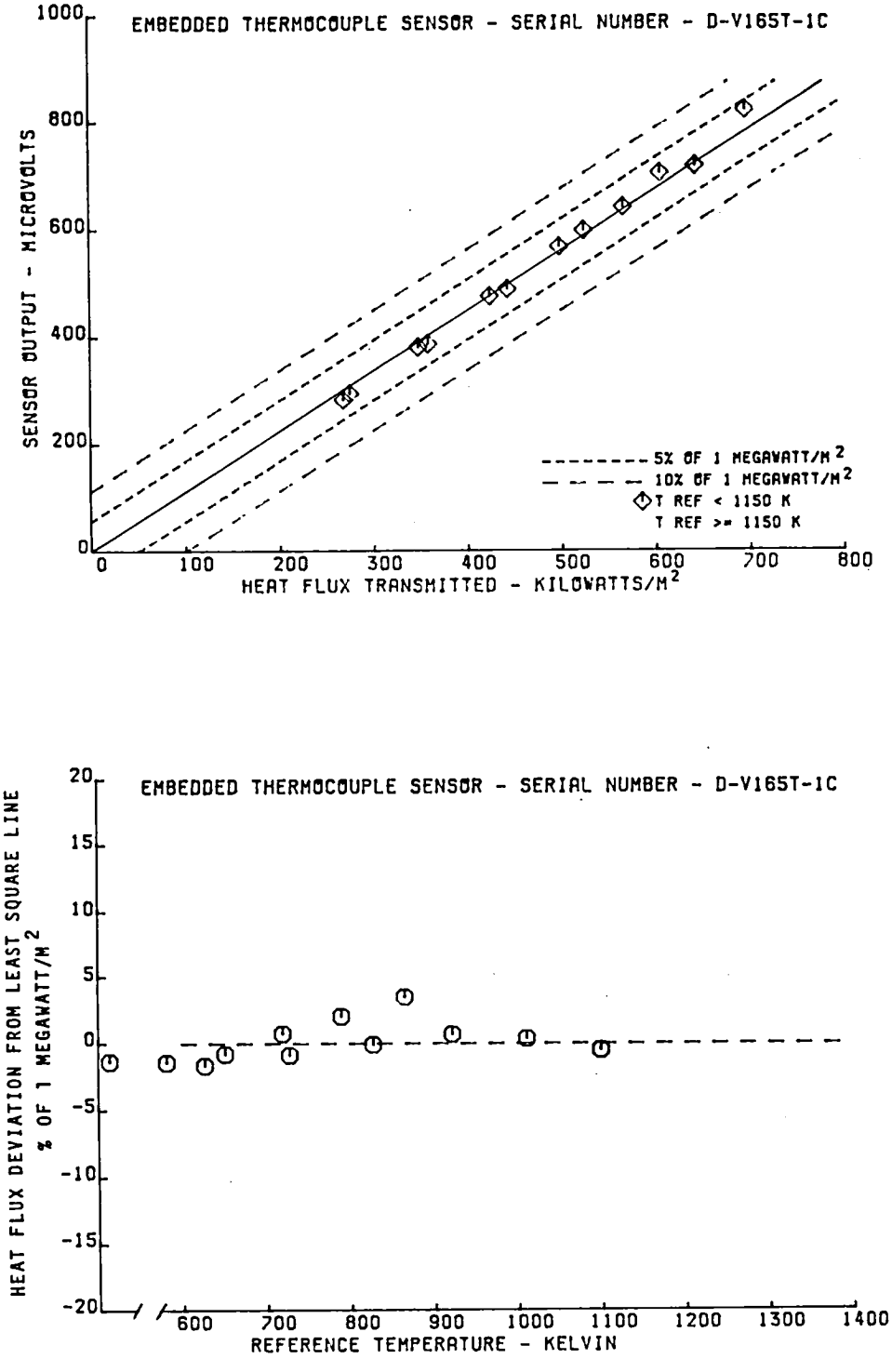

Figure 7.0-19 Calibration Data for Embedded Thermocouple Sensors Installed in Vanes for the High Pressure Facility

8.0 CONCLUSIONS AND RECOMMENDATIONS

8.1 CONCLUSIONS

The heat flux sensors developed in this phase of the Turbine Blade and Vane Heat Flux Sensor Development program met the objectives of the program. Specific conclusions drawn from the results are listed below.

- All of the blade and vane materials tested produced stable thermoelectric output to 1250K when paired with conventional thermocouple elements and can be used as a part of the thermoelectric circuitry of the heat flux sensors.
- The two heat flux sensor designs developed in this program produce accurate heat flux measurements and are capable of withstanding thermal cycle and thermal soak conditions in a laboratory environment.
- Fabrication techniques defined for the instrumentation of blades and vanes are suitable for engine testing.
- The calibration techniques for blades and vanes are affected by non-one-directional flow variations. Although these variations are evident in the data, the calibrations are still within $\pm$ 5% accuracy.

8.2 RECOMMENDATIONS

Based on the results achieved in this phase of the program and the conclusions drawn, the following recommendations are offered for the further development of heat flux sensors for application to turbine blades and vanes in an engine environment.

- Heat flux sensors fabricated into blades should be tested under rotation to ensure that the designs will withstand centrifugal loading.
- Heat flux sensors fabricated into both blades and vanes should be proof tested in an engine test to verify the design.
- The heat flux sensor calibration techniques should be analytically reviewed and changes made to the techniques and the calibration devices to minimize the non-one-directional flow effects.

APPENDIX A

LITERATURE REFERENCES

Steady State Heat Flux References

1 Atkinson, W. H.: Strange, R. R.; "Development of Advanced High Temperature Heat FLux Sensors"; NASA CR-165618 NASA Lewis Research Center, September, 1982.

2 Michard, J.; "Mesures De Flux de Chaleur Sur Aubes Fixes De Turbines"; NATA, AGARD; Symposium on High Temperature Turbines; Florence, Italy; September 21-25, 1970.

3 Burggraf, F.; "Local Heat Transfer Coefficient Distribution with Air Impingement into a Cavity"; ASME, Gas Turbine and Fluids Engineering Conference and Product Show; San Francisco, CA, March 26-30, 1972.

4 Hanus, G. J.; L'ecuyer, M. R.; "Turbine Vane Leading Edge Gas Film Cooling with Spanwise Angled Coolant Holes", AIAA-76-43; AIAA 14th Aerospace Sciences Meeting; Washington, D.C.; January 26-28, 1976.

5 Striegl S.A.; Diller, T. E.; "The Effect of Entrainment Temperature on Jet Imingement Heat Transfer"; accepted for publication in Journal of Heat Transfer; Transaction of ASME.

6 Kita, J. P.; Laganelli A.L.; "Gardon Heat Gage Temperature Response in Convective Heat Flux Measurement"; AIAA Journal, Vol. 13; No. 4 April 1975.

7 York, R. E.; Hylton, L. D.; Mihelc, M. S.; "An Experimental Investigation of Endwall Heat Transfer and Aerodynamics in A Linear Vane Cascade"; ASME paper 83-GT-52.

8 Nealy, D. A.; Mihelc, M.S.; Hylton, L. D. ; Gladden, H. J.; "Measurements of Heat Transfer Distribution Over the Surfaces of Highly Loaded Turbine Nozzle Guide Vanes"; ASME paper 83-6T-53

9 Prasad, B.V.S.S.S.; Mohanty, A. K.; "Analysis and Calibration of a Foil Heat Flux Sensor for Convective Measurements"; Journal of Physics & Scientific Instruments; Vol. 16; November, 1983.

10 Higuchi, H.; Peake, D. J.; "Bi-Directional, Buried-Wire Skin-Friction Gage"; NASA Technical Memorandum NASA-TM-78531.

11 Kornosky, R. M.; Perlmutter, M.; Fuchs, W.; Ruether, J. A.; "Apparatus Development for Measuring Heat Flux in a Direct Coal Liquefication Preheater"; DOE/PETC/TR-82/8.

Transient Heat Flux References

12 Dunn, M. G.; Hause, A.; "Measurement of Heat Flux and Pressure in a Turbine Stage", Journal of Engineering for Power; January, 1982; Vol. 104, p 215.

13 Godefroy, J. C.; "Thin Film Transducers for Temperature and Heat Flux Measurements"; LaRecherche Aerospatiale; No. 2, 1981.

14 Consigny, H.; Richards, B. E.; Ville, J. P.; "Short Duration Measurements of Heating to Cooled Gas Turbine Surfaces"; Journal of Engineering for Power; Vol. 100, July, 1978.

15 Francois J.; LeBot, Y.; Michard, S.; Deguest, P.; "Adaption of a Turbine Test Facility to High Temperature Research"; Royal Aircraft Establishment. December, 1980, Translation 2064.

16 Dunn, M. G.; Stoddard, F. J.; "Applications of Shock Tube Technology to the Measurement of Heat Transfer Rate to Gas Turbine Components"; Shock Tube and Shock Wave Research; Proceedings of the Eleventh International Symposium; Seattle, WA, July 11-14, 1977.

17 Jones, T. V.; Schultz, D. L.; Oldfield, M.L.G.; Daniels, L. C.; "Measurement of Heat Transfer Rate to Gas Turbine Components"; Shock Tube and Shock Wave Research; Proceedings of the Eleventh International Symposium; Seattle, WA, July 11-14, 1977.

18 Jones, T. V.; Schultz, D. L.; Oldfield, M.L.G.; Daniels, L. C.; "Measurement of Heat Transfer Rate to Turbine Blades and Nozzle Guide Vanes in a Transient Cascade"; International Heat Transfer Conference 6th, Toronto, Canada; August 7-11, 1978.

19 Louis, J. F.; "Heat Transfer in Turbines"; AFWAL-TR-81-2099, October, 1981.

20 Pochuev, V. P.; Shcherbakov, V. F.; 'Experimental Study of Heat Transfer at the Surface of Turbine Rotor Blades.", Aviatsionnaya Tekhnika, Vol. 24; No. 1, 1981

21 Richards, B. E.; Appels, C.; Ville, J. P.; Salemi, C.; "Film Cooling of Heated Turbine Surfaces at Simulated Conditions"; AIAA-77-947; AIAA/SAE 13th Propulsion Conference; Orlando, FL, July 11-13, 1977.

22 Paulon, J.; Portat, M.; Godefroy, J. C.; Szechenyi, E.; "Ultrathin Transducers Applied to Measurements in Turbomachines." Presented at Lecture Series on Measurement Techniques in Turbomachinery; May 18-22, 1981

23 Guernigou, J.; Indrigo, C.; Maisonneuve, Y.; Mentre, P. G.; "Development of Surface Temperature Fluxmeters"; La Rescherche Aerospatiale; May - June, 1980.

24 Polyakov, Y. A.; Degtyarev, S. A.; Klygin, A. V.; "Characteristics of a Film-Type Heat-Flux Transducer", Teplofizika Vysokikh Temperature; Vol. 20, No. 6, November - December, 1982.

25 Litchfield, M. R.; Norton, R.J.G.; "Heat Transfer Measurements of a Transonic Nozzle Guide Vane"; ASME paper 82-GT-247.

26 Dunn, M. G.; Rae, W. J.; Holt, J. L.; "Measurement and Analyses of Heat Flux Data in a Turbine Stage: Part I - Description of Experimental Apparatus and Data Analysis"; ASME Paper 83-GT-121.

27 Ligrani, P. M.; Camci, C.; Grady, M. S.; "Thin Film Heat Transfer Gage Construction and Measurement Details"; Von Karmon Institute for Fluid Dynamics Technical Memorandum 33. November, 1982.

28 Sucic, J.; "Exact Analytical Solution to a Transient Conjugate Heat - Transfer Problem; NASA Technical Note, NASA TN D-7101.

29 McBratney, W. F.; "Thin Film Gages for Ignition and Combustion Experiments"; U.S. Army Ballistic Research Laboratory Memorandum ARBRL-MR-03272, May 1983

Miscellaneous Heat Flux References

30 Emery, A. F.; Etemad, S.; Wolak, J.; "Interfacial Temperatures and Surface Heat Fluxes for Blade-Seal Process", AIAA-81-1165; AIAA 14th Fluid and Plasma Dynamics Conference; June 23-25, 1981; Palo Alto, CA.

31 Beacock, R. J.; Horton, F. G.; Kirker, T. J.; White, A. J.; "Measurements of Heat Transfer Coefficients on Gas Turbine Components - Part II Applications of the Technique Described in Part 1 and Comparisons with Results from a Conventional Measuring Technique and Prediction; ASME paper 82-GT-175.

32 Blair, M. F.; 'An Experimental Study of Heat Transfer and Film Cooling on Large-Scale Turbine Endwalls"; Transaction of the ASME, November, 1974.

33 Delyagin, G. N.; Shvartsshteyn, Y. M.; "Experimental Study of Heat and Mass Transfer in the Presence of a Controlled Protective Coating on Gas Turbine Blading"; Heat Transfer Soviet Research; Vol. 10, No. 2, March - April 1978.

34 Gladden, H. J.; Liebert, C. H.; "Method of Predicting Radiation Heat Transfer in Turbine-Cooling Test Facilities"; NASA Report TM-X-3172; January, 1975.

35 Johnson, B. V.; "Heat Transfer Experiments in Rotating Radial Passage with Supercritical Water", Gas Turbine Heat Transfer; 1978; Proceedings of the Winter Annual Meeting; San Francisco, CA, December 10-15, 1978.

36 Nicholson, J. H.; Forest, A. E.; Oldfield, M.L.G.; Schultz, D. L.; "Heat Transfer Optimized Turbine Rotor Blades - An Experimental Study Using Transient Techniques"; ASME82-GT-304.

37 Panteleev, A. A.; Slesarev, V. A.; Trushin, V. A.; "An Investigation of the Effect of Temperature Unsteadiness on Heat Transfer to Turbine Blades"; Teploenergetika 28; (10) 58-61; 1981.

38 Petrovskii, V. S.; Polyakov, A. M.; "Formulation of Unsteady Heat Conduction Problem for Radial Gas Turbine Rotor"; Aviatsionnaya Tekhnika; Vol. 16, No. 4; 1973.

39 Sundell, R. E.; Goodwin, W. W.; Kercher, D. M.; Dudley, J. C.; Triandafyllis, J.; "Boiling Heat Transfer in Turbine Bucket Cooling Passages"; ASME/AICHE National Heat Transfer Conference; Orlando, FL, July 27-30, 1980.

40 Trushin, V. A.; "Selection of Similarity Criteria in Studying the Effect of Rotation on Heat Exchange in Turbine Blades", Inzhenerno-Fizicheskii Zhurnal; Vol. 30, No. 2, February, 1976.

41 Turner, A. B.; "Heat Transfer Instrumentation"; NATO, AGARD, Symposium on High Temperature Turbines; Florence, Italy; September 21-25, 1970.

42 Winstanley, D. K.; Booth, T. C.; Dunn, M. G.; "The Predictability of Turbine Vane Convection Heat Transfer", AIAA81-1435; AIAA/SAE/ASME 17th Joint Propulsion Conference; Colorado Springs, CO; July 27-29, 1982.

43 Petukhov, B. S.; et al; "Experimental Study of the Heat Fluxes in a MHD Channel"; Teplofizika Vysokikh Temperature; Vol. 20; No. 4; July - August, 1982.

44 Iskakov, K. M.; Trushin, V. A.; "Unsteady Approach to Heat Transfer in Turbine Blade Cooling Passages"; Izvestiya Vuz; Aviatsionnaya Tekhnika, Vol. 25; No. 3; 1982.

45 Moody, H. L.; Jechel, K.; "Heat Transfer Measurements in Cold Wind Tunnels"; Air Force Weight Aeronautical Laboratories Report, AFWAL-TR-81-3176.

46 AGARD Conference Proceedings No. 281, "Testing and Measurement Techniques in Heat Transfer and Combustion", publication AGARD-CP-281, September 1980.

47 Merrill, B. R.; "An Alternate Approach to the Measurement of Soil Surface Heat Flux"; Thesis report AFIT-CI-81-33T.

48 Kidd, C. T.; "Determination of the Uncertainty of Experimental Heat-Flux Calibrations"; Arnold Engineering Development Center; AEDC-TR-83-13; August, 1983.

49 Kidd, C. T.; "A Durable Intermediate Temperature, Direct Reading Heat Flux Transducer for Measurements in Continuous Wind Tunnels"; Arnold Engineering Development Center; AEDC-T2-19; November, 1981.

50 Holanda, R; "Analysis of Thermoelectric Properties of High-Temperature Complex Alloys of Nickel-Base, Iron-Base, and Cobalt-Base Groups"; NASA TP-2278; February 1984

APPENDIX B

MATERIAL PROPERTIES USED FOR HEAT TRANSFER ANALYSES

The thermal analyses performed on the candidate sensors are discussed in Section 4.2. In order to perform these analyses, certain properties are required for each of the materials used. The material properties required are densities, thermal conductivities, and specific heats. These properties were readily available through internal literature and are presented in Table B-I and Figures B-1 through B-8.

TABLE B-I
DENSITIES OF MATERIAL

MAR-M-509	8.8 g/cm^3
Alloy 454	8.6 g/cm^3
B1900 + Hf	8.2 g/cm^3
Alumel	8.6 g/cm^3
Chromel	8.7 g/cm^3
MgO	3.8 g/cm^3
Wire	5.4 g/cm^3

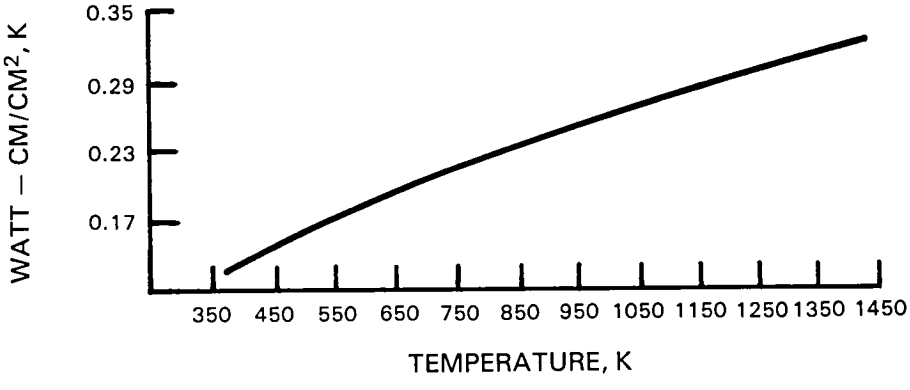

Figure B-1 Thermal Conductivity of MAR-M-509

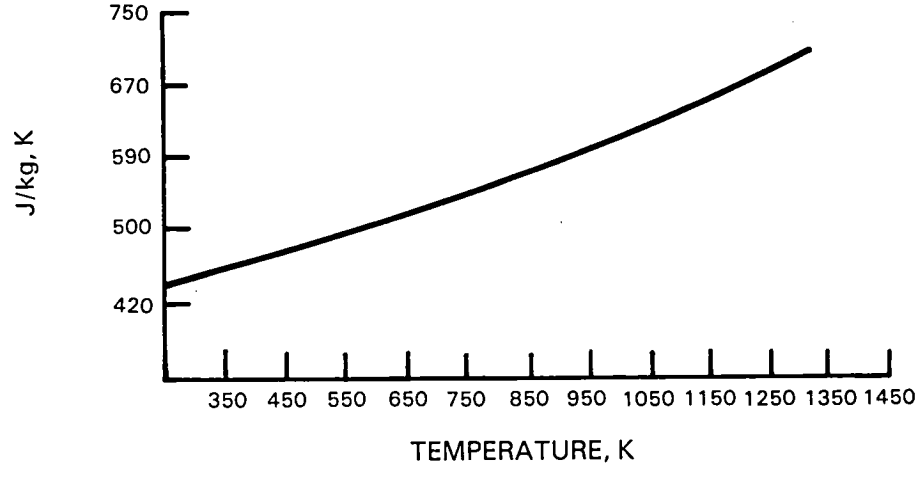

Figure B-2 Specific Heat of MAR-M-509

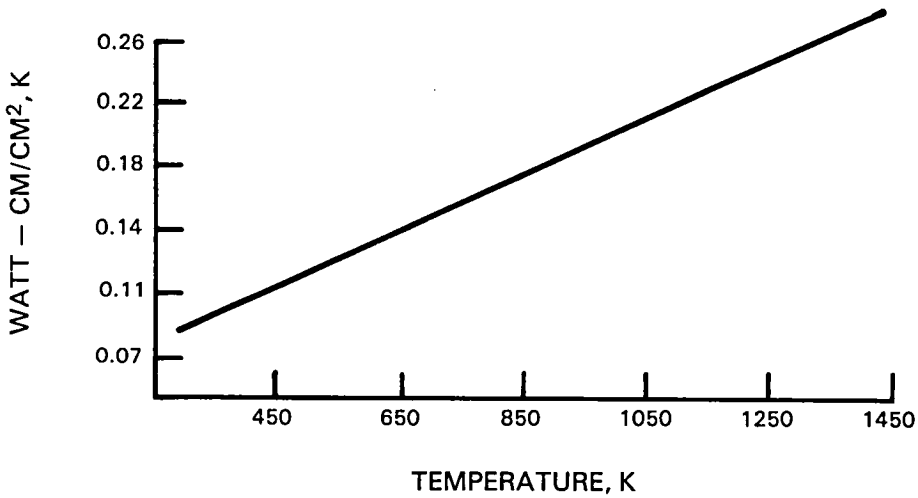

Figure B-3 Thermal Conductivity of Alloy 454

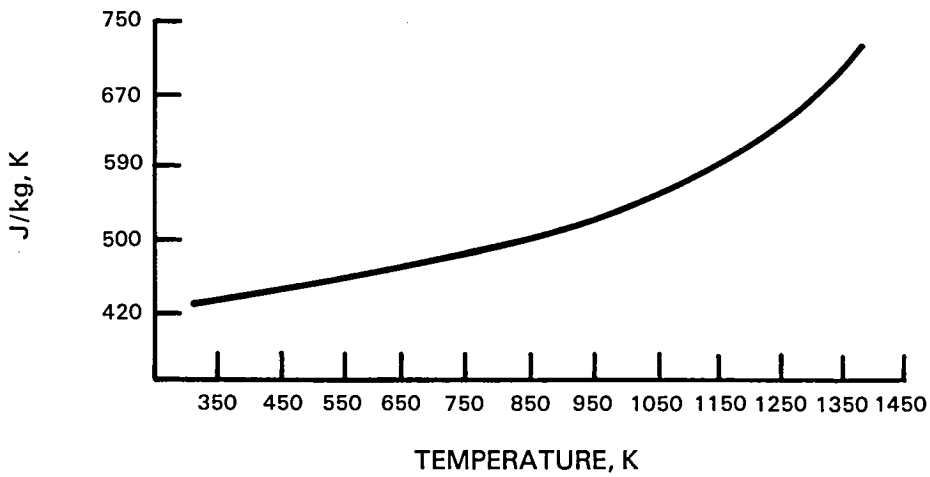

Figure B-4 Specific Heat of Alloy 454

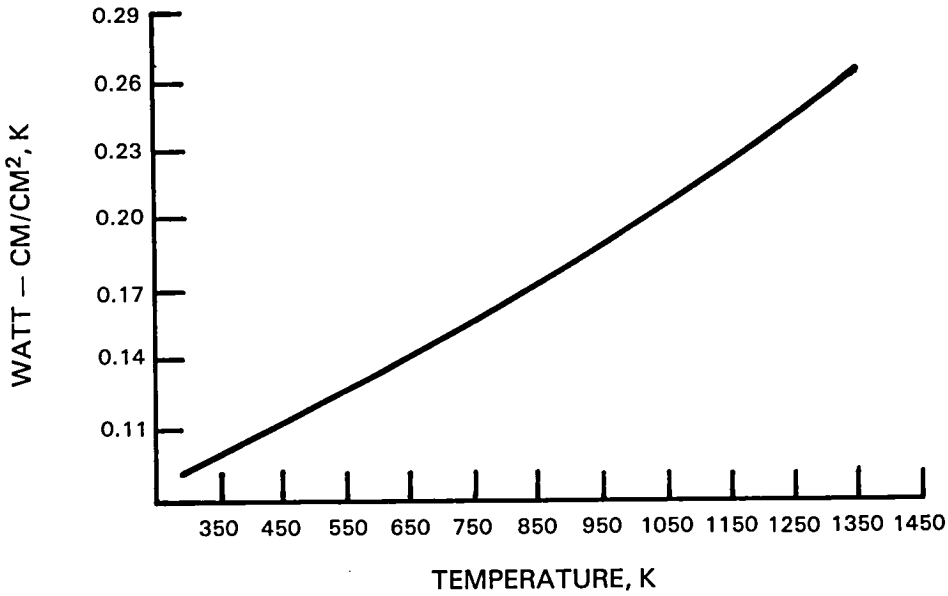

Figure B-5 Thermal Conductivity of B1900 + Hf

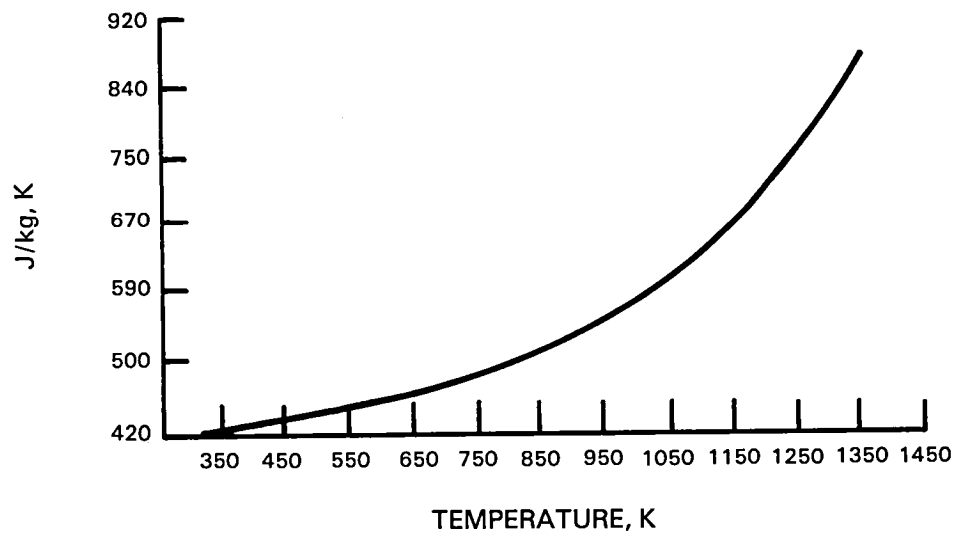

Figure B-6 Specific Heat of B1900 + Hf

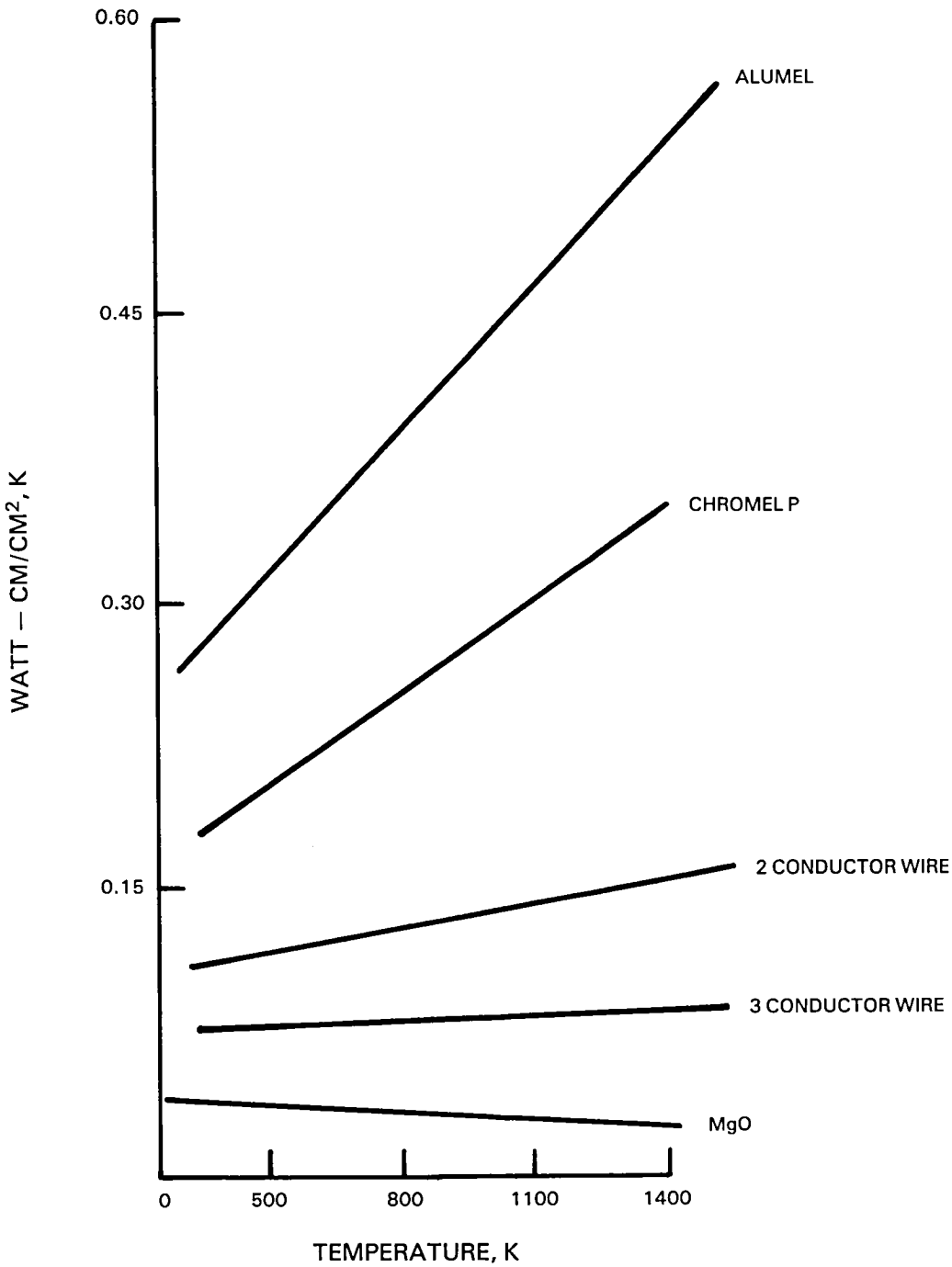

Figure B-7 Thermal Conductivities of Materials Used in Analyses

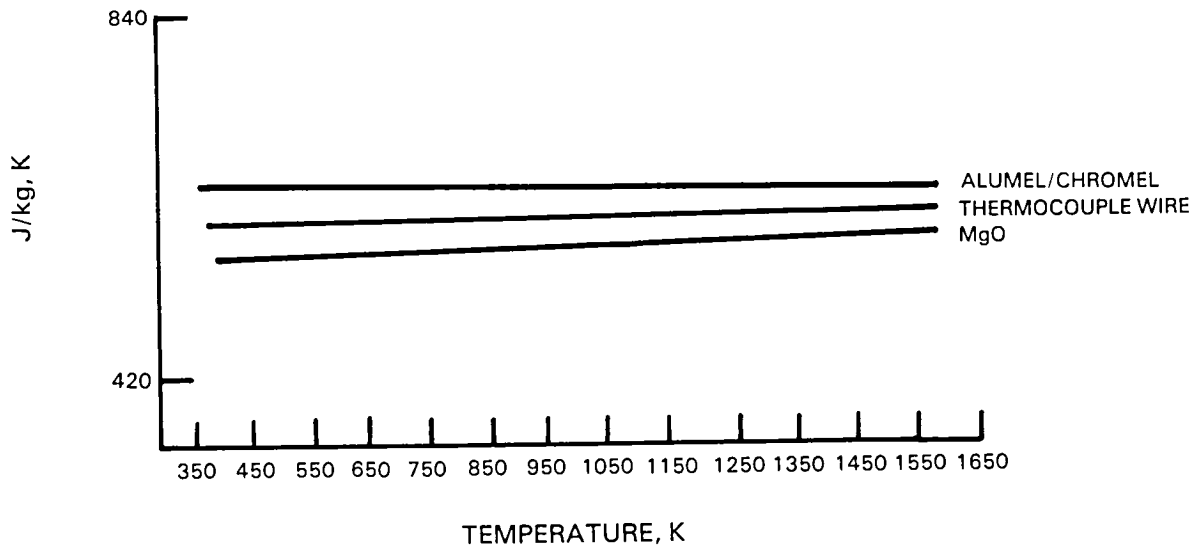

Figure B-8 Specific Heat of Materials Used in Analyses

APPENDIX C

THERMOELECTRIC PROPERTIES OF SUPERALLOYS

Table C-I lists the curves (Figures C-1 through C-11) which present the results of the thermoelectric tests versus platinum. In order to make the thermoelectric data easier to use, third order polynomial curve fits were produced for each of the data sets. Curve fits were produced for each superalloy versus both platinum and Alumel. The curve fit results are presented in Table C-II. Tabular data for these alloys has been computed from those equations and is presented at 100 C intervals versus platinum in Table C-III and versus Alumel in Table C-IV. The tables are produced to one decimal place to indicate the greater uncertainty in the thermoelectric output of these engineering materials compared to thermoelectric alloy materials. This uncertainty is the result of the larger allowable variation of the alloy constituents of engineering materials.

TABLE C-I

INDEX OF CURVES OF THERMOELECTRIC DATA VERSUS PLATINUM

Figure C-1	Summary Curve of Superalloy Thermoelectric Data vs Platinum	
	Nickel Base Materials	
Figure C-2	Alloy 454	(PWA 1480)
Figure C-3	B-1900	(PWA 663)
Figure C-4	B-1900 + Hf	(PWA 1455)
Figure C-5	Hastelloy-X	(PWA 1038)
Figure C-6	Inconel 792	(PWA 1456)
Figure C-7	Inconel 713C	(PWA 655)
Figure C-8	MAR-M-247	(PWA 1447)
Figure C-9	MAR-M-200 + Hf	(PWA 1422)
	Cobalt Base Materials	
Figure C-10	MAR-M-509	(PWA 647)
Figure C-11	WI-52	(PWA 653)

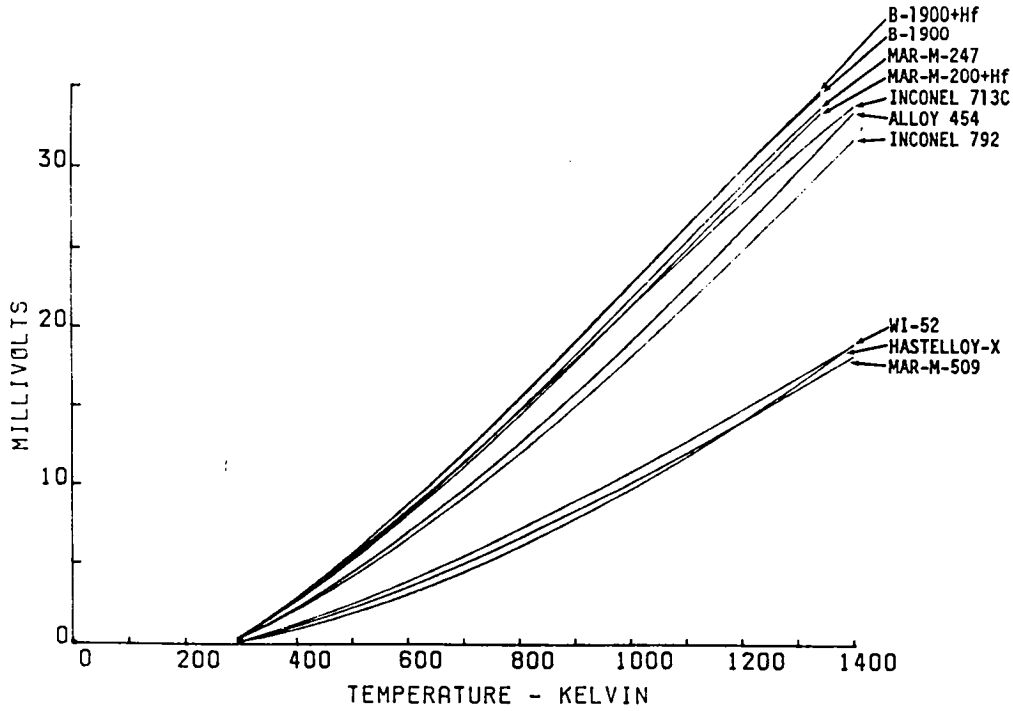

Figure C-1 Summary Curve for Thermoelectric Characteristics of Superalloys versus Platinum

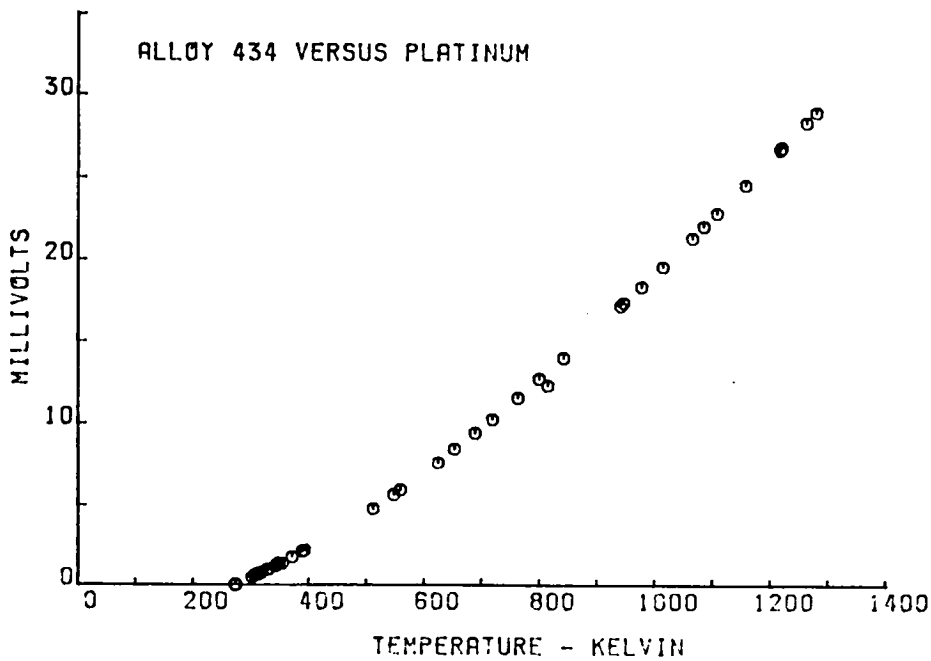

Figure C-2 Alloy 454 versus Platinum

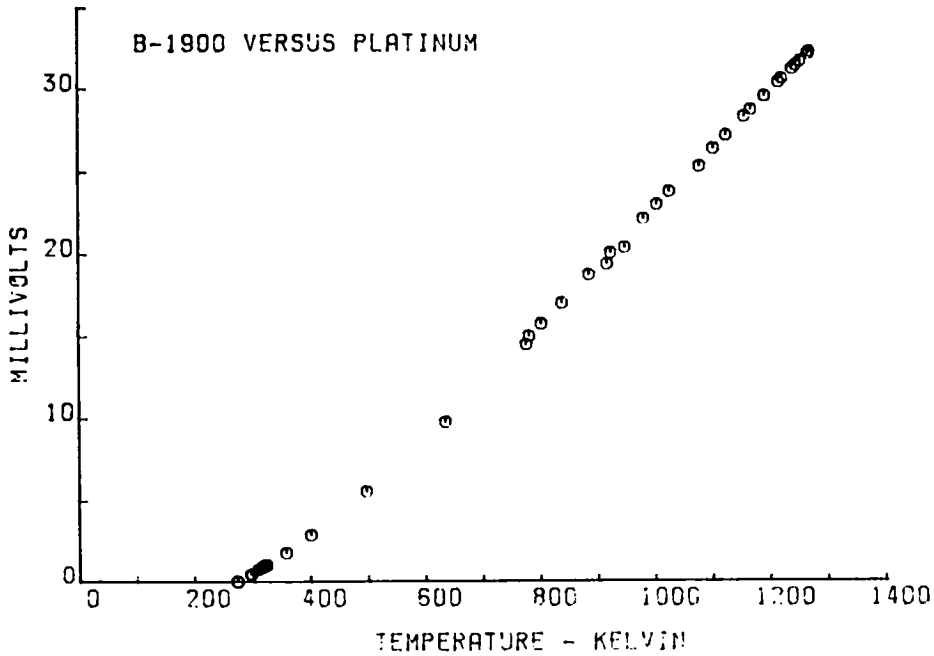

Figure C-3 B-1900 versus Platinum

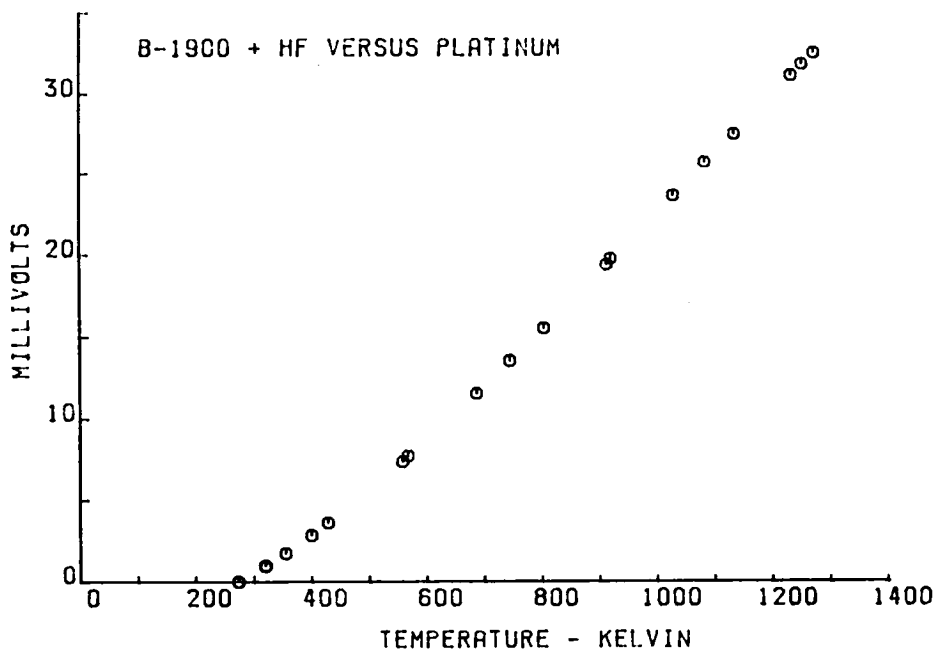

Figure C-4 B-1900 + Hf versus Platinum

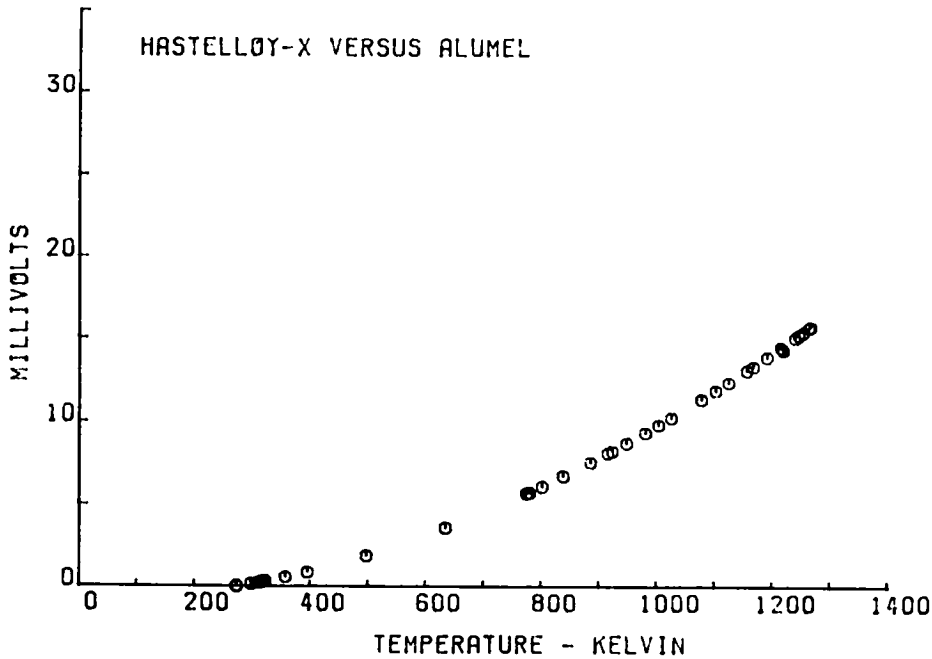

Figure C-5 Hastelloy - X versus Platinum

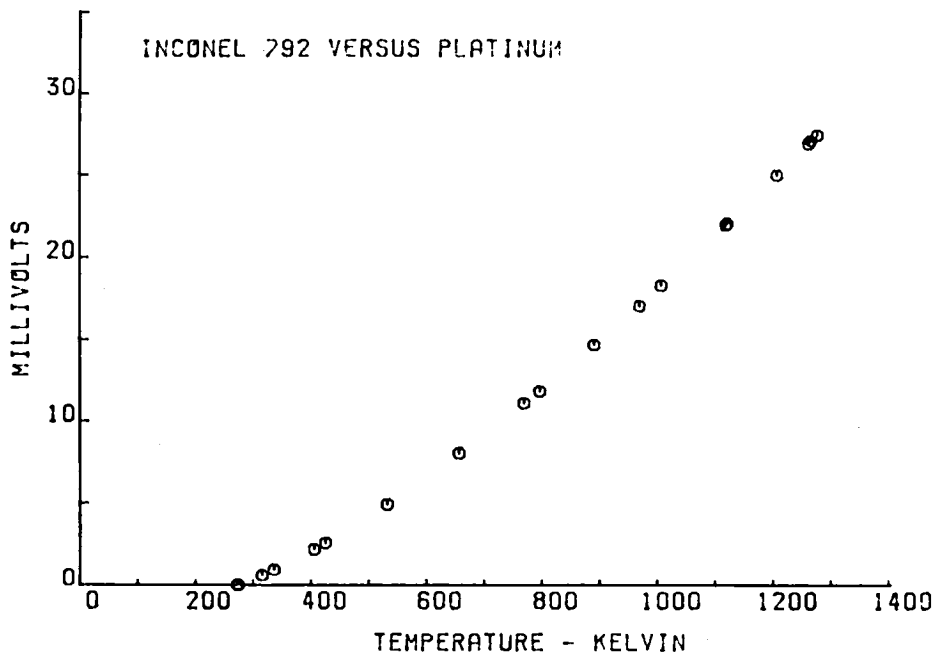

Figure C-6 Inconel 792 versus Platinum

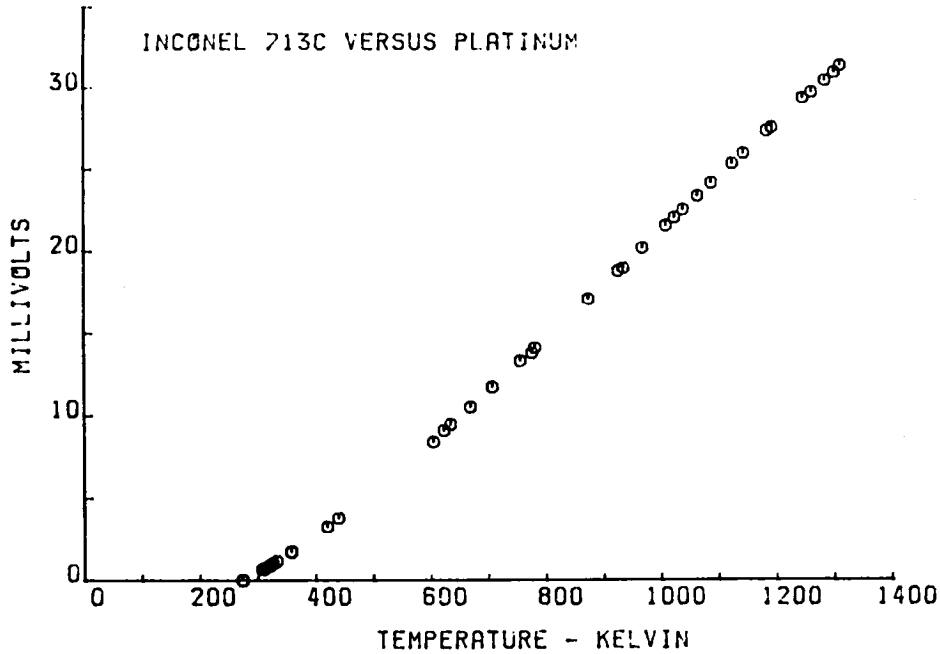

Figure C-7 Inconel 713C versus Platinum

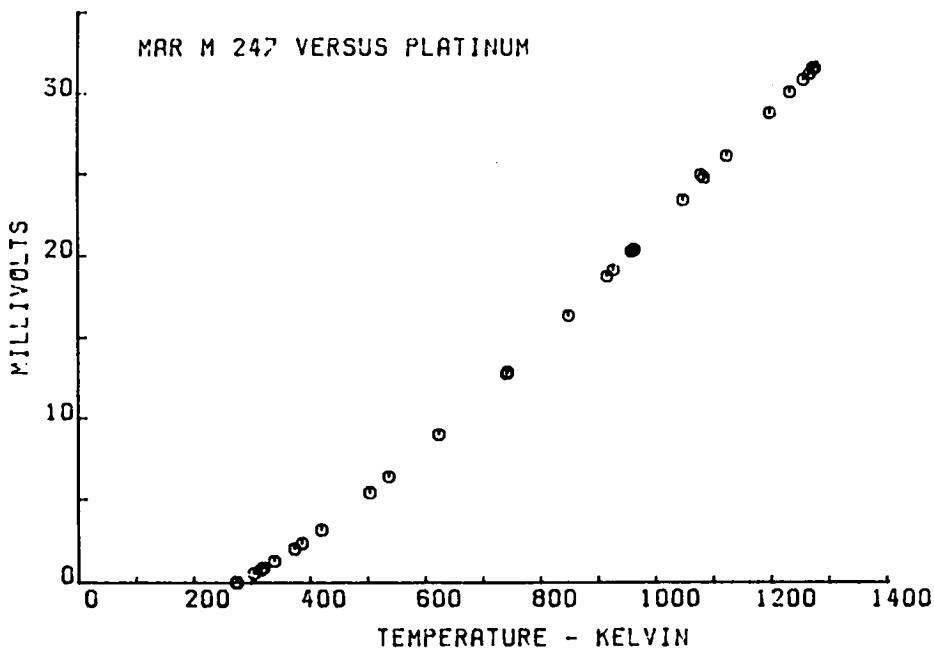

Figure C-8 MAR-M 247 versus Platinum

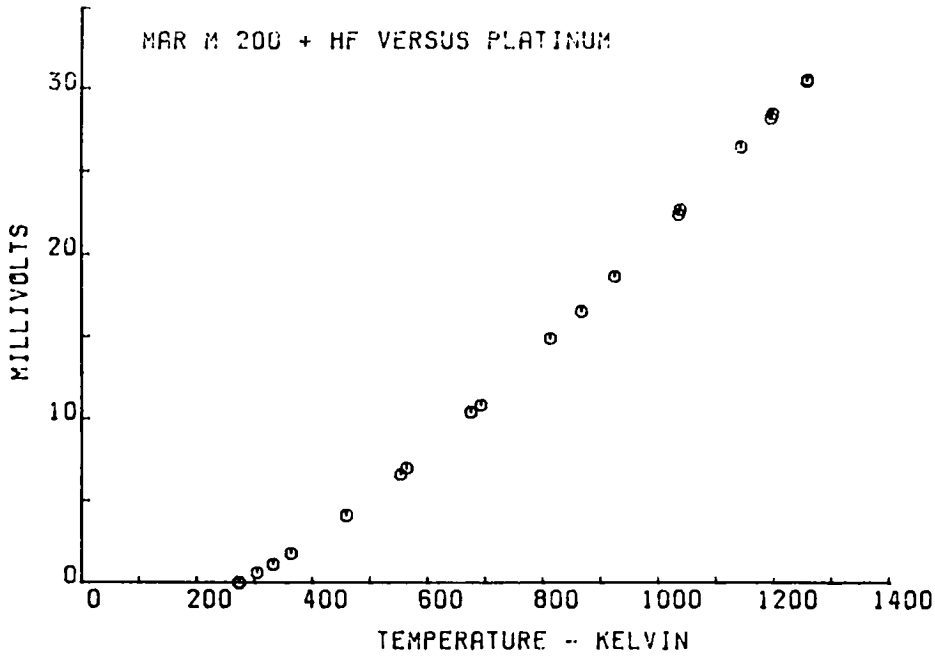

Figure C-9 MAR-M 200 + Hf versus Platinum

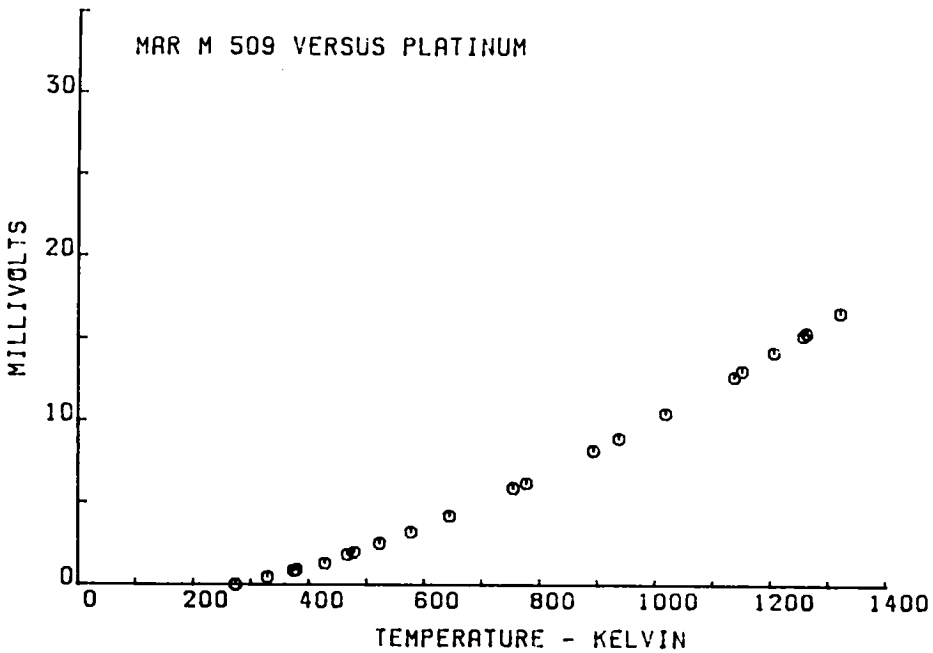

Figure C-10 MAR-M 509 versus Platinum

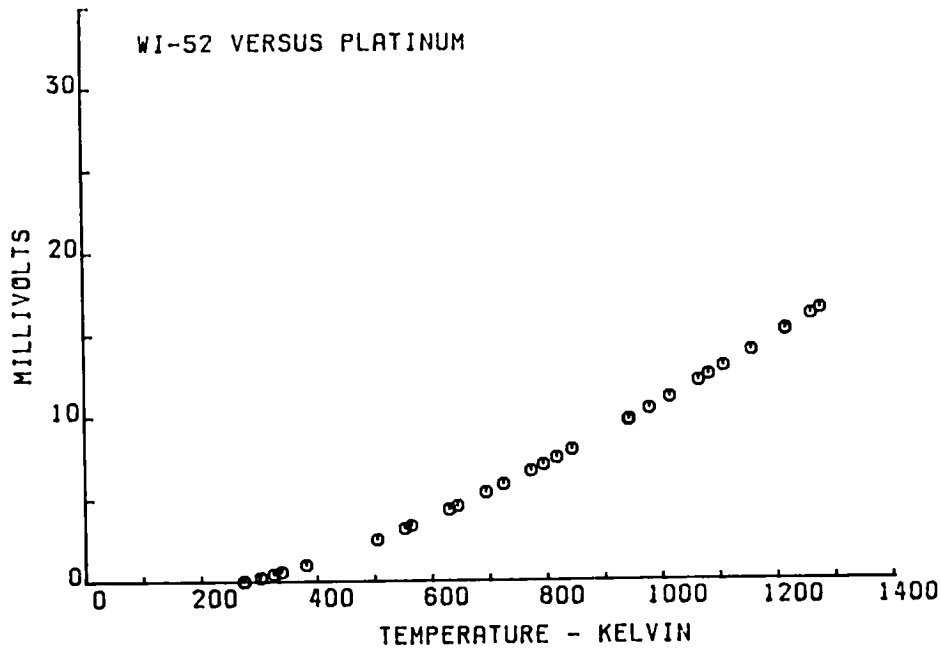

Figure C-11 WI-52 versus Platinum

Table C-II
THIRD ORDER CURVE FITS TO THE THERMOELECTRIC TEST DATA

Nickel Based Materials

Alloy 454 versus Platinum	$E.M.F. = -3.01 + 5.34 \times 10^{-3} T + 2.18 \times 10^{-5} T^2 - 4.98 \times 10^{-9}$
Alloy 454 versus Alumel	$E.M.F. = -6.31 + 1.98 \times 10^{-2} T + 1.38 \times 10^{-5} T^2 - 1.72 \times 10^{-9}$
B-1900 versus Platinum	$E.M.F. = -3.67 + 5.36 \times 10^{-3} T + 3.22 \times 10^{-5} T^2 - 1.12 \times 10^{-8}$
B-1900 versus Alumel	$E.M.F. = -6.84 + 1.90 \times 10^{-2} T + 2.55 \times 10^{-5} T^2 - 8.45 \times 10^{-9}$
B-1900+Hf versus Platinum	$E.M.F. = -3.81 + 6.47 \times 10^{-3} T + 3.00 \times 10^{-5} T^2 - 9.91 \times 10^{-9}$
B-1900+Hf versus Alumel	$E.M.F. = -7.36 + 2.21 \times 10^{-2} T + 2.01 \times 10^{-5} T^2 - 5.83 \times 10^{-9}$
Hastelloy-X versus Platinum	$E.M.F. = -0.86 + 3.36 \times 10^{-5} T + 1.17 \times 10^{-5} T^2 - 1.10 \times 10^{-9}$
Hastelloy-X versus Alumel	$E.M.F. = -4.18 + 1.44 \times 10^{-2} T + 3.50 \times 10^{-6} T^2 + 2.36 \times 10^{-9}$
Inconel 792 versus Platinum	$E.M.F. = -2.70 + 4.26 \times 10^{-3} T + 2.17 \times 10^{-5} T^2 - 5.12 \times 10^{-9}$
Inconel 792 versus Alumel	$E.M.F. = -6.27 + 1.99 \times 10^{-2} T + 1.20 \times 10^{-5} T^2 - 1.11 \times 10^{-9}$
Inconel 713C versus Platinum	$E.M.F. = -4.22 + 8.87 \times 10^{-3} T + 2.55 \times 10^{-5} T^2 - 8.90 \times 10^{-9}$
Inconel 713C versus Alumel	$E.M.F. = -7.21 + 2.17 \times 10^{-2} T + 1.97 \times 10^{-5} T^2 - 6.49 \times 10^{-9}$
MAR-M-247 versus Platinum	$E.M.F. = -3.23 + 4.02 \times 10^{-3} T + 3.12 \times 10^{-5} T^2 - 1.02 \times 10^{-8}$
MAR-M-247 versus Alumel	$E.M.F. = -6.89 + 2.02 \times 10^{-2} T + 2.06 \times 10^{-5} T^2 - 5.79 \times 10^{-9}$
MAR-M-200+Hf versus Platinum	$E.M.F. = -3.48 + 5.86 \times 10^{-3} T + 2.72 \times 10^{-5} T^2 - 8.26 \times 10^{-9}$
MAR-M-200+Hf versus Alumel	$E.M.F. = -6.93 + 2.09 \times 10^{-2} T + 1.83 \times 10^{-5} T^2 - 4.53 \times 10^{-9}$

Cobalt Based Materials

MAR-M-509 versus Platinum	$E.M.F. = -1.32 + 1.59 \times 10^{-3} T + 1.23 \times 10^{-5} T^2 - 2.46 \times 10^{-9}$
MAR-M-509 versus Alumel	$E.M.F. = -4.88 + 1.73 \times 10^{-2} T + 2.59 \times 10^{-6} T^2 - 1.52 \times 10^{-9}$
WI-52 versus Platinum	$E.M.F. = -1.66 + 2.80 \times 10^{-3} T + 1.26 \times 10^{-5} T^2 - 2.84 \times 10^{-9}$
WI-52 versus Alumel	$E.M.F. = -4.85 + 1.64 \times 10^{-2} T + 5.52 \times 10^{-6} T^2 - 1.03 \times 10^{-10}$

(E.M.F. is in millivolts and temperature is in Kelvin)

TABLE C-III

THERMOELECTRIC CHARACTERISTICS OF ENGINEERING MATERIALS VERSUS PLATINUM

Temperature Celsius	Output, millivolts				
	Alloy 545	B-1900	B-1900+Hf	HASTELLOY-X	INCONEL 792
0	0.0	0.0	0.0	0.0	0.0
100	1.8	2.2	2.3	0.7	1.6
200	3.9	4.9	4.9	1.7	3.6
300	6.3	7.9	7.9	2.8	5.9
400	8.9	11.1	11.1	4.1	8.4
500	11.8	14.5	14.5	5.7	11.2
600	15.0	18.1	18.1	7.4	14.2
700	18.2	21.7	21.8	9.2	17.3
800	21.7	25.3	25.4	11.3	20.5
900	25.2	28.9	29.1	13.5	23.9
1000	28.8	32.2	32.6	15.9	27.3

Temperature Celsius	Output, millivolts				
	INCONEL 713C	MAR-M-247	MAR-M-200 +Hf	MAR-M-509	WI-52
0	-0.1	0.0	0.0	0.0	0.0
100	2.2	2.1	2.1	0.9	1.0
200	4.7	4.6	4.5	1.9	2.2
300	7.6	7.4	7.3	3.2	3.5
400	10.6	10.5	10.3	4.6	5.1
500	13.8	13.8	13.5	6.1	6.7
600	17.0	17.3	16.9	7.8	8.5
700	20.4	20.8	20.4	9.6	10.4
800	23.7	24.4	23.9	11.5	12.3
900	26.9	28.0	27.5	13.5	14.4
1000	30.0	31.4	31.0	15.6	16.5

TABLE C-IV

THERMOELECTRIC CHARACTERISTICS OF ENGINEERING MATERIALS VERSUS ALUMEL

Temperature Celsius	Output, millivolts				
	Alloy 545	B-1900	B-1900+Hf	HASTELLOY-X	INCONEL 792
0	0.1	0.1	0.1	0.1	0.0
100	2.9	3.4	3.4	1.8	2.8
200	6.0	7.0	7.0	3.7	5.7
300	9.2	10.8	10.8	5.7	8.9
400	12.7	14.9	14.8	7.8	12.2
500	16.5	19.2	19.0	10.1	15.8
600	20.4	23.6	23.4	12.6	19.5
700	24.4	28.0	27.8	15.3	23.4
800	28.7	32.5	32.3	18.2	27.5
900	33.1	36.9	36.8	21.3	31.8
1000	37.7	41.2	41.3	24.7	36.2

Temperature Celsius	Output, millivolts				
	INCONEL 713C	MAR-M-247	MAR-M-200 +Hf	MAR-M-509	WI-52
0	0.1	0.0	0.1	0.0	0.0
100	3.3	3.2	3.2	1.9	2.0
200	6.8	6.7	6.6	3.7	4.1
300	10.5	10.4	10.2	5.6	6.3
400	14.3	14.3	14.0	7.5	8.7
500	18.3	18.4	18.1	9.3	11.1
600	22.4	22.6	22.3	11.2	13.6
700	26.6	26.9	26.6	13.0	16.2
800	30.7	31.4	31.0	14.8	19.0
900	34.9	35.8	35.5	16.5	21.8
1000	39.0	40.3	40.0	18.2	24.8

DISTRIBUTION LIST

HEAT FLUX PHASE I FINAL
706347-0003
DISTRIBUTION LIST & LABELS

NASA Lewis Research Center
21000 Brookpark Road
Cleveland, OH 44135
Attn: Ray Holanda, M.S. 77-1
(50 copies)

NASA Lewis Research Center
21000 Brookpark Road
Cleveland, OH 44135
Attn: Leonard W. Schopen, M.S. 501-11

NASA Scientific and Technical
Information Facility
P.O. Box 33
College Park, MD 20740
Attn: Acquisitions Branch
(22 copies)

NASA Lewis Research Center
21000 Brookpark Road
Cleveland, OH 44135
Attn: Library, M.S. 60-3
(2 copies)

NASA Lewis Research Center
21000 Brookpark Road
Cleveland, OH 44135
Attn: Report Control Office, M.S. 5-5

General Electric Company
Aircraft Engine Group
Evendale, OH 45215
Attn: Wayne Shaffernocker, MSH-78
Ronald Weise, MSH-78
William Stowell

Stanford University
Standford, CA 94305
Attn: Dr. R. J. Moffat
Asst. Prof. Mech. Engr.
Dir. Thermoscience
Measurement Center

Air Force Wright Aeronautical
Labortory
Wright Patterson AFB, OH 45433
Attn: R. Cox/POTC

Air Force Wright Aeronautical
Labortory
Wright Patterson AFB, OH 45433
Attn: Everett E. Bailey/AFWAL/NASA-PO

Air Force Wright Aeronautical
Labortory
Wright Patterson AFB, OH 45433
Attn: William Stange/POTC

Air Force Wright Aeronautical
Labortory
Wright Patterson AFB, OH 45433
Attn: M. Roquemore/POSF

DISTRIBUTION LIST

Roto Data, Inc.
10200 Anderson Way
Cincinnati, OH 45242
Attn: David Davidson

General Electric Company
Aircraft Equipment Division
50 Fordham Road
Wilmington, MA 01887
Attn: Ronald J. Casagrande

UTRC/OATL
Palm Beach Gardens Facility
West Palm Beach, FL 33402
Attn: John T. Carroll
Bldg. 30 (MS R-23)

Allison Gas Turbine Operations
General Motors Corporation
Box 894
Indianapolis, IN 46206
Attn: John Custer, W-16

Lewis Engineering Company
238 Wate Street
Naugatuck, CT 06770
Attn: C. B. Stegner

Allison Gas Turbine Operations
General Motors Corporation
Box 894
Indianapolis, IN 46206
Attn: Ken Cross

Arnold Engineering Development Center
Arnold Air Force Station, TN 37389
Attn: Marshall Kingery

Allison Gas Turbine Operations
General Motors Corporation
Box 894
Indianapolis, IN 46206
Attn: David Willis

Hitec Corporation
Nardone Industrial Park
Westford, MA 01886
Attn: Steve Wnuk

Allison Gas Turbine Operations
General Motors Corporation
Box 894
Indianapolis, IN 46206
Attn: Ralph Fox

General Electric Company
Aircraft Engine Group
1000 Western Avenue
Lynn, MA 01910
Attn: George Leperch, AL29dD

Battelle Columbus Laboratories
505 King Avenue
Columbus, OH 43201
Attn: Ross G. Luce, Energy &
Thermal Tech. Section

DISTRIBUTION LIST

Teledyne CAE
1350 Laskey Road
Toledo, OH 43612
Attn: R. Hugh Gaylord
Joseph Pacholec

Peter K. Stein
5602 East Monterosa
Phoenix, AZ 85018

Garrett Turbine Engine Company
P. O. Box 5217
Phoenix, AZ 85010
Attn: N. Fred Pratt

Pratt & Whitney
Main Plant
P. O. Box 2691
West Palm Beach, FL 33402
Atth: John Prosser (MS C-04)
William Watkins

FluiDyne Engr. Corporation
5900 Olson Memorial Highway
Minneapolis, MN 55422
Attn: T. Matsuura

National Bureau of Standards
Washington, DC 20234
Attn: Ken Kreider

AVCO Corporation
Lycoming Division
550 South Main Street
Stratford, CT 06497
Attn: E. Twarog, Mgr.
Electronics and Instr.

National Bureau of Standards
Washington, DC 20234
Attn: George Burns
Inst. for Basic Research

Thermonetics Corporation
1028 Garnet Avenue
San Diego, CA 92109
Attn: H. F. Poppendiek

General Electric Company
P. O. Box 8
Schenectady, NY 12301
Attn: Dr. David Skelley
Bldg. K-1, Rm. 3B24

Battelle Columbus Laboratories
505 King Avenue
Columbus, OH 43201
Attn: M. M. Lemcoe

Mechanical Technology, Inc.
968 Albany-Shaker Road
Latham, NY 12110
Attn: R. Hohenberg

DISTRIBUTION LIST

Boeing Aerospace Company
Engineering Laboratories
Seattle, WA 98124
Attn: Darrell R. Harting

Kulite Semiconductor Products, Inc.
1039 Hoyt Avenue
Ridgefield, NJ 07657
Attn: John R. Hayer

Engelhard
Engelhard Industries Div.
228 East 10th Street
Newport, KY 41075
Attn: Ronald G. Braun

Bolt Beranek and Newman, Inc.
50 Moulton Street
Cambridge, MA 02138
Attn: Richard E. Hayden

Williams International
2280 West Maple Road
Walled Lake, MI 48088
Attn: Henry Moore, Head
Instr. Dept.
J. H. Johnston

Caterpillar Tractor Company
Technical Center, Building F
100 Northeast Adams Street
Peoria, IL 61629
Attn: Mr. Donald Wilson

Virginia Polytechnic Institute
and State University
Mechanical Engineering Dept.
Blacksburg, VA 24061
Attn: W. F. O'Brien, Jr.
Wing F. Ng

Air Force Wright Aeronautical
Laboratory
Wright Patterson, AFB, OH 45433
Attn: Mr. Charles Bentz/POTC
Hot Section Technology

Naval Post Graduate School
Department of Aeronautics (Code 67)
Monterey, CA 93940
Attn: Prof. R. P. Shreeve

AVCO Corporation
Lycoming Division
550 South Main Street
Stratford, CT 06497
Attn: Mr. K. Collinge
IRAD Mechanical Projects
Manager

Pennsylvania State University
233 Hammond Building
University Park, PA 16802
Attn: Prof. B. Lakshminarayana

Eaton Corporation
Box 766
Southfield, MI 48037
Attn: Mr. Lamont Eltinge
Director of Research

DISTRIBUTION LIST

Public Service Electric & Gas Company
80 Park Plaza
Newark, NJ 07101
Attn: Dr. Melvin L. Zwillenberg
Research & Development Dept.

Massachusetts Institute of Technology
Cambridge, MA 02139
Attn: Dr. Alan Epstein
Rm. 31-266

Raychem Corporation
300 Constitution Drive
Menlo Park, CA 94025
Attn: Dr. David C. Chappelear
Director of Corporate
Research & Development

Sverdrup (AECD)
Arnold AFB, TN 37389
Attn: Paul McCarty

Fabrication Development Laboratory
Owens/Corning Fiberglas
Technical Center
Granville, OH 43023
Attn: Mr. Hugh W. Bradley, Jr.

Rosemont, Inc.
Mail Stop F-15
P. O. Box 959
Burnsville, MN 55337
Attn: Mr. Larry N. Wolfe

Xerox Electro-Optical Systems
1616 North Fort Myer Drive, 16th Floor
Arlington, VA 22209
Attn: Mr. Clifford I. Cummings
Manager, Intelligence &
Reconnassance

Thermogage, Inc.
330 Allegany Street
Frostburg, MD 21532
Attn: Charles E. Brookley

Construction Materials Support Group
Owens/Corning Fiberglas
CMG Process Technology Laboratory
Granville, OH 43023
Attn: Mr. J. W. Scott

Hycal Engineering
12105 Los Nietos Road
Sante Fe Springs, CA 90670
Attn: William Clayton

NASA Headquarters
Washington, DC 20546
Attn: M/Paul N. Herr

Medtherm Corporation
P. O. Box 412
Huntsville, AL 35804
Attn: Larry Jones

DISTRIBUTION LIST

Rocketdyne
6633 Canoga Avenue
Canoga Park, CA 91304
Attn: Dr. John C. Lee

Babcock & Wilcox R&D Division
P.O. Box 835
Alliance, OH 44601
Attn: John Berthold

Combustion Engineering
Dept. 9005-03D1
Windsor, CT 06095
Attn: John Fishburn

Applied Sensors International
7834 Palace Drive
Cincinnati, OH 45242
Attn: Richard Stillmaker

RdF Corporation
23 Elm Avenue
Hudson, NH 03051
Attn: Frank Hines

Carnegie-Mellon University
Dept. of Mechanical Engineering
Pittsburgh, PA 15213
Attn: Dr. Norman Chigier
Professor William J. Brown

Babcock & Wilcox R&D Division
P. O. Box 835
Alliance, OH 44601
Attn: Harold Wahle

Calspan Field Services, Inc./AEDC Div.
Arnold Air Force Station, TN 37389
Attn: C. T. Kidd

JEC Lasers, Inc.
253 Crooks Avenue
Patterson, NJ
Attn: Mr. John Wasko

Physical Sciences Dept.
Arvin/Calspan Adv. Tech. Ctr.
Buffalo, NY 14225
Attn: M. G. Dunn

NASA Langley Research Center
Hampton, VA 23665
Attn: R. E. Wright, Jr. (MS-234)
S. L. Ocheltree (MS-235A)

UNITED TECHNOLOGIES
PRATT&WHITNEY
AIRCRAFT

400 Main Street
East Hartford, Connecticut 06108

In reply please refer to:
WHA:D:0381Q - MS 165-37
Ref. No. PWA-5914-21

4 September 1984

To: National Aeronautics and Space Administration
Lewis Research Center
21000 Brookpark Road
Cleveland, Ohio 44135

Attention: Mr. R. Holanda, Project Manager, MS 77-1

Subject: Turbine Blade and Vane Heat Flux Sensor Development, Phase I Final Report, CR-168297

Reference: NASA Contract NAS3-22133

Gentlemen:

The attached report is submitted in compliance with the Reports of Work Clause of the referenced contract.

UNITED TECHNOLOGIES CORPORATION
Pratt & Whitney Aircraft Group
Engineering Division

W. H. Atkinson
Program Manager

cc: Air Force Plant Representative Office
UTC/Pratt & Whitney Aircraft Group
East Hartford, Connecticut 06108
Attn: Ira Goldberg, MS 104-08

DO NOT REMOVE SLIP FROM MATERIAL

Delete your name from this slip when returning material to the library.

NAME	MS
Scott Slaughter	170

NASA Langley (Rev. May 1988) RIAD N-75